EXPERIMENTAL INVESTIGATION ON THERMALLY ASSISTED MACHINING OF INCONEL 718 SUPERALLOY
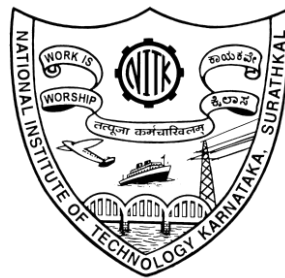
Thesis

Submitted in partial fulfillment of the requirements for the degree of

DOCTOR OF PHILOSOPHY

by

GANTA VENKATESH

DEPARTMENT OF MECHANICAL ENGINEERING

NATIONAL INSTITUTE OF TECHNOLOGY KARNATAKA

SURATHKAL, MANGALORE-575025

December, 2017

D E C L A R A T I O N

I hereby declare that the Research Thesis entitled "**EXPERIMENTAL INVESTIGATION ON THERMALLY ASSISTED MACHINING OF INCONEL 718 SUPERALLOY**" which is being submitted to the **National Institute of Technology Karnataka, Surathkal** in partial fulfillment of the requirements for the award of the degree of **Doctor of Philosophy** in **Mechanical Engineering** is a *bonafide report of the research work carried out by me*. The material contained in this Research Thesis has not been submitted to any other Universities or Institutes for the award of any degree.

Register Number: **123028ME12F03**

Name of the Research Scholar: **Ganta Venkatesh**

Signature of the Research Scholar:

Department of Mechanical Engineering

Place: NITK-Surathkal

Date:

C E R T I F I C A T E

This is to certify that the Research Thesis entitled "**EXPERIMENTAL INVESTIGATION ON THERMALLY ASSISTED MACHINING OF INCONEL 718 SUPERALLOY**" submitted by **Mr. Ganta Venkatesh (Register Number: ME12F03)** as the record of the research work carried out by him, *is accepted as the Research Thesis submission* in partial fulfillment of the requirements for the award of the degree of **Doctor of Philosophy.**

Research Guide

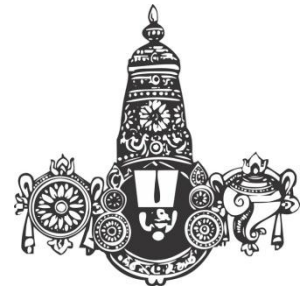**Dr. D. Chakradhar**
Assistant Professor
Department of Mechanical Engineering

Chairman-DRPC
Date

Dedicated to….

My Beloved Family Members…

ACKNOWLEDGEMENT

ABSTRACT

Nickel-based superalloys are widely used in the manufacture of various components and structures for aerospace, marine and nuclear power generation, chemical, petrochemical and process industries. Accounting for about 50 % weight of materials used in an aerospace engine, mainly in the gas turbine components. Aircraft engine constitute total materials about 30 % of nickel-based superalloys. These alloys are also used in structural material of various parts in the main engine like cryogenic tanks and in pressure vessels of nickel hydrogen batteries used in aviation. Nickel based superalloys desirable mechanical properties like high fatigue strength, high yield and ultimate strength, corrosion and oxidation resistance over a wide temperature range of -217 ^{o}C to 700 ^{o}C. Generally, superalloys are challenging to machining due to their peculiar characteristics such as low thermal conductivity, high hot hardness, high work hardening tendency, chemical affinity towards cutting tool and hard abrasive carbide particles present in the microstructure. Due, to these limitations nickel based superalloys are very difficult to machine. Conventional machining of nickel based superalloys exhibits poor machining performance due to high chemical affinity, strong work-hardening, and tendency to abrasive nature. To overcome these problems, thermally assisted machining of difficult to cut materials is an emerging technique; it is an alternative of conventional machining.

In present investigations, thermally assisted machining characteristics of Inconel 718 superalloy were studied. The most significant parameters and suitable cutting tool to machine Inconel 718 have been identified. The effect of process parameters on the cutting forces, surface roughness, tool wear, material removal rate, surface topography, heat affected zone (HAZ), microhardness, phase changes and residual stresses were investigated. The analysis of variance (ANOVA) was performed to find out the contribution of process parameters on the output responses and the regression equation has been developed using Minitab 17 software. L_{27} orthogonal array of experiments was conducted on Inconel 718 by using uncoated carbide, TiAlN nano multilayer, TiCN/Al$_2$O$_3$/TiN triple layer coated with considering process parameters of cutting speed, feed rate, depth of cut and workpiece temperature. Experimental results shows

that cutting speed, feed rate depth of cut and workpiece temperature are the most significant process parameters on cutting force; feed rate and workpiece temperature are most significant process parameters for surface roughness; cutting speed, feed rate and depth of cut are most significant process parameters for tool wear and metal removal rate. In extensive experimentation and analysis TiAlN multilayer coated tool was found to be appropriate to machine Inconel 718 superalloy than uncoated and $TiCN/Al_2O_3/TiN$ coated tool. Cutting forces in TAM were observed to be less compared to conventional machining; Surface roughness was improved remarkably in TAM by about 21.8 %. Tool wear was reduced by 29 %, and MRR increased by 5.9 % in TAM compared to conventional machining. However, the individual effects of cutting speed, feed rate, depth of cut and workpiece temperature on performance characteristics like cutting forces, surface roughness, metal removal rate, tool wear, heat affected zone, microhardness, surface topography, residual stresses and phase changes on the machined surface were analyzed. The cutting forces and surface roughness decrease as the cutting speed and workpiece temperature increase, but increases with increase in feed rate and depth of cut. The microhardness increases as the workpiece temperature increases, hence TAM improves the performance of the product. Thermally assisted machining reveals that there are neither phase changes, nor broadening of the peaks that were observed at different machining conditions. Tensile residual stresses are induced on the machined surface the workpiece temperature increases the residual stresses were decreased.

Central composite rotatable design of experiments was conducted to evaluate the cutting force, surface roughness, tool wear and metal removal rate. Based on the experimental results corresponding second order regression models have been developed. The developed regression models were utilized as fitness functions in particle swarm optimization algorithm (PSO). The lower and upper levels of process parameter were selected as constraints for the optimization. The simultaneous optimization of process parameters to minimize cutting force, surface roughness, and tool wear and to maximize MRR were performed by using particle swarm optimization algorithm. The optimized results were cross checked by conducting the confirmation experiments and the predicted

values found to have good agreement with the experimental values. PSO can also be used as a tool to optimize and predict the results during TAM machining of Inconel 718

CONTENTS

LIST OF FIGURES

LIST OF TABLES

NOMENCLATURE

MRR	:	Material Removal Rate
Ra	:	Surface Roughness
HAZ	:	Heat affected zone
SEM	:	Scanning Electron Microscope
EDAX	:	Energy Dispersive X-Ray Analysis
OA	:	Orthogonal Array
DOE	:	Design of Experiments
RSM	:	Response Surface Methodology
CCRD	:	Central composite rotatable design
ANOVA	:	Analysis of Variance
ANOM	:	Analysis of Mean
SS	:	Sequential sum of squares
Adj. SS	:	Adjusted Sum Of Squares
MS	:	Mean Square
F	:	F-Ratio Value
P	:	Percentage of Contribution
EA	:	Evolutionary Algorithm
GA	:	Genetic Algorithm
PSO	:	Particle Swarm Optimization
ABC	:	Ant Bee Colony Technique
TLBO	:	Teaching Learning Based Optimization
ANN	:	Artificial Neural Networks
BPNN	:	Back Propagation Neural Network
CFD	:	Computational Fluid Dynamics
FEM	:	Finite Element Method

CHAPTER 1

INTRODUCTION

In the modern industries machining of superalloys, smart materials and difficult to cut materials like nickel chromium alloys, high manganese steels, tool steels, high chrome white cast irons etc. have become very essential to meeting the design requirements for equipment in mining, agriculture, aerospace, defense, nuclear power plants and process industries. Machining of such materials, in particular nickel based superalloys have tough job (Sun et al., 2010). The high strength of the material is due to the presence of fine metastable γ' and γ'' precipitates, with intermetallic phases Ni_3 (Al, Ti) and Ni_3 (Al, Ti, Nb) distributed throughout the matrix. While machining of nickel based superalloys difficulties like high cutting forces, poor surface finish, severe tool wear tendency to form built up edge by welding the tool due to high temperatures (Choudhury, 1998). On the other hand ceramics and diamond like tools are used to overcome these difficulties but it requires high tooling cost (Bushlya et al., 2012; Sun et al., 2010).

High speed machining is one of the technique where frictional temperature is developed at the workpiece - tool interface which leads to annealing of the workpiece material opposite to the cutting tool, causes yield strength of the material to be reduced, thereby cutting forces are decreased increased metal removal rate, but cost of the tooling is increased due to severe tool wear. Therefore high speed machining requires high rotating drive of more than 10,000 RPM.

Hard turning process had been introduced to overcome the drawbacks of high speed machining of hard materials such as polycrystalline cubic boron nitride (PCBN) a cubic boron nitride cutting inserts were used. The advantages of hard turning over conventional grinding process are, complex and intricate geometry be done in a single set-up, less investment cost, less machining cost. But, time required to get cutting

temperature to soften the workpiece material depends on cutting speed and on cutting insert coatings and geometry.

In hard turning costly tools are used to soften the workpiece material, however, preheating is an another attractive technique. Preheating is also and is referred to as hot machining (HM) or thermally assisted machining (TAM) (Ranganathan et al., 2010; Xu et al., 2013; Thandra and Choudhury, 2010). In this method an external heat source is used on the workpiece to reduce the material strength and hardness which in turn leads to reduction of the cutting forces required for machining without material damaged (Ozler et al., 2001). Therefore strain hardening and flow stresses of the workpiece reduces significantly (Maity and Swain, 2007).

Selection of appropriate heating technique and locating of small heating zone is important in hot machining (Lajis et al., 2009). Faulty heating techniques may cause metallurgical damage of the workpiece. Heat sources vary from basic to advanced techniques such as induction heating, furnace heating, electric arc heating, electric current heating, flame heating, plasma arc heating, laser beam heating, flame heating (Thandra and Choudhury, 2010). But, localized heating techniques such as laser beam heating are potentially viable since unwanted of the workpiece causes subsurface and microstructure changes can be avoided. However, laser technique requires high machining cost and also it requires large space around the machine tool (Anderson et al., 2006). Using plasma gas to heat the workpiece is cheaper compared to laser machining, but it requires high energy consumption besides demanding large space around the machine tool (Sanchez et al., 2014). Among all the methods flame heating is a low investment techniques which is simpler and can be easily accommodated in all type of industrial space.

In hot machining process cutting forces, surface roughness, tool wear and metal removal rate plays a key role and is defined as the average temperature of the material as it enters the shear deformation zone (Sun et al., 2010). Since the deformation behavior of the workpiece material is strongly depend on this temperature requires thermal flux distribution analysis around the work surface to the thickness up to the cutting tool (Ozler

2

et al., 2001). Some of the remarkable advantages of hot machining operation are stated as follows:

> Tool life of the cutting tool is more.
> Cutting forces are less.
> Less power consumption.
> Greater productivity due to higher MRR.
> Strain hardenability and flow stresses in workpiece are reduced.
> Wear and abrasion of cutting tool is less resulting greater tool life.
> Better surface quality.
> Hot machining of brittle and ceramic materials is very much easier than any other known approaches.

1.1 NICKEL BASED SUPERALLOYS

Among all the nickel based superalloys, Inconel 718 is one of the most important alloys, because it has exceptional mechanical properties such as excellent wear resistance, high corrosion and oxidation resistance at elevated temperatures (650 $^{\circ}$C). Due to these properties Inconel 718 is extensively used in aerospace, gas turbine blades and nuclear power plants etc. Figure 1.1 shows different sections of gas turbine engine. Due to more advanced and sophisticated technology used in modern gas turbine engines, it is challenging for a material which is to be placed at the turbine inlet. This is because; it is subjected to extreme conditions such as very high temperature, great pressure, high rotational speed and vibration. The components of nickel-iron-based superalloys used in aircraft engines are blades and the discs in the high pressure compressor and turbine (Locq and Caron, 2011). However, this material is classified as difficult to cut material owing to its unique characteristics such as high tendency to work hardening, low thermal conductivity and hard abrasive particles such as γ' and γ'' (Ni_3Nb), (Ni_3 Al Ti) precipitates distributed throughout the matrix and high affinity for tool materials. For this reason, while machining Inconel 718 conventionally, the cutting speed cannot be higher than because of excessive tool wear, notching and tool chipping. Typically, at the cutting

zone during the machining of Inconel 718, the cutting temperatures can reach up to 1200 ^{o}C. Due to these limitations nickel based superalloys are very difficult to machine. Figure 1.2 shows the classification of superalloy. (Choudhury and El-baradie, 1999).
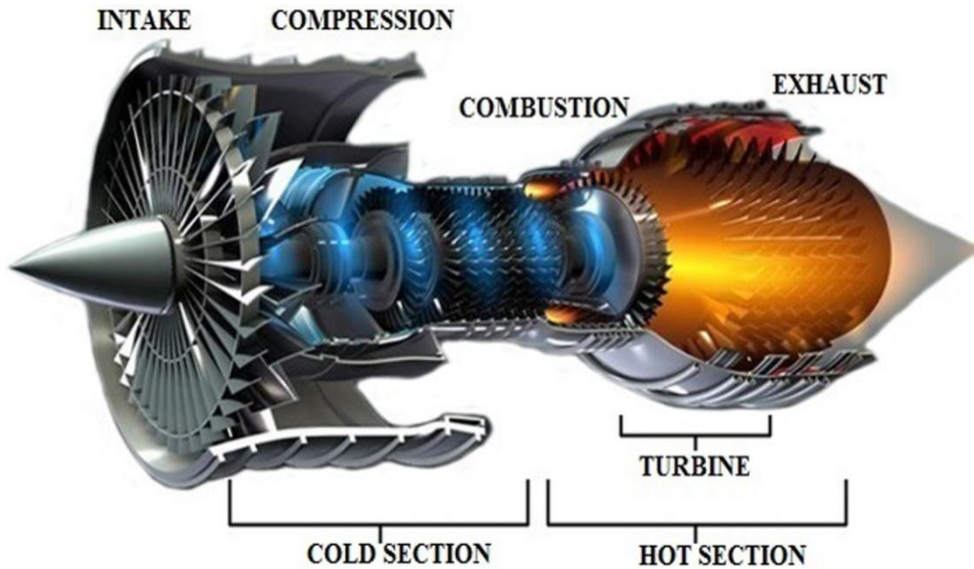
Figure 1.1 Schematic representation of Rolls Royce turbofan engine
(Rolls Royce, 2015)
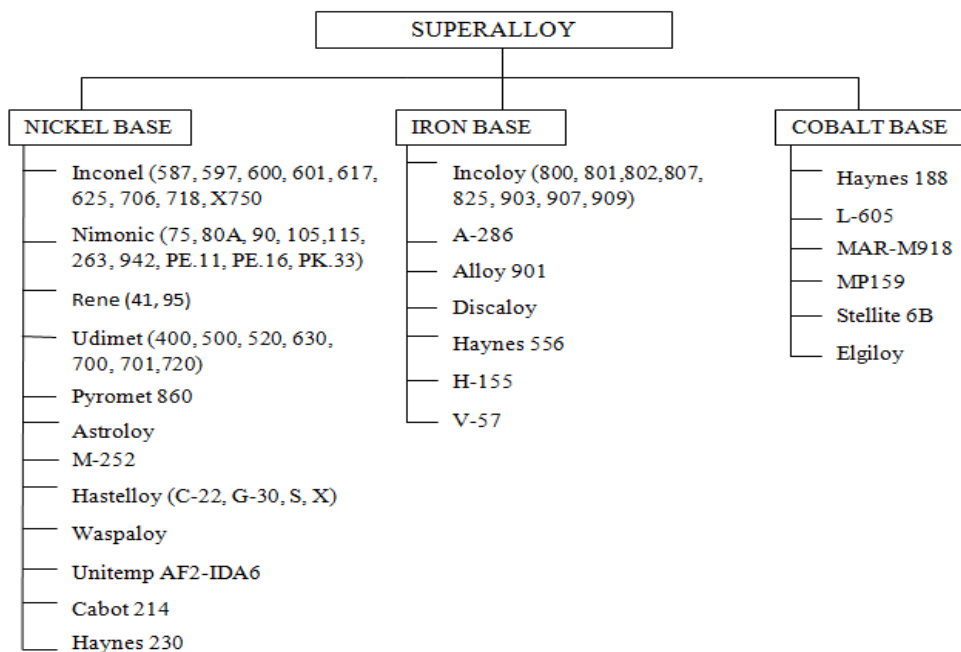
Figure 1.2 Classification of super alloys (Choudhury and El-baradie, 1999)

Many researchers and engineers have concentrated on improving the machinability of difficult to cut materials, through the use of number of methods. Currently non-traditional machining methods/processes like Electro discharge machining (EDM), wire electro discharge machining (WEDM), electrochemical machining (ECM), water jet machining are widely used in industries for machining the components, but they requires high machining costs and have low metal removal rates. Some other conventional machining techniques like minimum quality lubrication, cryogenic coolants, compressed coolants, new synthetic coolants, hybrid combinations techniques required coolants to obtain better surface finish and improved tool life (Kaynak et al., 2014). However, these techniques involve high machining cost due to cutting fluid disposal and chip cleaning cost. To overcome these difficulties hot machining is one of the preferred methods to improve the machinability of difficult to cut metals

1.2 RESEARCH OBJECTIVES AND APPROACH

This research work mainly focuses on improving and investigating the machinability of Inconel 718. Industries would benefit from improved machinability of Inconel materials are improved. In view of this, hot machining is the right choice to enhance the machinability characteristics. Oxy-acetylene flame was selected as the preheat source. Extensive investigations were made experimentally to evaluate the machinability characteristics at different cutting conditions. Microscopic studies were done at various stages to support experimental work. The performances of the cutting tools (three different cutting inserts such as uncoated, TiAlN nano multilayer and $TiCN/Al_2O_3/TiN$ triple layer) were analyzed by conducting series of microscopic, EDAX and XRD tests at different stages. Chip morphology explores the behavior of the machining process. Most importantly, DOE techniques (Taguchi, ANOVA/RSM, and Regression) found to be more useful tools in optimizing the cutting process. Experimental design, correlation of the derived results and the development of the higher order mathematical models to build the relationship among the process parameters and responses are the other key tasks

covered by these tools. The graphical presentation behavior of the process parameters and its interactive effects enrich the analysis job.

1.3 SCOPE OF THE INVESTIGATION

Hot machining of difficult to cut materials is an emerging technique; it is an alternative of conventional machining. The surface quality of the machined products produced by this process has been achieved in earlier investigations, due to above mentioned reasons some of these methods remain of academic interest only and they are not viable for industrial adoption. The quality and integrity of machined surfaces of difficult to cut materials depends on various factors such as cutting parameters, tool materials, tool geometry etc. Therefore, this dissertation addresses the machinability studies of Inconel 718 by hot machining, which is difficult to cut material by conventional machining. Three different cutting inserts i.e., uncoated carbide, TiAlN nano multilayer, $TiCN/Al_2O_3/TiN$ triple layer coated were used at different machining conditions to investigate the machinability characteristics and performance. In addition, this study includes surface and sub surface alterations and residual stresses during hot machining.

1.4 OBJECTIVES OF THE PRESENT RESEARCH

- ➢ To investigate the effects of cutting speed, feed rate, depth of cut and workpiece temperature on cutting forces, tool wear, metal removal rate, and surface roughness in hot machining.
- ➢ Optimization of process parameters to achieve better surface and sub-surface properties.
- ➢ To study the effect of hot turning and their process parameters on surface integrity.
- ➢ To study the effect of process parameters on residual stresses as well as surface and sub-surface alterations.
- ➢ Developing a correlation model between process parameters and performance characteristics by using statistical methods.

To execute the research objectives, the research is performed through the following approach.

1. Based on the literature review the experimental studies, a methodology is developed to understand the problems in existing method of machining the difficult to cut the materials.
2. Experiments are performed to study the machinability characteristics of Inconel 718 by three different cutting inserts like uncoated carbide, TiAlN nano multilayer and $TiCN/Al_2O_3/TiN$ triple layer coated.
3. The effect of hot machining process parameters on the quality of machined surface , tool wear are studied
4. The tool wear and the surface integrity of machined surface are studied through SEM analysis
5. Statistical analysis is performed to study the significant influencing parameters and their interactions on the response factors.
6. The multiple linear regression models are presented and validated using confirmation tests.

1.5 THESIS OUTLINE

This thesis is divided into seven chapters.

Chapter 1 gives a general introduction on hot machining, nickel based superalloys, heat treatment of super alloys, cutting tool materials, various problems in hot machining. Scope and research objectives of the thesis work and outline are presented and discussed.

Chapter 2 shows the select survey of literature on characteristics of the machining of nickel based superalloys; presents the influence of process parameters on cutting forces, surface roughness, tool wear and chip morphology. Also, surface roughness plays a major role on product quality and in case of technical requirement for mechanical products. In this chapter, surface integrity of nickel based superalloys are reviewed and presented.

Chapter 3 represents the experimental procedure and setup used to measure the cutting forces, surface roughness, tool wear, surface topography and residual stresses were explained. In this chapter selection of workpiece material, cutting tools selection of process parameters and optimization techniques were discussed.

Chapter 4 focuses on the effect of process parameters on the performance characteristics such as cutting forces, surface roughness, tool wear, metal removal rate in machining of Inconel 718 superalloy.

Topics covered in this chapter are

- Selection of major influencing process parameters affecting on performance characteristics.
- Finding of optimal set of hot machining process parameters.
- Selection of best cutting tool for machining of Inconel 718 superalloy based on output responses.

The Taguchi parameter design is used to obtain the above objectives.

Chapter 5 shows the studies on the effect of individual parameters such as cutting speed, feed rate, depth of cut and workpiece temperature on cutting forces, surface roughness, tool wear, metal removal rate, microhardness, and chip morphology. Further analyses were carried out to study the phase changes on the machined surface and residual stresses of Inconel 718 super alloy.

Chapter 6 explains central composite rotatable design for conducting experiments on Inconel 718. Mathematical models were developed to correlate thermally assisted machining process parameters and response like cutting force, surface roughness, tool wear and MRR using Response surface methodology.

Topics covered in this chapter are

- Developing a single response optimization model using Response Surface Methodology.
- Developing multi response optimization models using particle swarm optimization approach.
- Confirmation experimental verification was performed for optimized process parameter combinations.

Chapter 7 presents the summary of conclusions on the investigations carried out in this research work and also includes further recommendations addressing various issues for the future work.

CHAPTER 2

LITERATURE REVIEW

2.1 INTRODUCTION

This chapter reviews the present research work carried out in the field of hot machining (HM). The literature review mainly discusses about the literature related to basic metal cutting, hard machining, thermally enhanced machining, different pre heating techniques, cutting tools, design of experiments used in the present research work.

2.2 METAL CUTTING

In metal cutting process, the components are produced by application of external forces on tools which causes the fracture (Figure 2.1). This occurs from the combined effect of shearing stress and the bending stress. The bending stress existence in the deformation zone divides the metal cutting and manufacturing process. System deliberation of the metal cutting processes shows that the competition between deformation hardening and thermal softening forms the chip formation process. Due to various parameters on metal removal rate vary chip formation.
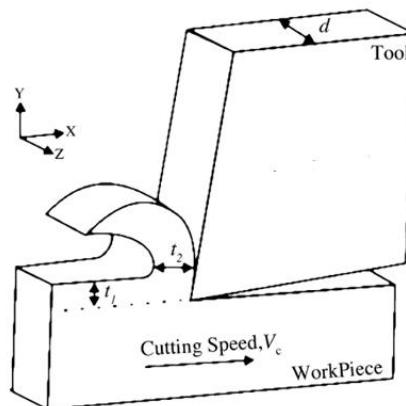
Figure 2.1 Metal cutting process interaction between chip and tool rake face

(Mitrofanov et al.,2015)

2.3 CONVENTIONAL MACHINING

In the present time, metal cutting plays a significant role in manufacturing industries and is indispensable. In view of cost-effective importance of metal cutting, it is necessary to have a complete understanding of the cutting process. It is possible to adopt a new machining technique/equipment or finding the optimal machining conditions, which are required for the following;

1. To utilize the expensive cutting machines and high cost of labor at the highest productivity.
2. To allow machining of new alloys, which are generally difficult to machine due to improved mechanical properties.
3. To improve the dimensional accuracy of the machined product.

2.4 HARD TURNING

Hard turning is a metal cutting process in which high accuracy surfaces are produced in hard metals like hardened steel and difficult to cut materials having a hardness value of 45-60 HRC. This process is normally used for machined parts, where surface finish and accuracy are not too demanding. In grinding still ultra and high precision parts commonly used in manufacturing processes. But in some cases complimented and dedicated finishing process still better surface finishes are required. Hard turning processes have many advantages over precision grinding for improving the product and process quality (Chryssolouris et al., 2014).

Hard turning is successfully implemented, differences in the physics of the cutting process for machining soft steels (hardness below 50 HRC). There are several of researchers who have reported on the features of the hard turning process and machinability of different materials. Masood et al. (2011) reported that in hard turning, higher cutting speed is in order to produce maximum friction at the cutting zone (tool-work) interface. Thus frictional heat generated at the primary shear zone softens the

workpiece at the cutting zone, after completion of the machining removing by the tool itself leaving the machined surface unaffected. Therefore, cubic boron nitride (CBN) cutting tools are very costly compared to other tools like carbide and ceramic tools (Lin and Chen, 1995). Fewer researchers have addressed the features of hard turning of different materials. Among them, Hasan and Rizwan (1998) explained the benefits of hard turning process in bearing industry, in which production steps are heat treatment followed by grinding. This process is used to manufacture bearings of high and medium carbon steels (e.g. ASTH5115, AISI1050, 52100). Gaurav Bhattacharya et al., (2003) review shows that the type of tool material, cutting edge geometry and cutting parameters affect the process efficiencies in terms of tool forces, surface integrities integrity, and white layer. Nowadays trends have changed with the costly and slow grinding process having been replaced by the turning process for roughing and finishing of parts prior to super finishing. Another industrial example of the grinding operation to hard turning in the machining of blisks and blings of Inconel 718 reduces the tool life of ceramics when machined (Zhou et al., 2012).

Hard coated tools have been commercially available since 1980 and have brought improvements to the hard turning technology. After the detailed study on coated carbide tools, Li et al. (2002) reported the encouraging properties of TiAlN such has high hot hardness, high strength, good heat resistance, and high wear resistant. Also the tool used has negative rake angle, dry machining and high speed turning has high temperature around 900 $^\circ$C generated at the shear zone.

The experimental investigations of Bushlya et al. (2012) on Inconel 718 super alloy (~45 HRC) with two different cutting tools such as coated TiN and uncoated PCBN reveal that at low cutting speeds the advantage of the coating over PCBN tools is limited. As the cutting speed increases to 300 m/min, there is no benefit in terms of tool life. Jindal et al. (1999) employed differently coated PVD inserts such as TiN, TiCN and TiAlN with workpiece materials as Inconel 718, SAE 1045 steel and ductile Iron. TiAlN shows better machining performance among all the cutting tools. TiAlN coated tool even

show greater performance at higher cutting speeds. TiAlN coating has high oxidation resistance, high temperature chemical stability, low thermal conduction, high hot hardness temperatures generated at the tool tip during machining operation.

Sahin (2009) conducted experiments on hardened bearing steels to compare the tool life of both ceramics and CBN tools, and reported that cutting speed has dominant effect on tool life at 90 % confidence level. The cutting speed has highest percentage contribution of 41.63, tool hardness has 32.68 and feed rate has 25.22 on the tool life. Suresh et al. (2012) performed experiments with hard coated multilayer carbide (TiC/TiCN/Al$_2$O$_3$) tools for hardened AISI 4340 turning. They observed that the optimum combination of high cutting speed, low feed rate and low depth of cut is beneficial to reducing the machining force, surface roughness. The tool wear and machining power increases linearly with increase of feed rate and cutting speed.

The investigations made by Jiang et al. (2006) evaluated the surface roughness, tool wear, surface morphology, chemical composition, crystal structure, microhardness and wear mechanisms of CBN coated deposits on carbide inserts (SNMG432) for hard turning of AISI 4340 they reported that CBN coated tools demonstrated a tool life of about 10 min per cutting edge, the white layer was characterized by using SEM and nano-indentation, which revealed no discernible difference in hardness between the white layer and bulk material. Gaitonde et al. (2009) performed a series of experiments to investigate the machinability characteristics of high chromium AISI D2 cold worked tool steel with CC650WH, CC650 and CC650WG inserts. The experimental results reveal that CC650WG wiper insert had superior performance in tool wear and surface finish. However the CC650 insert was useful in reducing the machining force, power and specific cutting force. Ozel et al. (2005) conducted series of experiments with two distinct edges of cubic boron nitride insert, finish turning of AISI H13 steel.

The hard turning experiments Dudzinski et al. (2004) conducted by Round inserts of SiC whisker-reinforced ceramic improve the cutting performance for milling of Inconel 718, in comparison with the square ones. Ceramics are poor conductors and vulnerable to

thermal cracks and dry machining is recommended with them. Ozel et al. (2005) studied the effect of cutting edge geometry, workpiece hardness, cutting speed and feed rate on cutting forces and surface roughness. The experimental results shows that honed edge geometry and low workpiece hardness shows lower better surface roughness and lower cutting forces.

Aslan (2005) used X210 Cr12 to investigate machining of cold worked tool steel (62 HRC) to analyze the performance and wear of CBN, TiCN/TiAlN coated carbide tool, TiAlN coated cermets, and mixed ceramic with Al_2O_3 + TiCN. Among all the cutting inserts, the CBN tool had the best given the better performance on surface roughness, tool wear and metal removal rate.

Limitations of Hard turning

Considering the economic feasibility of the hard turning process, especially for large production volumes may particularly prevail against the other favorable factors offered by grinding (Lin and Chen, 1995). As the machining parts goes to the final stages of production, increased marginal costs are added to the part making it continually more valuable. Even a small defect at the machining stage or system instabilities in the final stage, will damage the part, making very expensive scrap. Due to these problems many authors are very cautious opting to manufacture them for very slow, but highly reliable grinding processes, particularly when manufacturing large and expensive components. Hence, it requires more innovations to make the hard turning process more competitive and economically effective than grinding (Masood et al., 2011).

2.5 HOT MACHINING

The drawbacks with the hard turning process creates a window of opportunity for high speed machining, as the speed of the workpiece is kept considerably high to increases then the friction between tool-work interface (Chryssolouris and Anifantis, 1994). The high amount of heat produced at the tool-work-chip (cutting zone) is sufficient to anneal

the material there by diminish the material's shear strength. This reduction in shear strength leads to increase of metal removal rate due to resistance reduced at the hot stock (Lajis et al., 2009). However, the high cutting speed causes severe tool wear, hence the cutting tool's cost also very high. Therefore, advanced tool technologies suitable for difficult to materials like Inconel 718 and to improve the machinability characteristics are required. There is a lot of demand for difficult to cut materials in engineering applications, many machine tool manufacturers came forward to machine this type of materials and developed advanced coating techniques and tool materials.

As hard turning process is a costly process, researchers invented thermally enhanced machining (TEM) also called hot machining. TEM used localized heat is applied in front of the cutting zone (tool- work) to reduce the strength of the material. The heat generated at the tool workpiece interface will match the heat produced at the high speed machining (Ozler et al., 2001). Lajis et al., (2009) in hard turning quoted tensile strength of different materials at various temperatures (Figure 2.2). From the Figure 2.2 it is observed that the strength of the material decreases as the temperature increases in between 400 $^{\circ}$C to 800°C.
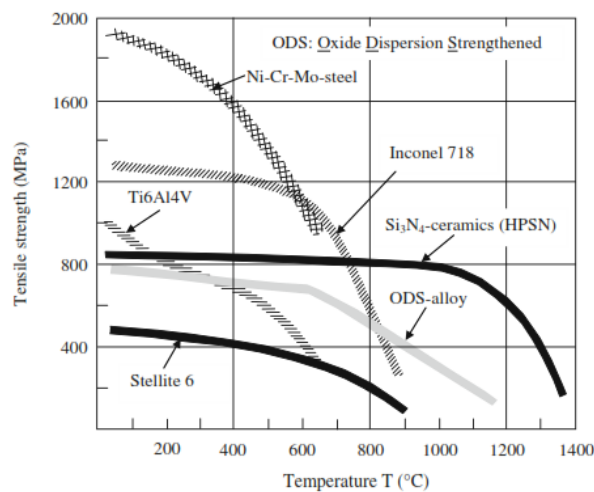
Figure 2.2 Effect of temperature on ultimate tensile strength for different difficult to cut materials (Sun et al. 2010)

15

Figure 2.3 shows the comparison of shear strength of Inconel 718 at various temperatures. The characteristic curve shows the decrement of yield strength of the Inconel 718 for the increase of temperature. Even though the data is limited, Figure 2.3 a shows drop of 160 ksi at 750°C, which makes machining at 750 °C easier than at room temperature (Leshock et al., 2001). Normally, hot machining experiments were conducted on conventional lathe machine where the workpiece is heated by moving heat source. From the external heat source provides intense localized heat, which might soften the work metal may be moved in the form of chip, leaving the workpiece relatively cool and metallurgical undamaged. The preheating method makes a positive influence on the process responses. Literature review on hot machining, shows the following benefits compared to conventional methods:

➢ Lower cutting forces and hence low power consumption.
➢ Reduced strain hardening and flow stresses in the workpiece.
➢ Lower wear and abrasion of cutting tool resulting greater tool life.
➢ Better surface quality
➢ Higher metal removal rate and so high productivity.
➢ Easier hot machining of brittle ceramic materials than any other known approaches (Thandra et al., 2010)
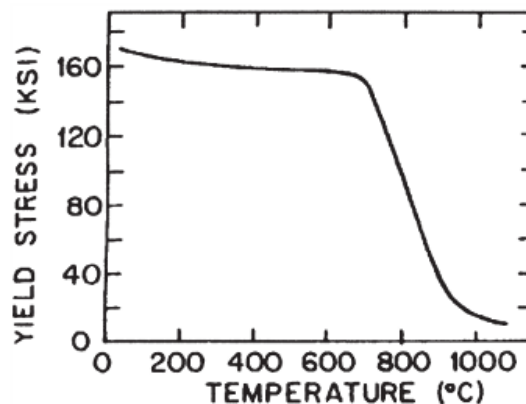
Figure 2.3 Shear strength of Inconel 718 vs temperature (Leshock et al., 2001)

16

Literature review shows that advantages of hot machining have been explored in milling, shaping and turning operations due to their experimental constraints. Industries such as aerospace, defense and aviation are few examples where hot machining would be the most beneficial. Normally, the materials machined by hot machining process are super alloys, Ni-Cr steel, high manganese steel, ceramic materials, NH4 (Ni-hard steel), high-chrome white cast iron alloys, Cr-Mo white cast iron, AISI 4340, stainless steel, navy grade steel, S-816 alloy, Titanium alloys, Timken 16-25-6, (Masood et al., 2011, Rozzi et al., 2000, Maity and Swain, 2007).

Hot machining was first introduced by Tigham, J.R Macy whose patented method of electrical resistance heating of the workpiece produced successful results in his experiments (Maity and Swain, 2007). From this encouragement many researchers introduced different type of heating techniques to study the benefits of hot machining (Thandra and Choudhury, 2010). Rozzi et al. (2000) reported that during hot machining, and resistance to cutting were minimized.

Conventional and thermally assisted machining experiments by Konig and Zaboklicki (1994), reveals that tool wear has been reduced by 90 % during laser assisted machining of Stellite 6. Dandekar et al. (2010) performed the experiments to investigate the machinability characteristics of Ti-6Al-4V alloy used for laser assisted hybrid machining; and observed excellent improvement in metal removal rate and tool life. Skvarenina and Shin (2006) compacted graphite iron material is used to machine the laser assisted machining and observed that improvement in tool life and surface finish. In the investigations made by (Ozler et al., 2001) on austenitic manganese steel established that, as the workpiece temperature increases the tool life also increases, but decreases as the feed rate and cutting speed increased. They confirmed that the increase of workpiece temperature reduces the frictional force on the tool. Mukherjee and Basu (1973) concluded that machining with nickel chromium steel and reported that influence of preheating on surface roughness is much more articulated than tool life.

2.5.1 Pre heating techniques

There are different types of preheating techniques used in hot machining process in industries as follows:

- Laser heating
- Plasma arc heating
- Electrical heating
- Flame heating

From the above all heating techniques, laser heating and flame heating are widely used (Ravi et al., 2014) discussed the effective utilization of preheat; in this process the heating zone must be as small as possible. To avoid the metallurgical changes the depth of heat penetration of the workpiece should not be deep. The introduction of newly developed hot machining techniques gives relief to industry. Due to the preheating process, the cutting forces are reduced up to 40 %, therefore it causes improvement in tool life.
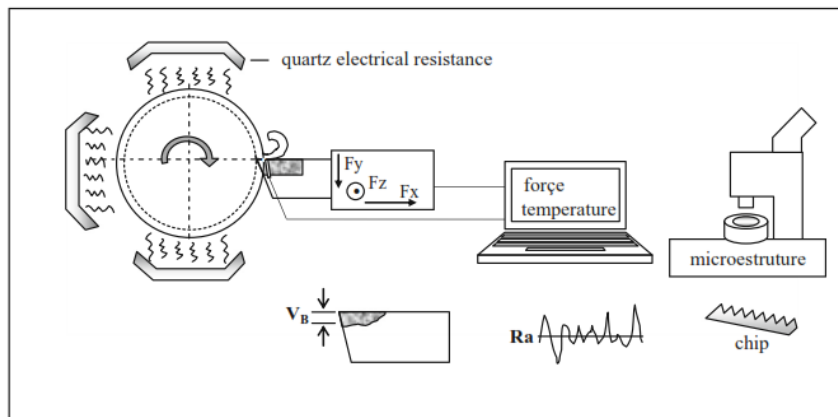
Figure 2.4 Quartz electrical resistance pre heating experimental setup

(Sanchez et al. 2014)

2.5.2 Electric heating

The first pre heating setup was developed by Macy J.R, by using electrical heating (Figure 2.4) to heat the material during machining (Sanchez et al., 2014). In this process

the workpiece is heated by using electric current flow for various machining processes such as drilling, milling, turning etc. There is no temperature rise in the machined surfaces. The drawback of this technique is that initial cost of the equipment is high.

2.5.3 Plasma heating

Plasma arc heating is another pre heating technique used to heat the workpiece material as shown in Figure 2.5. In this process the temperature developed in the machine zone is very high at around 16000 ^{o}C to 30000 ^{o}C. The flow of the gas in plasma arc heating is very high and is able to support low voltage and high electric arc current. This technique is suitable for high production rates, but works effectively in interrupted machining method. The main disadvantage of this technique is that cost of the equipment is high, plasma arc heating is mainly suitable for low permeability materials, and the temperature can be easily adjustable and due to high temperature at the machining zone the structure/metallurgical damage of the workpiece.
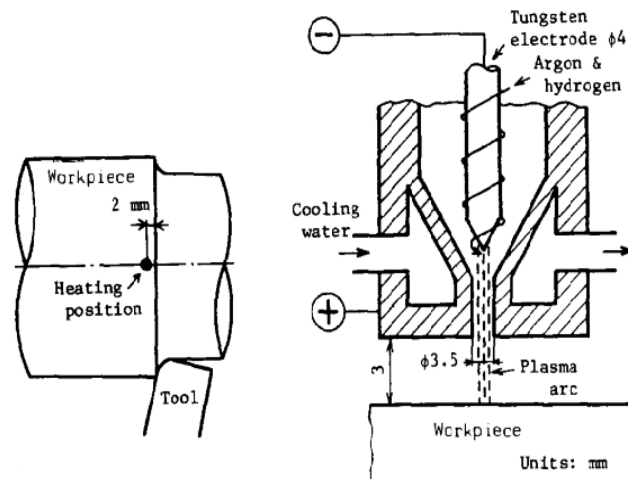
Figure 2.5 Plasma heating experimental setup

2.5.4 Laser assisted machining (LAM)

Laser assisted machining is most widely used technique before the invention of flame heating here the workpiece is heated using laser beam on to the specific region. In LAM

is normally used in conventional turning, milling and drilling process. A high energy laser beam directly focused in to the workpiece just near to the tool work interface. Due to this laser beam the workpiece becomes softens the primary shear zone of the material. The main drawback of this technique is during machining the surface of the workpiece will melt (Konig and Zaboklicki, 1994). The high amount of heat added by the laser can damage the microstructure of the workpiece, which may sometimes require finish operation (Chryssolouris and Anifantis, 1994). Moreover, there are subsurface cracks with effects the surface integrity of the workpiece. Due to this limitation the usage of laser assisted machining for producing simple parts like slurry pumps made by high chrome white cast iron (Masood et al., 2011).

Nowadays, many innovative techniques have been developed to widen the applications of the laser assisted machining. Among them, one application is CO_2 laser to cut the ceramic materials like silicon nitride and metal alloys with minimum cost (Konig and Zaboklicki, 1994, Madhavulu., 1994, Chryssolouris and Anifantis., 1994). Several researchers have adopted this heating technique to soften the workpiece material. Rozzi et al., (2000) performed experiments using silicon nitride ceramic using laser heating and found that due to softening of the stock material a reduction of magnitude of cutting forces. They reported that strength of material permits visco-elastic flow this leads to reduce the friction between tool work and chip. They confirm that 93% of energy is added by laser beam and remaining is generated during cutting process.
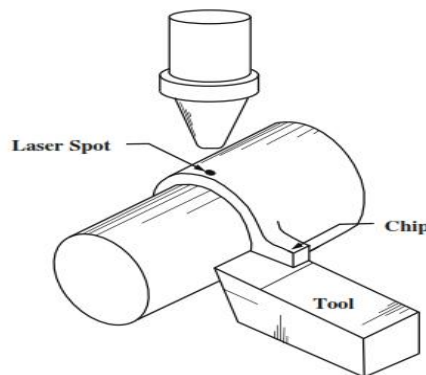
Figure 2.6 Laser assisted machining experimental setup (Sun et al., 2010)

Germain et al., (2011) performed laser assisted machining on 42CrMo4 steel and they reported that due to high temperatures generated within the shear zone would reduce the shear stress and hence cutting force is reduced about 40% and residual stresses. In a similar kind of work, Ding and Shin. (2010) developed a three dimensional transient model to study the temperature distribution of hallow shaft of varying thickness by laser turning. They investigated the effect on surface integrity, microhardness, microstructure and residual stresses. Their experimental results reveal that good surface finish of Ra (< 0.3μm), uniform surface hardness and no microstructure change. Patrick et al. (2002) adopted the LAM of pressureless sintered mullite ceramics with the application of laser power and they studied on cutting force, surface temperature, chip morphology, tool wear, surface roughness and subsurface damage for a variety of operating conditions.

Masood et al. (2011) studied machinability on high chrome white cast iron using CBN cutting tool by adopting laser heating and concluded that reduction of cutting forces by 24 % and thrust force by 22 %. Attia et al., (2010) adopted laser assisted high speed machining of Inconel 718 by using (SiAlON) ceramic tool and their results shows that at optimum machining conditions metal removal rate is increased by eight times and the significant improvement in surface finish and tool life by comparing conventional machining. There has been very less amount of research work conducted on LAM of Inconel 718 super alloy and there is no detailed work on machinability and material characterization using flame assisted machining.

Limitations of preheating methods

There are some drawbacks in the heating methods which opens the window for further investigations on hot machining, this technique is successfully implemented in the industries, by using electrical heating of intricate designs, in electrical heating consumption of power is very high, but mechanical damage of the workpiece is due to high temperature arc is the main issue in the case of plasma arc heating.

Several researchers are reported the drawbacks of the laser assisted machining method while solving hard turning problems (Masood et al., 2011). The major drawbacks of this method are as follows:

➢ The cutting speeds used in the industry are twice their cutting speed (50 m/min) due to this the penetration of the heat is drastically reduces, which is normally happen at higher depth of cut.

➢ Minimizing the cutting speed may improve the depth of heat penetration, but it results in increased machining time. Any demand to use very high power laser may prove to be uneconomical (Masood et al., 2011; Ding and Shin, 2010)

➢ LAM requires high safety precautions before applying to the workpiece. The laser beam is harmful when viewed in the naked eye, but it requires appropriate shielding.

➢ The reflections of the laser beam may be hazardous to nearby equipments and machineries as discovered by Konig and Zaboklicki. (1994). Incorrect distance setting between the laser and the tool may reflect the laser beam towards the operator or back onto the lens of the equipment (Masood et al. 2011).

From these limitations researchers has to think for another alternate preheating technique. Among all the techniques, flame heating method appears to be an attractive alternate method for its simple design. This technique requires high power industrial lathe machine, and the workpiece material requires uniform hardness and microstructure.

2.5.5 Flame heating

In flame heating method, the workpiece is heated by a continuous flame that is produced by burning proportions of oxygen- liquid petroleum gas (LPG) or oxygen-acetylene. Among, the two oxy-acetylene is widely used, it is found to be the better alternative of TEM process. The design and setup of oxy-acetylene flame heating is

very simple. Figure 2.7 shows the flame heating setup and the torch is placed near to the workpiece.
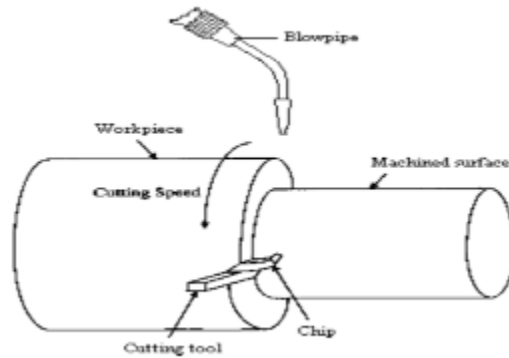
Figure 2.7 Flame heating experimental setup

Advantages of oxy-acetylene gas over other gases

The following are some of the advantages of oxy-acetylene gas over other gases

- ➢ Higher flame temperature than other fuel gases
- ➢ Heats as fast as other gases- superior heating value (neutral flame temperature, inner and outer flame temperature) transfer of heat to the metal is very fast (Choudhury 2010).
- ➢ Safer and operators friendly: non toxic and no back fire
- ➢ No sensitive to shock and has low explosive range.
- ➢ Less cost compare to other gases

Only few researchers have adopted this heating method to soften the workpiece material. Thandra and Choudhury (2010) performed experiments on EN 26 steel with the assistance of oxy-acetylene flame heating. The regression equation has been developed to know the effect of cutting speed, feed rate and depth of cut on cutting forces, surface roughness and tool flank wear. The results confirm that cutting forces, surface roughness and flank wear about 34 % compare to conventional machining.

Bermingham et al. (2012) performed machinability studies on Ti-6Al-4V with two different tool geometry using Oxy-acetylene flame heating. They found that TAM reduces the cutting forces, and this process has significant effect on tool life and dominant wear mechanisms associated with diffusion wear. At 350 $^{\circ}$C shortest tool life has been noticed and at 150 $^{\circ}$C and 250 $^{\circ}$C the tool life has slightly improved up to a maximum of 7 %.

The literature review reported many constraints in the LAM, Plasma and Electrical heating methods, and significant advantages in flame heating technique. Therefore flame heating technique has been selected for the present research work to investigate the machinability characteristics of Inconel 718.

Selection of preheating temperatures

Selection of preheating temperature of the workpiece material is the major issue in flame heating method. Generally, temperature of the material depends on yield strength, microstructure, especially recrystallization temperature, cutting tool geometry, and other constraints in the experimental setup (Ding and Shin, 2010). Many researchers used preheating temperatures are listed in the Table 2.1. Ozler et al. (2001) performed experiments on austenitic manganese steel using Oxy-LPG flame heating the maximum surface temperature is 600 $^{\circ}$C. Whereas, the optimum experimental results obtained at 400 $^{\circ}$C. Bermingham et al. (2012) conducted experiments using oxy-acetylene heating on Ti-6Al-4V, the surface temperature used in the range of 150 $^{\circ}$C to 350 $^{\circ}$C. But, the best tool life has been reported in the range of 150 $^{\circ}$C to 250 $^{\circ}$C. Lajis et al. (2009) kept the preheat temperature range at 250 $^{\circ}$C to 450 $^{\circ}$C to machine the hardened AISI D2 steel using coated carbide tool, and observed the best results at 336 $^{\circ}$C.

As per the literature review, and constraints of the equipment, the material properties of Inconel 718. The preheating temperature selected for the present research work in the range of 200 $^{\circ}$C to 600 $^{\circ}$C

2.6 CUTTING FORCES

The forces acting on cutting tool are the important aspect in hot machining. The knowledge of cutting forces in very important to estimate the power required and ensures the required cutting tool geometry, tool-holders and fixtures are effectively rigid and vibrations free. The overview of cutting forces, surface roughness and tool wear are shown in Table 2.1.

Many researchers have reported that cutting forces are subjected to number of factors such as machine tool, cutting parameters, hardness of the workpiece, cutting time and tool geometry (Ozler, 2004; Taylor et al., 2007). Chen (2000) investigated that when machining high hardened steel (55- 65 HRC) with CBN cutting tool, among all the three cutting forces they observed that radial force has largest cutting force. Lima et al. (2005) reported that as the cutting speed increases the three cutting forces namely radial force, tangential force and axial force are decreasing. The reason might be as the cutting speed increases, the temperature generated at the cutting zone increases leads to increase in the shear plan area, resulting reduction in the shear strength of the material. Many authors reported the same results (Sanchez et al., 2014; Thandra and Choudhury, 2010). Bermingham et al. (2012) reported that by thermally enhanced machining of Ti-6Al-4V with two different tool geometry such as CNMX tool with 45 ^{o}C entry angle and WNMG with 95 ^{o}C entry angle and they observed that 45 ^{o}C experiences lower cutting force than 95 ^{o}C. And at CNMX tool has higher thrust force and lower feed force than WNMG tool. The temperature of the workpiece plays a significant effect on cutting forces, with increase in preheating temperature at 350 ^{o}C the cutting forces is decreasing drastically up to 30%.

Thandra and Choudhury (2010) investigated with both conventional as well as hot machining with EN-21 as workpiece and tungsten carbide as cutting tool and reported that the cutting forces in hot machining is less compared to conventional machining the reason might be as the temperature of the material increases the shear strength of the material decreases and the machinability improves by heating.

25

Sanchez et al. (2014) conducted experiments with conventional, cutting fluid and hot machining of quartz resistance electric current of 500 W to heat the (sae xev—f) steel machined with triple layer coating cutting tool $TiCN/Al_2O_3/TiN$ and observed that the lowest cutting forces were reached at hot machining due to low tool wear. The highest cutting forces were noticed at cutting fluid which cools the primary shear zone and increase shear resistance. But, due to cutting fluid the tool wear is less than conventional machining. Xi et al. (2014) to study the chip formation and cutting forces, Smoothed particle hydrodynamics (SPH) method was employed with both 2D and 3D models to study the TAM of Ti-6Al-4V. The simulation results reveals that cutting forces predicted by machining models showed excellent correlation between the experimental data and both simulation results and the experimental results shows that as the temperature of the workpiece increases will significantly decrease the cutting forces.

Ravi et al. (2014) conducted experiments with oxy-LPG gas heating with high chrome white cast iron (HCWCI) high manganese steel machining with CBN cutting tool and found that the main cutting force decreases with increase in cutting speed and surface temperature. From all the control parameters depth of cut and surface temperature has significant effect on cutting force. The optimal cutting parameters for cutting force were cutting speed at 132 m/min, depth of cut at 0.1 mm, feed rate at 0.096 mm/rev, and workpiece temperature at 450^oC. Maity and Swain (2007) found that at 350 ^{o}C the thrust force and cutting force increases with increase in feed. The non dimensional cutting force is higher than non dimensional thrust force which shows a normal machining operation.

Hot machining experiments conducted by Kitagawa et al. (1990) plasma heating with different workpiece materials such as Pyrex, Mullet, Zirconia, silicon nitride and high speed steel and three different cutting tools CBN, Sintered diamond tool, and cemented carbide tools were used depend on the workpiece material. The experimental results shows that when machining of Pyrex and Mullet the cutting forces decreases as the temperature increases. Cutting forces increases with increase in temperature while

machining with alumina and also there is no change in chip formation. The total workpiece was broken when the temperature reached to 700 ^{o}C. While machining with zirconium the cutting forces decreases with increase in temperature the chip changes from powder form to transition type. Feyzi and Safavi (2013) conducted experiments on hybrid machining and conventional machining of Inconel 718 and they reported that all the cutting force components of hybrid machining is reduced by 9 – 14 % than conventional machining of all the cutting speeds. And also in both the methods thrust force has highest among all the components followed by axial force and tangential force.

2.7 TOOL WEAR AND TOOL LIFE

Tool wear and tool life are very essential aspects of hot machining as tool wear causes white layer formation and tensile residual stresses on the machined surface. In hot machining, less cutting forces, high hardness of the material, and high temperatures generated at the tool-work interface leads to thermal softening of the workpiece causes less tool wear and resistance of the tool increases. Generally different type of tool wear mechanisms observed in hot machining such as abrasive, adhesive, and diffusion wear. But, tool wear is depend on various factors such as tool geometry, tool material and cutting parameters.

Many researchers carried different investigations to study the performance of uncoated, coated, ceramic and CBN tools during hot machining of difficult to cut materials. When machining with EN-21 steel by tungsten carbide tool with both conventional as well as hot machining as the cutting speed increases the tool flank wear decreases the reason might be during heating the shear strength of the workpiece material decrease at the cutting zone, leading to reduction of forces and flank wear. However, during heating workpiece becomes soft and friction between tool and chip reduces. The percentage improvement with conventional over hot machining is around 33.95 % (Thandra and Choudhury, 2010). Ozler et al. (2001) conducted experiments with oxy-LPG flame heating on austenite manganese steel. The experimental results reported that at low cutting speed 22 m/min longest tool life was observed the probable reason is reduction in

Table 2.1 Overview of cutting forces, surface roughness and tool wear on hot machining.

Ref.No	Material	Process	Cutting speed (m/min)	Feed rate (mm/rev)	Depth of cut (mm)	W/P temperature (^oC)	Machinability Characteristics
Ranganathan et al. (2011)	stainless steel (type 316)	Hot Turning	29.68,73.04,113.1	0.25,0.376, 0.381.	0.4,0.8,1.	200, 400, 600.	Surface roughness, tool life, MRR.
Thandra and Choudhury (2010)	EN-24	Hot Turning	400 to 1260 rpm	0.1 to 0.25	0.5 to 0.9	200, 400, 600.	Cutting Forces, Surface Roughness, Flank Wear
Maitya et al. (2008)	High manganese steel	Hot Turning	21, 43.	0.05, 0.7	0.5, 1.5.	200, 600.	Tool life.
Tosun and Ozler 2004	High manganese steel	Hot Turning	22, 46, 75.	0.1, 0.2, 0.4.	0.5, 1.5, 2.5.	200, 400, 600.	Surface Roughness, Tool Life.
Tosun and Ozler (2002)	High manganese steel	Hot Turning	22 to 75.	0.1	1.5	200, 400, 600.	Tool Life.
Ozler et al. (2001)	austenitic manganese steel	Hot Turning	22, 33, 46, 62, 75.	0.005, 0.1, 0.2, 0.4.	0.5, 1.5, 2.5.	200, 400, 600.	Tool Life.
Ranganathan et al. (2010)	Stainless steel (Type 316)	Hot Turning	29.68,73.04,113.1	0.25,0.376, 0.381.	0.4,0.8,1.	200, 400, 600.	Surface Roughness

Author	Material	Process	Speed	Feed	Depth	Temp	Output parameters
Dabade et al. (2016)	Al/SiCp type MMC	Hot Turning	25,50.75, 100.	0.05,0.1,0.15,0.2	0.4,0.6,0.8,1.	60,80,100.	Cutting Forces, Surface Roughness, Microhardness
Sanchez et al. (2014)	sae xev-f steel	Hot Turning	109,139, 176,216	0.232	0.5	230	Cutting forces, surface roughness,tool life, micro hardness, chipmorphology
Ravi et al. (2014)	High chrome white cast iron	Hot Turning	53,84,132	0.096,0.124,0.179	0.1,0.2,0.3	200,325,450	Cutting forces, surface roughness,tool wear.
Upadhay et al. (2013)	Ti-6Al-4V	Hot Turning	70	0.2	1.5	200,300,400, 500	Cutting forces, surface roughness,Flank wear,Chip analysis.
Bermingham et al. (2012)	Ti-6Al-4V	Hot Turning	50-145, 45-150.	0.1-0.3, 0.07-0.23.	0.5-3.0,0.8-6	150,250,350	Cutting forces, Flank wear.
Lajis et al. (2012)	AISI D2	Hot Milling	40-80.	0.02-0.044.	1	30-450	Surface Integrity, workhardening, Microhardness.
Baili et al. (2011)	Ti-5553	Hot Turning	35	0.15	3	300-640	Cutting forces, Surface Integrity, Tool wear, Chip Morphology
Davami et al. (2008)	AISI 1060	Hot Turning	35	0.08	1.5	180-200	Surface roughness
Madhavulu et al.(1994)	SS 410, Alloy steel,	Hot Turning	29	0.75	5		MRR, Tool life
Kitagawa et al. (1990)	High speed steel	Hot Turning	10	0.05	0.2	700,800.00	Cutting forces, surface roughness, Tool wear, chip morphology

the resistance of chip tool interface as a result decrease in size of the tool chip interface. And also noticed that as the feed rate increases corresponding decreases in the tool life the reason might be inefficient transfer of heat at the machining zone during hot machining, because shear strength of the workpiece was not reached at high feed rate. Depth of cut has very less significant on tool wear, a minimal decrease of tool wear were observed. Bermingham et al. (2012) performed experiments on Ti-6Al-4V with two different uncoated carbide tools.

According to Sanchez et al. (2014) investigated with three different methods like conventional, hot machining by quartz electrical resistance of 500 W, and cutting fluids on sae-xev-f steel with $TiCN/Al_2O_3/TiN$ coated tool. They reported that at cutting speeds 109, 139, 176 and 219 m/min a meaning full improvement in hot machining over conventional machining. Cutting speeds at 109, 139, 176 and 219 m/min the corresponding improvement were 80, 117, 200 and 340% the reason might be yield strength of the material decreases by heating, even which in inferior temperature to the one necessary for micro structural changing, shear resistance of the workpiece material reduces leading to increase in tool life. In hot machining tool life produced is high over conventional machining and it decreases when feed rate increases at low feed rates the tool life is improved by 80 % and at intermediate feed rate around 150 %. But, at higher feed rate it is moderate to 40 % than conventional machining. Among all the machining conditions hot machining shows better performance than cutting fluid, this method is considered better for human health and environment.

2.8 SURFACE INTEGRITY

The machined quality surface becomes the significant in view and high demand for safety, performance, reliability, preventive, life cycle cost and reliability of the products. The machined components used in aerospace, marine, automotive, gas turbines and other industries are subjected to high thermal stress and temperature. Hence, surface integrity plays an important role which affected by hot machining conditions and indicates the machined surface and subsurface properties. Surface integrity consisting of (a) surface

30

roughness; (b) surface morphology; (c) Microhardness; (d) Recast or white layer formation; (e) Residual stresses (Rech and Moisan, 2003) Thermally assisted machining is known for better surface integrity and high production rate. Nowadays this technique is rapidly growing in manufacturing industries. The surface produced in hot machining is comparatively less affected by the phenomena such as cracks, defects, phase transformation, work hardened layer, residual stresses compared to conventional machining.

The machined products having good surface quality are lot of demand for majority of applications. Surface integrity shows the quality of machined surface and it sub surfaces. Surface textures of the machined surface are expressed in terms of roughness and waviness. The surface changes have occurred during machining are the surface hardness and other mechanical properties. This modifications is due to metallurgical changes, microstructure, grain size, residual stresses, phase transformation contributes to the machines surface performance of the product. Several researchers have been studied on surface integrity of the hot machined components. Some brief discussions are reported in the following sections.

2.9 SURFACE ROUGHNESS

Surface roughness is the major parameter to estimate the performance of the machined components, further depending upon type of contact, friction, accuracy and deformation. There are lots of machining parameters which quantify the surface roughness such as amplitude parameters that characterizes the surface topography. The surface deviation is most commonly used parameter as the arithmetic mean average roughness. The selection of hot machining parameters is an important criterion to get better surface for the workpiece material. Some of the authors reported that surface roughness is mainly depending on the cutting speed and feed rate.

Attia et al. (2010) investigates the high speed machinability using laser assisted machining on Inconel 718 by (SiAlON) ceramic tool. The experimental results revels

that surface roughness is improved by 25%. Leshock et al. (2001) performed experiments on Inconel 718 using plasma enhanced machining and they observed improvement of surface roughness by varying surface temperature in the range of 200 $^{\circ}$C to 700 $^{\circ}$C at different cutting speeds of 2, 3.5, 5.5 and 6.5 m/sec. From all the cases surface roughness was improved up to surface temperature 500 $^{\circ}$C. Beyond 530 $^{\circ}$C surface oxidation was observed, which leads to poor surface finish. The oxidation effect can be controlled by accurate control of plasma arc.

Dabade and Jadhav (2016) conducted experiments on Al/SiC particulate metal matrix composites with PVD coated carbide inserts by hot machining process. The experimental results reported that feed rate and pre heating temperature is significantly affecting the surface roughness. The micro hardness near to the machined surface is high and then gradually decreasing. Sanchez et al. (2014) reported that in hot machining lower surface roughness values preserves the cutting tool geometry especially at severe machining conditions.
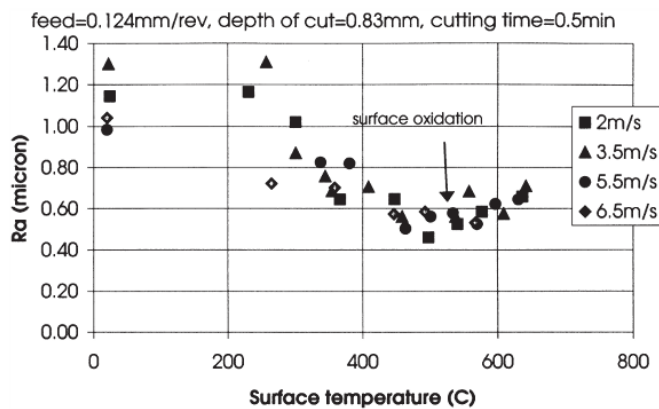
Figure 2.8 Surface roughness vs surface temperature at different speeds (Leshock et al., 2001)

In the hot machining experiments conducted by Ravi et al. (2014) machining of difficult to cut materials like HCWCI of thermally assisted machining (TEM) the ANOVA results shows that feed rate has significant effect on surface roughness and the optimum surface roughness were obtained at speed at 84 m/min, feed rate at 0.096 mm/rev, depth of cut at

0.1 mm and workpiece temperature at 350°C. Ranganathan and Senthilvelan (2011) performed hot machining experiments on stainless steel (316) with tungsten carbide insert and reported that cutting speed at 131.1 m/min, feed rate at 0.381 mm/rev, and workpiece temperature at 400 ^{o}C are the optimum process parameters.

Thandra and Choudhury (2010) investigated the hot machining performance of EN 21 steel with tungsten carbide tool. Conducted experiments with both conventional as well as hot machining, the experimental results reported that compared to conventional machining surface roughness of hot machining is giving better performance the probable reason might be explained in to three steps (i) While heating decrease of chatter vibrations with the decrease of cutting force (ii) discontinuous type of chips to continuous type (iii) the absence of built up edge formation.

2.10 SURFACE TOPOGRAPHY
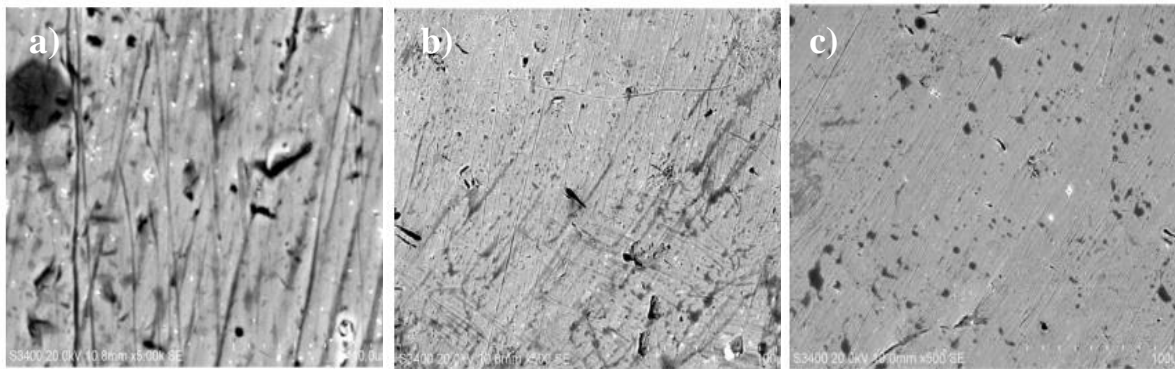
Figure 2.9 The SEM micrographs of surface texture at a) 200 ^{o}C b) 400 ^{o}C and c) 600 ^{o}C during hot machining of 316 SS (Ranganathan et al. 2010)

The surface texture is formed on the machined surface is mainly depends on the machining conditions, mechanical properties and the workpiece material. This connection is more evident in some materials and under machining operation. The surface texture as observed in Figure 2.9 It is varied with different temperatures. At 200 ^{o}C and 400 ^{o}C surface temperatures it is observed that the surface has non uniform and at 600 ^{o}C the surface obtained yields better surface finish compared with other

33

temperatures. This is due to working temperature towards recrystallization temperature. The higher temperature is desirable for uniform surface (Ranganathan et al., 2010). The hot machining gives the less surface roughness values and conserve the cutting tool geometry, particularly in more severe machining conditions (Sanchez et al., 2014)

2.11 SURFACE METALLURGY

During hot machining, the surface of the workpiece will affect the thermal and mechanical energy. Surface metallurgy is the metallurgical changes occurred at near the machined surface. Due to several reasons can be recognized to poor surface integrity, including, phase transformation, subsurface plastic deformation, residual stresses distribution, thermal softening or hardening, micro as well as macro cracks, intergranular attack, recrystallization. Some other surface integrity problems include cracks on the surface, machining burns, lower fatigue strength of parts residual stresses and stress corrosion (García et al., 2013). Some researchers are studied the metallurgical aspects of hot machining (Sanchez et al., 2014) under conventional and hot machining. From the Figure 2.10 it was observed that, hot machining condition the structure suffered the plastic deformation in the outer surface, due to high temperature was able to reduce the yield strength and also subsurface layer formed with elongated grains which were deformed in hot machining, but in conventional machining it was not present in the same intensity.
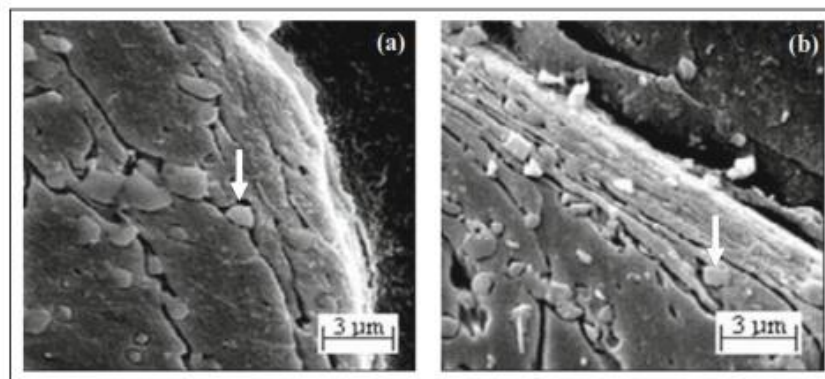
Figure 2.10 Microstructure obtained a) conventional b) hot machining (luiz et al., 2014)

34

2.12 MACHINED SURFACE HARDNESS

During hot turning with different surface temperatures, thermal softening of the workpiece material is very rapid and causes recast layer on the machined surface. This recast layer appears below the presence of heat affected zone may be observed. The machined surface the hardness is varying in hot machining with different temperatures and workpiece material. Hardness of the machined surface increases to certain depth up to 100 μm. Then further increase the depth of the measurement, surface hardness value remains constant as the normal hardness of the material.
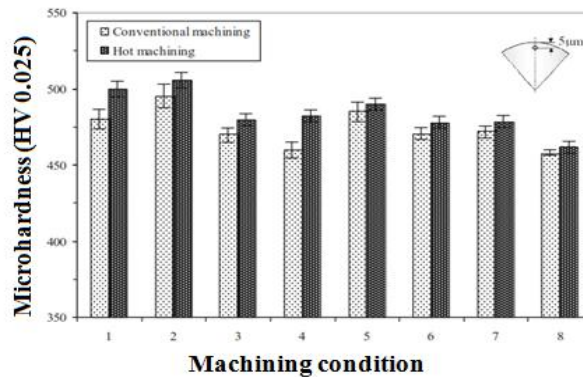
Figure 2.11 Microhardness of the workpiece subsurface layer at 5μm depth (Sanchez et al. 2014)

In the hot machining due to high temperatures generated at the machining zone the formation of oxides and carbides appears on the machined surface is common. From the Figure 2.11 it was observed that the hardness values are slightly higher in hot machining compared to conventional machining. The reason might be small strain hardening of the workpiece outer layer produced by heating and the following passage of the cutting tool. If the workpiece is not cooled in the hot machining there is a tendency towards the formation of compressive residual stresses into plastically deformed layer (Sanchez et al.,2014). Zhuang et al. (2015) plasma pre heating condition on Inconel 718 the hardness test performed with two machining conditions with load of 20gf. The micro hardness of machined surface varies with different machining conditions the plastic deformation

takes place and also depth of work hardening varies different machining conditions. From the Figure 2.12 it can observe that in dry cutting depth of hardness reached more than 0.4 mm, but in plasma preheating condition the depth of preheating is less than 0.3mm.
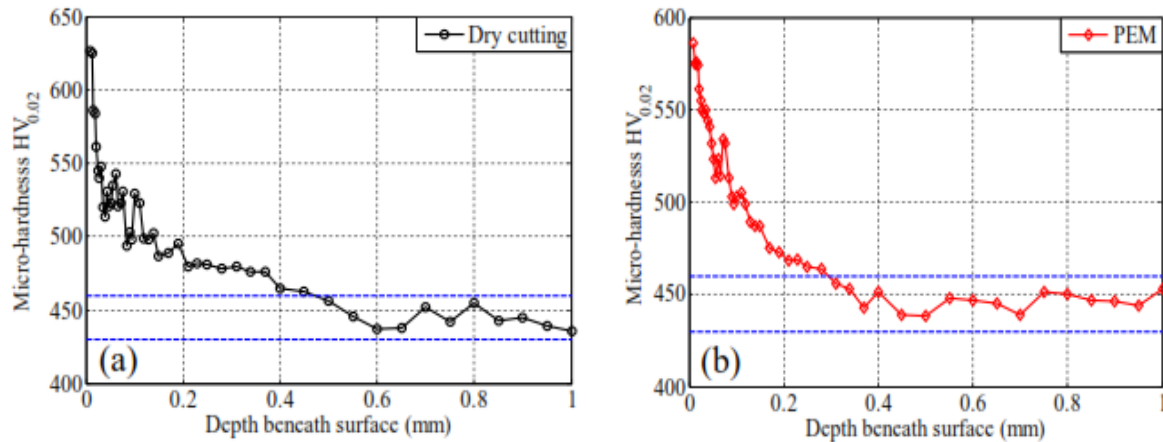
Figure 2.12 Microhardness beneath the surface under a) Dry cutting b) Plasma enhanced machining (v = 150 m/min) (Zhuang et al. 2015)

2.13 CHIP FORMATION MECHANISM

In hot machining metal removal process, chips produced as a result of workpiece shearing. The chip mechanism in hot machining is quite different from other machining processes. Here two types of segmented chips are normally observed. In hot machining serrated/ saw toothed chips, twisted and straight continuous chips are formed. Due to these chips some interrelated mechanism such as adiabatic shear, localized shear and catastrophic shear in the form of cracks (Komanduri and Brown, 1981). The chip morphology depends on various factors like thermo-mechanical properties of the workpiece material. Input parameters of the cutting condition, interaction between primary and secondary zone, divergence of shearing in the shear zone, dynamic response of the machine tool structure all these are influence for the chip formation (Poulachon and Moisan, 2000). Different stages of chip formation are shown in Figure 2.13. The first stage of the chip mechanism, due to negative rake angle, the compressive stresses

distributed around the cutting tool. The cutting tool and the free surface of the workpiece, the combined effect of low compressive stresses and high shear stresses leads to crack formation. The crack is followed by a slip plane, which runs towards the cutting edge. The second stage of chip formation is observed between the crack and the edge chamfer where chip comes outside without any deformation. In the third stage plastic deformation of the chip is very high, the gap crack initiation line and the cutting tool chamfer is so narrow the ejection of chip is very fast, at this time the chip thickness is reduces and chip cooling is very fast. The final stage shows the formation of the chip is closed.
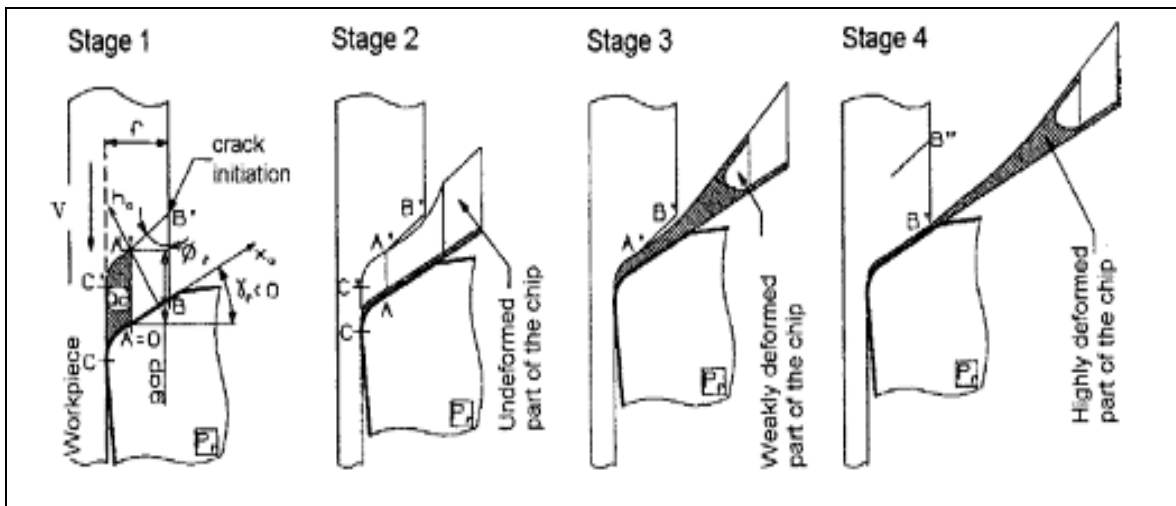
Figure 2.13 Different stages of chip formation in machining (Poulachon and Moisan, 2000).

Attia et al. (2010) observed that continuous ribbon like chips while laser assisted machining of Inconel 718**.** This tendency is due to thermal softening effect of LAM, shear localization and large strains in primary shear zone. The cutting speed increases shows thinner chips i.e lower strain because speed increases, cutting temperature increases the absorption of the heat from the laser source reduces. Further, as the cutting speed increases above 300 m/min, the temperature level (650-700 ^{o}C) significant thermal softening effect is not reached. The undeformed and saw tooth chips is attributed at this cutting condition as shown in Figure 2.14. Sanchez et al. (2014) observed that chips

37

produced are continuous lamella type in hot machining is higher than conventional machining as shown in Figure 2.15 Energy required for plastic deformation of the layer being removed in to conversion into chips is lower in hot machining than conventional machining. The formation of the chip mainly depends on the workpiece material and the cutting speed.
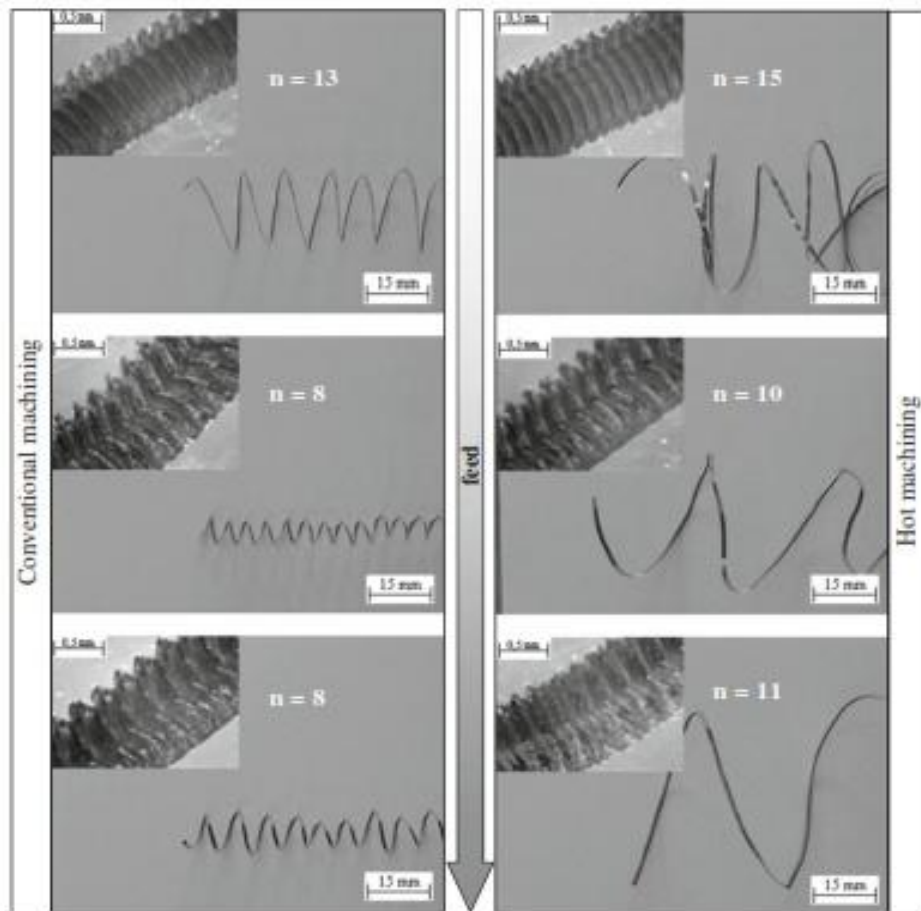
Figure 2.14 Chips produced in conventional and hot machining under different feeds (Sanchez et al., 2014)
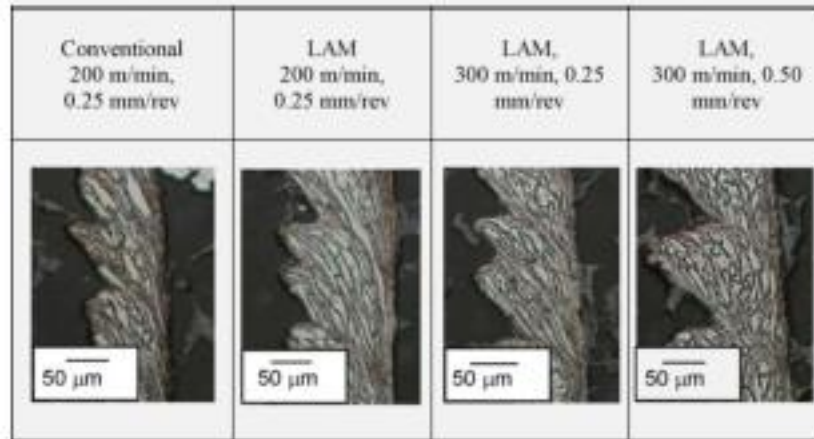
Figure 2.15 Effect of cutting conditions on chip morphology (Attia et al., 2010)

Upadhyay et al. (2012) experimentally investigated the chip formation in machining of Ti-6Al-4V with different surface temperatures. At without preheating condition the chip back surface roughness was found to be highest, as the surface temperature increases the chip back surface roughness is reducing. This is because as the surface temperature increases the workpiece material becomes softer and softer and the number of asperities on the chip during flow over the cutting tool face.

2.14 RESIDUAL STRESS

Life of the machined product significantly depends on the residual stress present in it. In metal cutting processes, the range of residual stress developments are depends on the temperatures developed during machining. On the other way, the quantity and type of residual stress is mainly depends on the type of cutting insert, type of workpiece material, tool geometry, cutting parameters and machining environment respectively. Inconel 718 is one of the hard materials and conventional machining of this kind of materials develops more cutting zone temperatures during machining process due to more friction between the tool-workpiece interfaces respectively. There are two types of residual profiles are available

1) Compressive residual stress

2) Tensile residual stress

In general, compressive residual stresses are favorable to the product life and tensile stresses are not desirable. During machining with fresh insert, at initial stages, the expected stresses are compressive at the surface and subsurface. Afterwards as tool wear progress, the tensile stresses are expected. There are five main factors that could drastically affect the residual stress distribution in finish machining (Liu et al. 2011, Sharman et al. 2006).

- Insert grade
- Tool geometry, including nose radius and edge preparation (chamfer angle and length, hone radius)
- Machining parameters such as cutting speed, feed rate and depth of cut
- Tools wear development
- Hardness and chemical composition of workpiece material

Residual stresses in high performance alloys are of considerable industrial importance because they can affect failure by fatigue, creep or cracking (Lee and Mathew, 2007) few researchers are reported that the residual stresses distribution in Inconel 718.
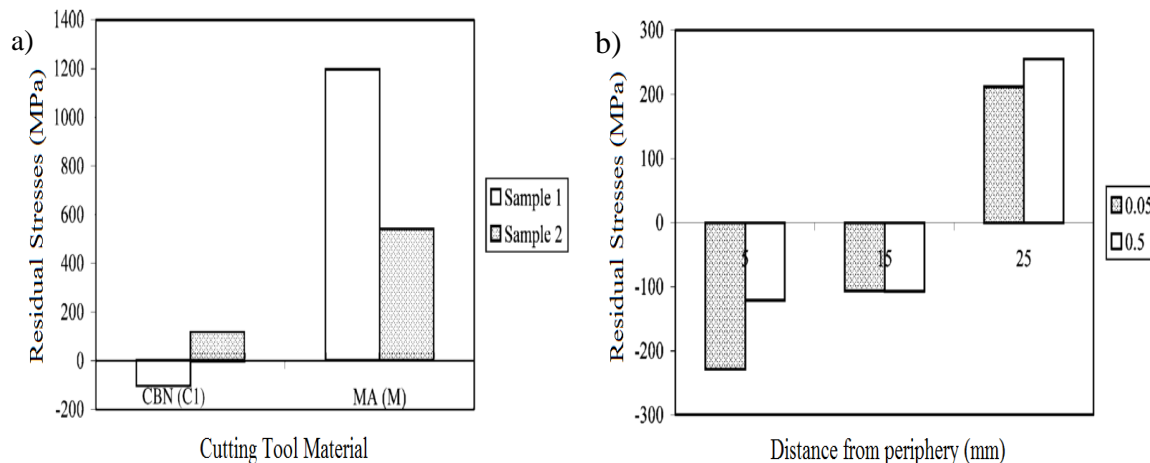
Figure 2.16 a) Comparison of CBN and ceramic tools on residual stresses b) Comparison of CBN tools of round and square shape on residual stresses (Arunachalam et al., 2004)

40
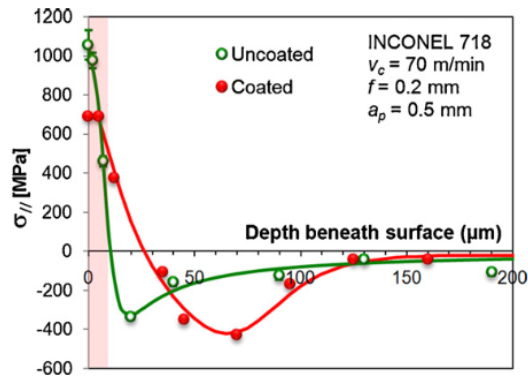
Figure 2.17 Residual stresses distribution in the machining of Inconel 718 (Outeiro et al. 2008)

Anderson et al. (2006) conducted experiments with LAM of Inconel 718, the residual stresses were about 200-300 MPa in the hoop direction and -90 to -220 MPa in the axial direction. In the axial direction, compressive axial stresses which indicate that LAM does not give any affect on the resultant subsurface.

The residual stresses were measured with both CBN and mixed alumina ceramic inserts of round shape from the Figure 2.16. It was observed that machining with ceramic tools causing much higher values of tensile residual stresses compared to CBN tools. Because due to poor thermal conductivity of ceramic tools which causes higher values of residual stresses due to dominance of thermal effect. In CBN tools the thermal conductivity is quite high this leads to lower values of residual stresses. From the Figure 2.17 Two different geometries of round and square shape CBN cutting tools at 5, 15 and 25 mm from the periphery. It was observed that round type insert showing compressive residual stresses up to 15 mm from the periphery where as square type insert showing only tensile residual stresses from the beginning of machining. The one to one comparison cannot do because the cutting edge was different from the two inserts (Arunachalam et al., 2004). Figure 2.17 shows the residual stresses induced by uncoated and coated cutting tools. Residual stresses are tensile at the machined surface and gradually shifted to compressive stresses with both the tools. At the near machined surface the tensile residual stresses

are very high about 1000 MPa with coated carbide tools lower residual stresses were observed on the sub-surface (Outeiro et al., 2008)

2.15 RECAST OR WHITE LAYER FORMATION

White layer is a hardest material, can observed at the subsurface level of the machined surface. It can propagate the cracks rapidly compared to bulk material. White layer thickness on the machined surface depends on the tool tip contact nature. On the other hand, it is depends on the type of machining environment, type cutting tool, tool geometry and hardness of the workpiece material respectively. White layer thickness is not a desirable surface quality characteristic. The formation of white layer thickness may leads to development of more tensile residual stresses, resulting product failure occurs (Ding and Shin, 2010; Jiang et al., 2006; Ezugwu et al., 1999) The characteristics of such layers appear to vary considerably in structure and thickness (few microns) depending on the operating machining conditions suggesting different possible mechanisms.

- Mechanical grain refinement due to severe plastic deformation
- Thermally-induced phase transformation due to rapid heating and cooling.
- Surface reaction with the environment such as carburizing, nitriding, oxide Ploughing.

2.16 MATHEMATICAL MODELING

Optimization techniques are popularly used for different engineering problems and industrial fields and many real world issues. Optimization is the thing to get the best results for a given issue under given environment. An optimization is performed by using different algorithms to find an optimal solution. The obtained mathematical equation describes exact relationship between decisions, constraints and objectives. The suitable algorithm has to be used to get the proper solution. Some researchers used different optimization algorithms to optimize the input parameters to acquire the best results, and are represented in the following sections. The researchers carried out

different studies (Ozler, 2004; Thandra and Choudhury, 2010; Ranganathan et al., 2010; Ravi et al., 2014; Xu et al., 2013) are used to study the experimental results with different modeling techniques, and finally they are developing a mathematical regression equation for the output responses with input parameters. There are many optimization techniques such as Taguchi design, artificial neural networks (ANN), response surface methodology (RSM), particle swarm optimization (PSO), fuzzy logic etc. The thermal related FEM models like CFD, Ansys, Deform 3D, LS Dyna and so on are to analyze the cutting forces, surface roughness, tool wear, residual stresses, white layer with the combination of input parameters with certain constraints (Xu et al., 2013; Xi et al., 2014). These techniques give good results from the experimental values with very less errors. Few researchers attempted for turning/hot turning on real time evaluation and online cutting forces. Xi et al. (2014) analyzed the cutting forces and chip formation mechanism in thermally assisted machining using 3D and 2D models.

Optimize the process parameters of hot turning for different materials by design of experiments, which is reported in Table 2.2. Several researchers have adopted multi objective optimization (Ranganathan and Senthilvelan, 2011) to optimize the output parameters such as surface roughness, tool wear and metal removal rate by using Taguchi based grey relation analysis, full factorial design and response surface methodology based regression mathematical models are developed. Ranganathan et al. (2010) reported that surface roughness of hot turning parameters can be optimized by using response surface methodology based artificial neural networks. The experimental results revels that surface roughness produced at 200 $^\circ$C was poor and when temperature raised between 400 $^\circ$C and 600 $^\circ$C the surface roughness improved to satisfactory limit.

Furthermore, the authors are using different optimization techniques to predict the cutting forces, surface roughness, tool wear and MRR in thermally assisted machining as shown in Table 2.2. Finite element method is used to simulate the results without performing the number of experiments. The researchers were used to evaluate and predict the cutting forces, cutting temperature and residual stresses appeared in the hot machined surface.

The finite element simulation is also used to avoid the tool cracking (Xu et al., 2013). The white layer formation, surface roughness in the thermally enhanced machining was predicted by using central composite design experimentation (Ravi et al., 2014).

In the Table 2.2 different researchers used various tools and techniques to optimize and correlating the experimental results. Very few researchers (Zhao et al., 2012) online temperature detecting system for hot machining to get better surface roughness. The literature review reported in Table 2.2 reveals that there is a scope to apply newly developed optimization techniques to correlate the experimental results such as artificial bee colony technique (ABC), particle swarm optimization (PSO), Tabu search, simulated annealing, mixed orthogonal array, hybrid methods, teaching learning based optimization (TLBO), cloud computing, modeling and simulation packages and computational system for the process design. Amid all the optimization techniques, PSO is commonly used for optimize the process parameters as compared to other techniques.

2.17 PARTICLE SWARM OPTIMIZATION

PSO was first introduced by Eberhart and Kennedy in the year 1995 (Yu et al., 2004). This approach is newly developed meta-heuristic method and evolutionary computational algorithm. PSO was adopted by many researchers in different engineering problems all around the world. The main advantage of this technique is very simple. Easy to apply, less time consuming compared to other computational algorithms with high efficiency. Hence, for the present study is adopting the application of PSO to optimize the thermally assisted machining process parameters. Sarah et al. (2010) used PSO technique in the pulp industry to get optimal solution to direct the input parameters to diminish the resources utilization and wastage of the finished paper. The experimental results were compared with both genetic algorithm (GA) and PSO. PSO gave the better computational efficiency with less time than GA. Ciurana et al., (2009) performed experiments on laser micromachining (laser milling) process to study the surface roughness, geometrical and dimensional features of the grooves on AISI H13 tool steel. PSO technique is adopted to optimize the laser micromachining process parameters. The results indicate that the

proposed swarm intelligent approach for solving the multiobjective optimization problem with complex objectives is efficient, and can assist the user in process design. Gupta et al., (2015) used RSM based PSO technique to optimize the process parameters in turning of Titanium(Grade II) alloy using cubic boron nitride insert tool under minimum quality lubrication (MQL). The experimental results showed that the selected responses predicted on PSO much closer as that of the values acquired in the view of desirability approach. Lee and Ponnambalam (2012) performed using PSO and GA multi objective optimization of turning process. These two techniques show similar trend in Pareto optimal fronts but PSO produced optimal solution with less time compared to GA.

Table 2.2 Techniques used for correlation.

Author	Processes	Techniques used
Ranganathan et al. (2010)	Hot turning	Artificial neural networks and Response surface methodology was applied to determine the optimal process parameters
Ranganathan et al. (2011)	Hot turning	Grey relational analysis was used to determine the multiple machining performance characteristics
Thandra and choudhury (2010)	Hot turning	Response surface methodology was used to optimize the hot machining parameters
WenjiXu et al. (2014)	Hot turning	Finite element simulation based calculation was used for cutting forces and workpiece temperature
Tosun et al. (2002)	Hot turning	Regression analysis method and artificial neural networks were used to optimize the hot machining parameters.
Kamdar and Patel (2012)	Hot turning	Design of experiments were adopted to optimize the hot machining parameters
Dabade and Jadhav (2016)	Hot turning	Design of experiments were adopted to optimize the hot machining parameters
Ginta et al. (2009)	Hot milling	Optimization of process parameters by using design of experiments
Ravi et al. (2014)	Hot turning	Taguchi L_{27} orthogonal array was used to optimize the process parameters.
Ciurana et al. (2009)	Laser micro machining	Hybrid neural networks and particle swarm optimization were used to optimize the process parameters
Raja and Bhaskar et al. (2012)	Face milling	Mathematical model has been developed for surface roughness prediction using Particle Swarm Optimization

Karpat and Ozel, (2007)	Turning	Multi objective optimization using neural networks and Particle Swarm Optimization to optimize the process parameters
Lee et al. (2007)	Grinding	Particle Swarm Optimization was adopted to optimize the process parameters
Shukla and Singh (2016)	Abrasive water jet machining	Taguchi and evolutionary optimization techniques were used to optimize the process parameters
Vijaykumar et al. 2003	Turning	Ant colony optimization technique was used to optimize the process parameters
Yildiz Ali (2013)	Multi pass Turning	Artificial bee colony-based approach was adopted for optimization
Yao Xi et al. (2014)	TAM	Finite element simulation both 2D and 3D was used chip formation and cutting forces.
Sanchez et al. (2014)	Hot turning	Design of experiments was used to optimize the process parameters
Yang et al. (2010)	LAM	3D finite element prediction was adopted to predict the heat affected zone.
Chang and Kuo (2007)	LAM	Taguchi L_9 orthogonal array was used to optimize the process parameters.
Manjaiah et al. (2013)	WEDM	Design of experiments Taguchi L_{27} was used to optimize the process parameters.
Sardinas et al. (2006)	Turning	Genetic algorithm- based multi optimization approach was used to optimize the process parameters.
Guptha et al. (2016)	MQL turning	Different evolutionary techniques were used to optimize the process parameters
Senthilkumar et al. (2012)	Facing and Turning	Hybrid genetic algorithm coupled with artificial neural networks is an intelligent optimization technique to optimize the process parameters
Jafarian et al. (2014)	Turning	Simultaneous Optimizing residual stresses and surface roughness

2.18 SUMMARY OF LITERATURE REVIEW ON HARD TURNING

- High speed machining an another machining method, where frictional heat developed at the tool-work interface anneals the metal in front of the cutting tool, thereby reduces the yield strength of the stock material.

- Benefits of hard machining over grinding are complex workpiece shapes in a single set-up with less cost, and reduced working cost and risk.

- Hard turning proved that as the cutting speed increases tool life increases up to certain limit after which the tool life decreases.

- Hard turning is environmental friendly, because carbide, coated carbide, ceramics and CBN tools are used for dry machining therefore to avoid coolants. Further, preparation setup is very easy and can do the faster rate.

- In hard turning, tool wear is mainly responsible for adhesion and chipping mechanism, therefore there is no diffusion takes place during machining.

- A small defect due to cutting or system instabilities in the final stages will damage the part, making it very expensive scrap.

- Lack of rigidity of machine tool leads to increased tool wear due to chipping because of the brittle nature of the tool.

- High speed machining cost is very high.

2.19 SUMMARY OF THE LITERATURE REVIEW ON THERMALLY ASSISTED MACHINING

- Due to external heat source provided on the workpiece material leads to reduce the yield strength of the material causes decreased cutting forces, surface roughness, tool wear and increased metal removal rate.

- The temperature maintained in the primary and secondary shear zone below recrystallization temperatures leads to no metallurgical changes in the workpiece((Madhavulu et al., 1994).

- The addition of preheat softens the work surface layer, so that ductile deformation rather than brittle deformation occurred during cutting.

- Preheating methods used in industry are laser-assisted heating, plasma heating, electric heating and flame heating. Among all the heating techniques flame heating simpler and low setup cost all kinds of industries can accommodated this technique.

- The main drawbacks of laser assisted machining was due to high laser temperature causes workpiece to be melt, micro structural changes, sub surface cracks.

- Tool life increased drastically with lower manufacturing cost.

Difficult to cut materials can easily machine with this simple thermally assisted machining technique.

2.20 MOTIVATION FROM LITERATURE REVIEW

Due to requirements of advanced manufacturing industries, the usage of nickel super alloys is increasing day by day. Nickel based alloys such as Inconel 718 is suited for application in extreme conditions as combustor and gas turbines where elevated temperature is maintained. Especially, Inconel 718 has been used in aircraft engines because of its high corrosion resistance and creep rupture strength of over 700°C. Most of the literature discussed about the conventional machining of Inconel 718. But, only a few researchers have concentrated on thermally assisted machining of Inconel 718. Therefore there is a scope to study the machinability performance characteristics of Inconel 718 superalloy.

However, earlier literatures have shown the usage of different optimization techniques (i.e., Taguchi technique, desirability approach, ANN, GRA, RSM and DOE) in the field of TAM of Inconel 718 superalloys. These conventional techniques of optimization can yields local optimum solution because experimental design based on the discrete levels, although, in the reality control parameters changing continuously. The global optimum solution may lie outside the experimental domain In order to obtain global optimum solutions some evolutionary algorithms such as GA, PSO, ABC, TLBO etc are discussed in the literature. Hence in the present study PSO algorithm has been adopted.

49

CHAPTER 3

EXPERIMENTAL WORK

The chapter describes the hot machining of Inconel 718 superalloy, material properties and its composition. Cutting tool materials and its geometry used in the present work, experimental setup and experimental procedure used to measure the cutting forces, surface roughness, tool wear, metal removal rate, micro hardness, phase changes on the machined surface and chips examination during hot machining of Inconel 718 super alloy with three different type of cutting tools under various cutting conditions.

Table 3.1 Chemical composition of Inconel 718

Element	C	Ti	Cr	Fe	Ni	Nb	Mo
Percentage	8.24	0.59	14.81	15.46	54.39	4.10	2.41

Table 3.2 Mechanical properties of Inconel 718

Properties	Value
Yield stress (MPa)	1110
Tensile stress (MPa)	1310
Strain (%)	23.3
Elastic modulus (GPa)	206
Thermal conductivity (W/m^2K)	11.2
Density (Kg/m^3)	8470

3.1 WORK MATERIAL

Inconel 718, a nickel based super alloy is widely used in aerospace industry, particularly in the hot sections of gas turbine engines, due to their peculiar characteristics like high strength, high corrosion resistance at elevated temperatures. The chemical composition

of Inconel 718 were evaluated using an optical emission vacuum spectrometer, the obtained chemical composition is listed in Table 3.1. The mechanical properties are listed in Table 3.2.

3.2 MICROSTRUCTURAL STUDY

For microstructural study a specimen of 8 mm is used for optical microscopy. First the specimens were cold mounting by using acrylic resign and allowed to set. Polishing these mounted samples by grinding at 1/0, 2/0, 3/0 4/0 and 600, 1000, 1200, 1600, 2000 SiC papers to get flat and smooth surface. Then the samples were polished by velvet cloth using diamond paste to attain mirror polish. Finally 10 gms CuSo4 + 20 ml HNO3 + H_2O etchant was applied on the specimen for few seconds then immediately wash the specimen with water. After applying the etchant the shiny surface turns in to dull surface. The samples were placed on the scanning electron microscope to capture the microstructure.
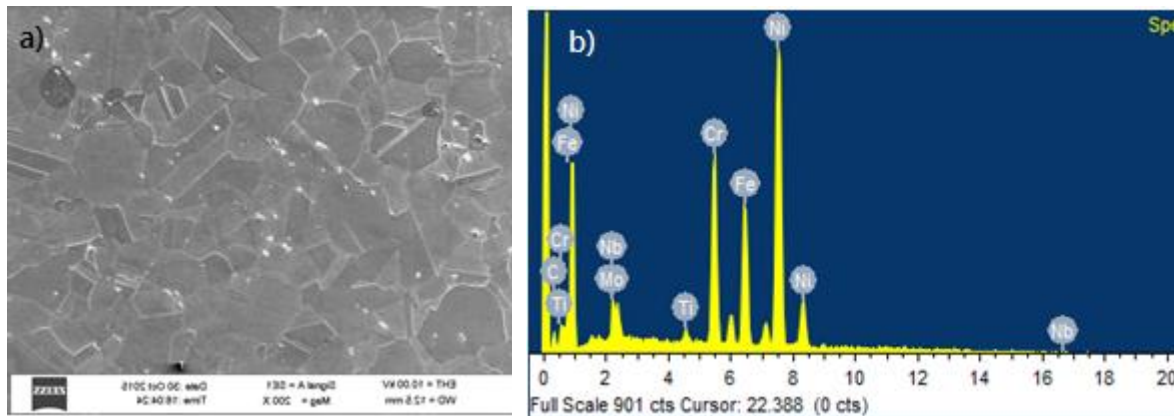
Figure 3.1 (a) SEM microstructure of Inconel 718 (b) EDS analysis of Inconel 718.

Figure 3.1 (a) shows the SEM image of Inconel 718 superalloy is comprised of austenitic face-centered cubic (FCC) matrix phase known as gamma (γ) phase, which is a solid solution of Fe, Cr, and Mo in nickel together with other secondary phases. The main structure of Inconel 718 is a face-centered cubic (FCC) austenitic solid solution matrix known as the gamma (γ) phase with a precipitated nickel aluminum titanium [Ni3(Al Ti)]

known as the gamma prime (γ′) phase as the main strengthening phase. Another strengthening phase present in Inconel 718 is the nickel niobium (Ni3Nb) phase known as gamma double prime (γ″).

3.3 EDAX ANALYSIS

From the Figure 3.1(b) shows the elemental diffraction X-ray analysis of Inconel 718 superalloy. This test was performed to confirm the percentage addition elements in to the alloy. It is confirmed that the weight percentage and atomic percentage of all the elements of same are shown in Table 3.3.

Table 3.3 Elemental composition of Inconel 718

Element	Ni	Cr	Fe	Ti	Nd	o	Mo
Atomic %	54.38	13.64	16.72	1.89	7.95	2.66	2.76

3.4 XRD ANALYSIS
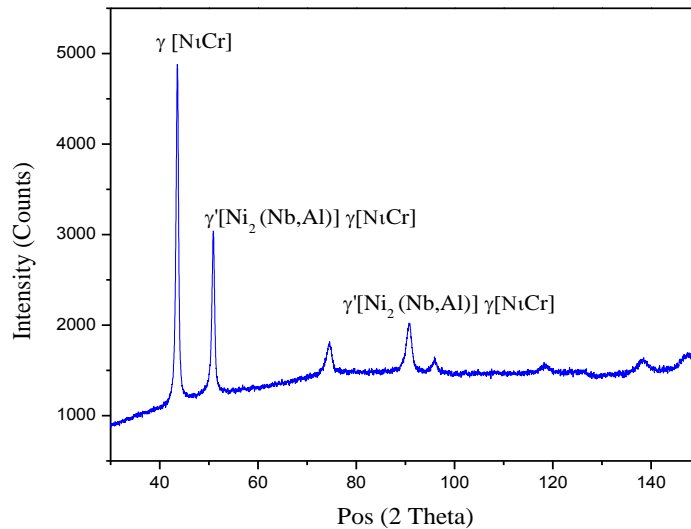
Figure 3.2 XRD result of Inconel 718 super alloy

X- ray diffraction analysis was conducted on Bruker D8 advance machine to identity the phase analysis of the material. Figure 3.2 represents the XRD pattern of the Inconel 718 superalloy. The machined samples were examined using X- ray diffraction (XRD). The peaks were observed at 43.06 ^{o}, 50.79 ^{o} and 74.67 ^{o}. The peaks reveal that presence of γ-Ni matrix precipitates with face-centered cubic (FCC) crystal structure. The intermetallic phases such as γ-NiCr, γ' Ni_3Al and γ'-Ni_3Nb are precipitated in the γ-Ni matrix.

3.5 CUTTING TOOLS

Inconel 718 super alloy with average hardness of 46 HRC were machined using three different tools of ISO grade (K313, WS10PT and KC9105) cutting tools. The properties of the cutting tools used are shown in Table 3.4. All the cutting tools have same ISO geometry designed by ANSI as SNMG 120408. The cutting tools were mounted on a PSBNR2020 K12 (ISO) tool holder as shown in Figure 3.3. The tool geometry of the insert with inclination angle: $- 6^{o}$, rake angle: $- 6^{o}$, clearance angle: 6°, Major cutting edge angle: 75°. The geometry of the cutting tools and order of multilayer and triple layer for coated carbide tool is shown in Figure 3.3.
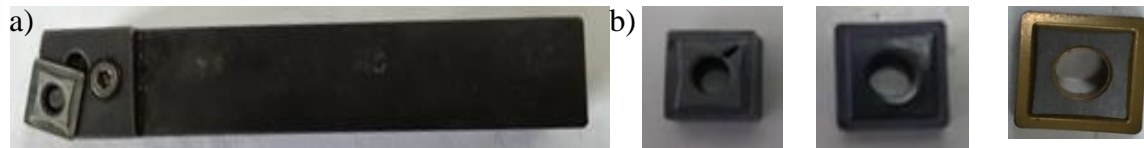
Figure 3.3 (a) PSBNR 2020 K12 Tool holder (b) cutting inserts (i) Uncoated (ii) TiAlN (iii) TiCN/Al$_2$O$_3$/TiN

Table 3.4 Properties of the cutting tools.

Properties	K313 (uncoated)	TiAlN	TiCN–Al$_2$O$_3$–TiN
Hardness (HRA)	93	93	90.6
Density (g/cm^3)	14.9	14.9	13.9

Tensile strength, (Mpa)	3100	3100	-
Avg. grain size (mm)	Fine (~1 μm)	Fine (~1 μm)	Medium(>1 μm)
Binder	6 % Co	6 % Co	7 % Co

3.6 EXPERIMENTAL DESIGN AND METHODOLOGY

Design of experiments is necessary to minimize and to perform the experiments productively. Generally, in any experimental research, experimental procedures are usually expensive and time consuming, with less number of experiments need to satisfy the objectives is an important requirement. In the late 1920's R.A. Fisher in England introduced the design of experiments (DOE), which is a powerful statically tool to study the effect of multiple variables at the same time (Ranjith Roy 2001). This technique has much developed in the academic environment to solve many engineering applications in the production floor. Dr. Genechi Taguchi in the year 1940 carried out a significant research with DOE techniques. He made an extensive effort to make the experimental technique more easily, and applied in the manufacturing field to improve the product quality. Dr. Taguchi's standard version of DOE, widely known as Taguchi approach or Taguchi method. Taguchi technique is used to determine the optimum settings of the design parameters for performance and cost, the designer can easily adopt this systematic and efficient approach for experimentation. For Engineering analysis Taguchi technique is popularly used. It is a robust experimental design of experiments. The experimental plan and analysis of results flow chart is shown in Figure 3.4

3.7 TAGUCHI EXPERIMENTAL DESIGN

Taguchi approach consist set of experimental plans for obtaining experimental results in a controlled manner. This technique involves laying out the experimental conditions using specially designed tables known as 'orthogonal arrays'. By using orthogonal arrays considerably decreases the number of experimental configuration to be studied. Experiments were performed based on orthogonal array allows the effects of different

parameters to be determined proficiently. The conclusions obtained from less number of experiments are suitable more than the entire experimental region spanned by the process parameters and their settings. In the current study, in order to determine the influence of process parameters and their effects on the machining characteristics of Inconel 718 superalloy, Taguchi technique with four parameters at three different levels are considered.

The orthogonal array criteria was selected based on the degrees of freedom for the orthogonal array must be greater than or equal to sum of process parameters. From the list of experimental designs Taguchi L_{27} orthogonal array was selected. It consists of 13 columns and 27 rows is shown in Table 3.6 By using this orthogonal array can be studied the individual as well as interaction effects of the process parameters on the response of the study. Therefore, it is best suitable for the conditions being investigated, 4 parameters each at 3 levels (3^4) along with the interaction effects. The effect of noise sources are tried to remove by employing the each experimental trial thrice under same conditions at different times. In addition, the run order of experiments was random in order to avoid noise sources, which had not been considered initially and perhaps take place during experimental run and it affect the results in negative manner.

Taguchi approach is used to identify the most significant process parameters to produce the product or process insensitive to noise factors (Ross, 1996 and Phadke, 1989). Taguchi design of experiments technique is created based on the matrix experiments known as orthogonal arrays (Ross, 1996 and Phadke, 1989) used to study the effects of numerous factors competently. The main reason of performing orthogonal experiments is to identify the optimum levels for all the parameters using analysis of means (ANOM) and to find the comparative significance of each parameter using analysis of variance (ANOVA) on the proposed performance characteristics. Taguchi suggests signal to noise ratio (S/N) as the objective function for matrix experiments (Ross, 1996 and Phadke, 1989). Objective function broadly divided in to three categories such as smaller the better, nominal the best and larger the better. In the present study the cutting forces,

54

surface roughness, tool wear to be minimized thus smaller the better is selected and MRR to be maximized and therefore larger the better is selected.

3.8 PARAMETERS AND THEIR LEVELS

The selected process parameters and their levels for hot machining operation are shown in Table.3.5 for Taguchi L27 orthogonal array experiments, the combined input parameters is set and the workpiece of Inconel 718 super alloy were machined using carbide, TiAlN nano multilayer coated, TiCN/Al$_2$O$_3$/TiN triple layer coated tool. In order to keep away the error creeping in to the system the experiments were randomized. Four output responses such as cutting forces, surface roughness (R$_a$), tool wear, and MRR were measured for each trails of orthogonal array.

Table 3.5 Control parameters and three levels

Symbol	Process Parameters	Units	Levels		
			I	II	III
A	Cutting speed	m/min	34.08	54.97	85.21
B	Feed rate	mm/rev	0.048	0.096	0.143
C	Depth of Cut	mm	0.2	0.4	0.6
D	Temperature	^{o}C	200	400	600

3.9 EXPERIMENTAL DESIGN

In the present research work, four parameters namely, cutting speed, feed rate, depth of cut, workpiece temperature were identified and each parameters levels were selected based on preliminary experiments. For each process parameter was investigated at three different levels to study the non linear effect of the parameters.

From the literature review the three best cutting tools were selected such as uncoated carbide, TiAlN multilayer coated, TiCN/Al$_2$O$_3$/TiN triple layer coated carbide tool for machining of Inconel 718 to study their effect on the machining characteristics. These cutting tools were utilized for better machining of Inconel 718 and to study the cutting

forces, surface characteristics, tool wear and MRR. The experiments were performed on 'Kirloskar lathe machine' and setup is shown in Figure 3.5. For the hot machining experiments, cylindrical workpieces of 32 mm diameter and 150 mm length were considered. Each workpiece is first pre machined and centre drilled on two sides. It is necessary to support the material from both the ends while machining on the lathe, due to this, the vibrations of the workpiece will be reduced and also minimizes the impact forces on the cutting tool. The workpiece materials were first heat treated in the electric furnace to relieve the internal stresses and to get the required hardness. Initially, the Inconel 718 super alloy workpiece were heat treated at 950 $^{\mathrm{o}}$C for 1 hour and removed from the furnace followed by air cooling one hour.

The cutting parameters were considered were cutting speed, feed rate depth of cut and workpiece temperature and their levels were shown in Table 3.4. First the workpiece is heated in the electrical furnace to get the desired temperature to improve the machinability and reduce its shear strength, after the required temperature is achieved. The workpiece is fixed on the steel points on the lathe machine to perform the experiments. While fixing the workpiece in the lathe temperature loss to the atmosphere. To maintain equilibrium of heat oxy acetylene torch heating was used. The oxy acetylene torch was fixed opposite side of the tool carriage to sustain the temperature of the workpiece properly as shown in Figure 3.5. The temperature of the workpiece is measured by using non contact type infrared thermometer. A fresh cutting tool and 4 minutes of machining time were maintained for each experiment to evade the effect of tool wear on the given responses.

Table 3.6 Taguchi L27 orthogonal array

Trial No.	Parameters												
	A	B	C	D	E	F	G	H	J	K	L	M	N
1	1	1	1	1	1	1	1	1	1	1	1	1	1
2	1	1	1	1	2	2	2	2	2	2	2	2	2
3	1	1	1	1	3	3	3	3	3	3	3	3	3
4	1	2	2	2	1	1	1	2	2	2	3	3	3
5	1	2	2	2	2	2	2	3	3	3	1	1	1
6	1	2	2	2	3	3	3	1	1	1	2	2	2
7	1	3	3	3	1	1	1	3	3	3	2	2	2
8	1	3	3	3	2	2	2	1	1	1	3	3	3
9	1	3	3	3	3	3	3	2	2	2	1	1	1
10	2	1	2	3	1	2	3	1	2	3	1	2	3
11	2	1	2	3	2	3	1	2	3	1	2	3	1
12	2	1	2	3	3	1	2	3	1	2	3	1	2
13	2	2	3	1	1	2	3	2	3	1	3	1	2
14	2	2	3	1	2	3	1	3	1	2	1	2	3
15	2	2	3	1	3	1	2	1	2	3	2	3	1
16	2	3	1	2	1	2	3	3	1	2	2	3	1
17	2	3	1	2	2	3	1	1	2	3	3	1	2
18	2	3	1	2	3	1	2	2	3	1	1	2	3
19	3	1	3	2	1	3	2	1	3	2	1	3	2
20	3	1	3	2	2	1	3	2	1	3	2	1	3
21	3	1	3	2	3	2	1	3	2	1	3	2	1
22	3	2	1	3	1	3	2	2	1	3	3	2	1
23	3	2	1	3	2	1	3	3	2	1	1	3	2
24	3	2	1	3	3	2	1	1	3	2	2	1	3
25	3	3	2	1	1	3	2	3	2	1	2	1	3
26	3	3	2	1	2	1	3	1	3	2	3	2	1
27	3	3	2	1	3	2	1	2	1	3	1	3	2
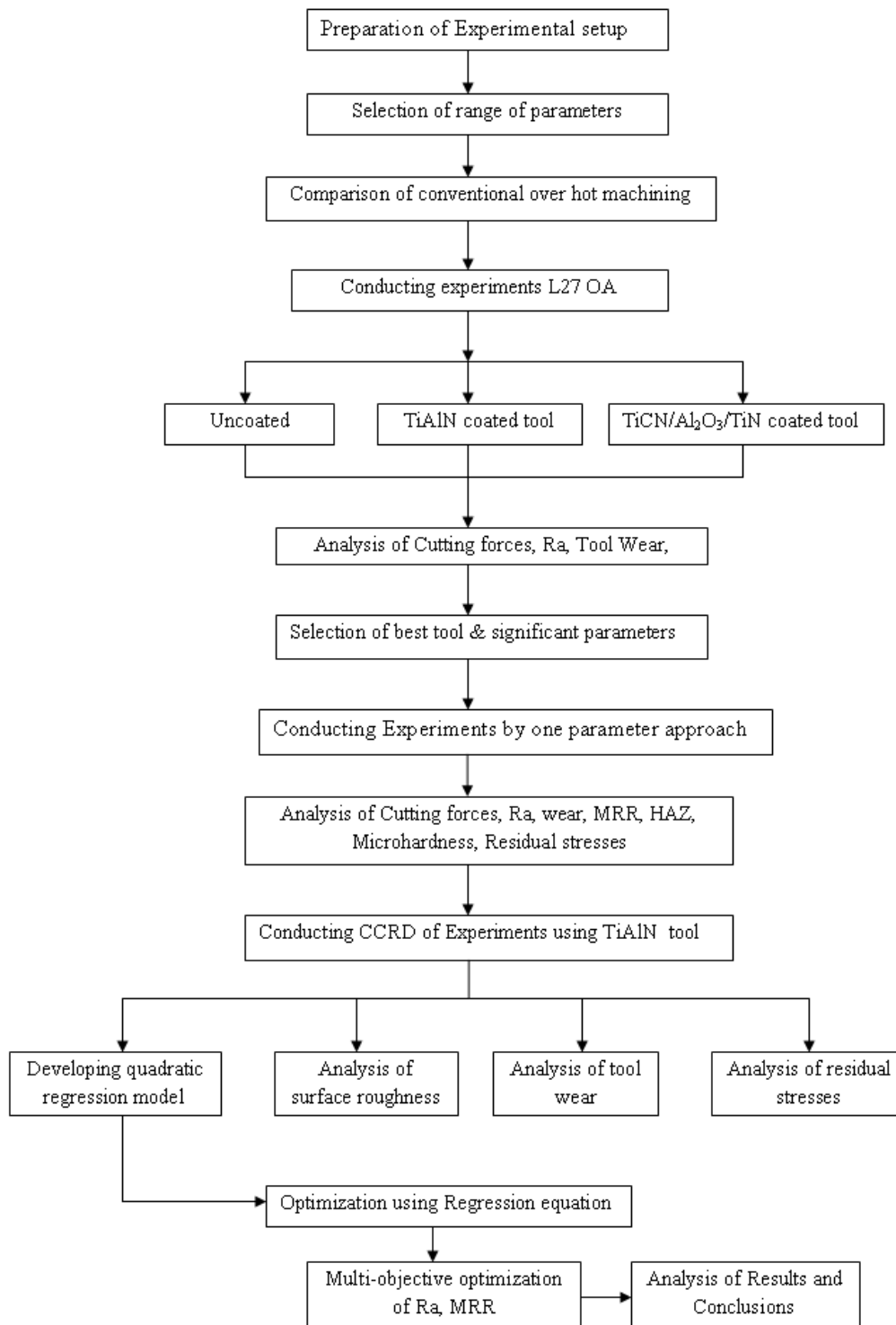
Figure 3.4 Flow chart of plan of experiments design and analysis
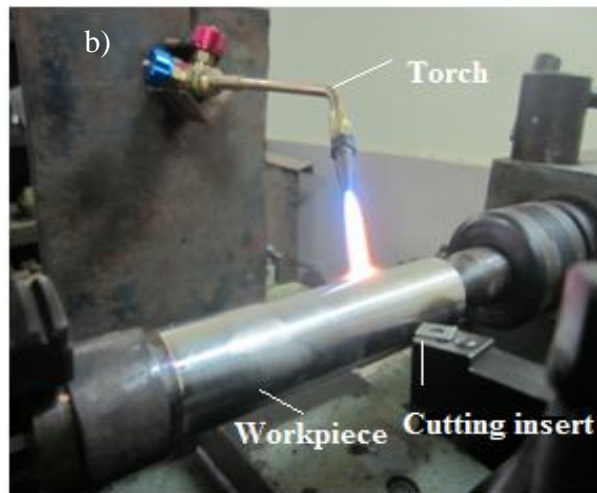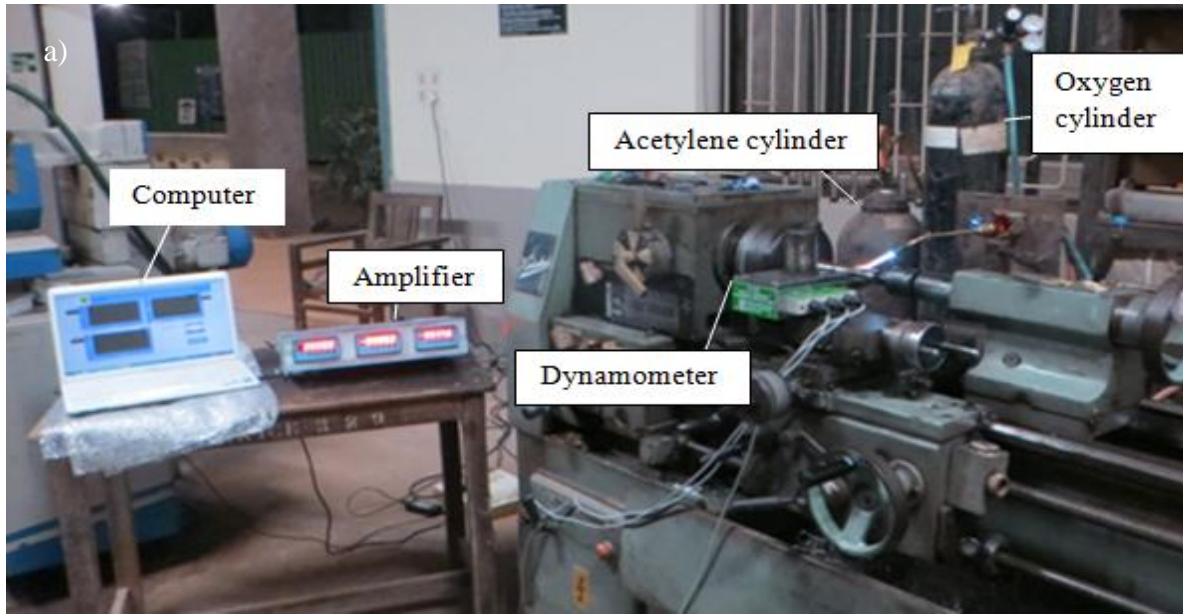
Figure 3.5 a) Experimental setup b) machining zone
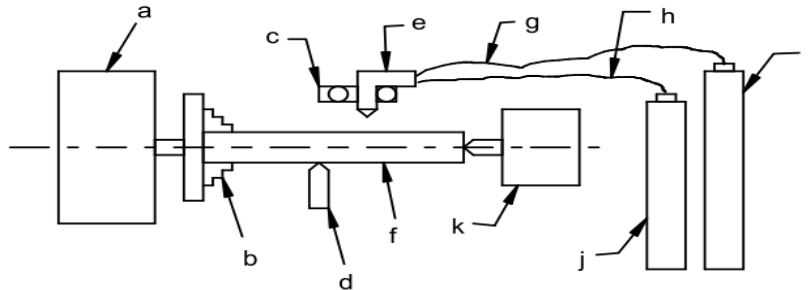
Figure 3.6 Schematic diagram of hot machining setup

(a) Lathe head stock (b) 3 jaw chuck; (c) Torch distance adjustable screws

(d) Cutting inserts (e) Torch (f) Workpiece

(g) O_2 flow pipe (h) Acetylene flow pipe; (i) O_2 cylinder;

(j) Acetylene cylinder (k) tail stock.

In the present research work Taguchi L_{27} OA is used to study the significant effect on responses on cutting forces, surface roughness (Ra), tool wear and MRR. The process parameters were selected from a limited set of values available on the machine. To evaluate the effect of machining parameters on performance characteristics like cutting forces, surface roughness (Ra), tool wear, MRR and to select the best cutting tool to machine Inconel 718 superalloy. The process parameters are used to identify the best machining conditions to design the manufacturing process, where as noise factor represents all parameters that cause variation. Present study deals with the performance of four process parameters viz., cutting speed (v), feed rate (f), depth of cut (d) and workpiece temperature (T). The experimental results are further transformed in to signal to noise ratio (S/N). There are different types of S/N ratios obtainable depending upon the type of characteristics. The characteristics that have lesser values shows the better machining performance, such as cutting forces, surface roughness and tool wear is called

60

'smaller the better' η_1. The characteristics that have larger values better machining performance such as 'larger the better' η_2 in order to get optimal machining parameters. The loss function is defined as MRR.

$$\eta_1 = -10 \log_{10} [R_a^2] \tag{3.1}$$

$$\eta_2 = -10 \log_{10} [\frac{1}{MRR^2}] \tag{3.2}$$

From the taguchi experimental results the best cutting tool and significant hot machining process parameters were selected for further continuation of the work.

3.10 ONE FACTOR AT A TIME APPROACH

One factor at a time approach experiments were performed by considering four significant parameters of five levels, keeping other three parameters constant when one parameter is varying based on the previous experimental data. The four machining parameters such as cutting speed, feed rate, depth of cut and workpiece temperature to study the individual effect of the output parameters like cutting forces, surface roughness, tool wear, MRR, micro hardness, heat affected zone (HAZ), residual stresses. The process parameters of 5 levels were selected, cutting speed 26 to 130 m/min, feed rate 0.048 to 0.143 mm/rev, depth of cut 0.2 to 0.6 mm and workpiece temperature 200°C to 600°C. The TiAlN nano multilayer coated carbide tool was selected to machine Inconel 718 superalloy based on the pervious study. The selected process parameters and their ranges are listed below.

3.11 RESPONSE SURFACE METHODOLOGY

Response surface methodology (RSM) a combination of both statistical and mathematical technique used for analysis and design of experiments. This technique is helpful for modeling and analysis of parameters, in which response of interest is affected by a several variables and the purpose is to optimize this response. A five level four factor central composite rotatable design (CCRD) was employed to develop the response models using RSM. From the Figure 3.7 it can be observed that the low level represents

Table 3.7 Machining parameters and their levels.

Symbol	Control parameters	Levels				
		Lowest (-1.682)	Low (-1)	Centre (0)	High (+1)	Highest (1.682)
v	Cutting speed (m/min)	26	52	78	104	130
f	Feed rate (mm/rev)	0.048	0.071	0.096	0.119	0.143
d	Depth of cut (mm)	0.2	0.3	0.4	0.5	0.6
T	W/P temperature (^oC)	200	300	400	500	600

the value (−1.68) and the middle level represents by the value (0) and the high level represents the value (1.68). This facilitates in fitting the regression model belonging to output parameters of the levels
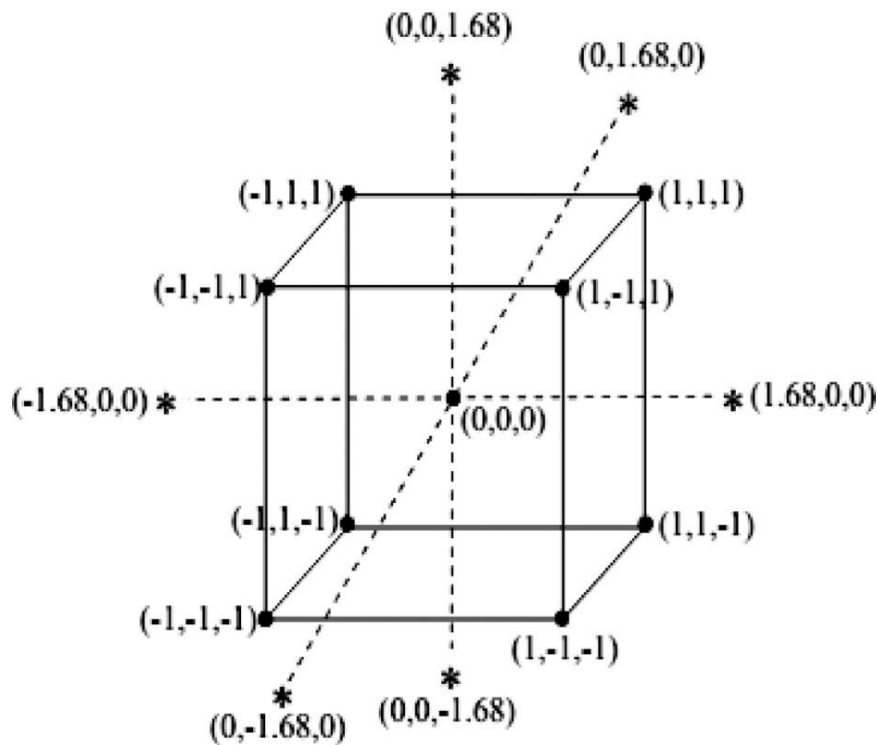
Figure 3.7 All combinations representation of central composite rotatable design

Response surface methodology is the most commonly used approach in design of experiments. In this study RSM based central composite rotatable design experiments of all possible combination of levels of the cutting speed, feed rate, depth of cut and workpiece temperature were investigated. The parameters and their levels are shown in Table 3.7. Four parameters of five levels of central composite rotatable design and to conduct 30 experiments in this present study. The design consists of axial points, center points and star points. The axial points consist of 16 trails of experiments and the star point consists of 8 experiments and the centre point consists of 6 experiments. The experimental design is shown in Table 3.8. The RSM permitted use to determine 30

Table 3.8 Central composite design

Run Order	Std order	A	B	C	D
1	6	-1	-1	-1	-1
2	9	1	-1	-1	-1
3	19	-1	1	-1	-1
4	7	1	1	-1	-1
5	18	-1	-1	1	-1
6	25	1	-1	1	-1
7	24	-1	1	1	-1
8	22	1	1	1	-1
9	13	-1	-1	-1	1
10	5	1	-1	-1	1
11	26	-1	1	-1	1
12	16	1	1	-1	1
13	23	-1	-1	1	1
14	27	1	-1	1	1
15	15	-1	1	1	1
16	30	1	1	1	1
17	2	-2	0	0	0
18	4	2	0	0	0
19	28	0	-2	0	0

20	29	0	2	0	0
21	3	0	0	-2	0
22	14	0	0	2	0
23	11	0	0	0	-2
24	17	0	0	0	2
25	21	0	0	0	0
26	10	0	0	0	0
27	8	0	0	0	0
28	1	0	0	0	0
29	20	0	0	0	0
30	12	0	0	0	0

values to determine 30 values of each response and to proficiently estimate the coefficients of a reduced second order model, which revealed a link between the cutting forces, surface roughness, tool wear and MRR. This can be represented in the following equation:

$$Y = \beta_0 + \beta_1 V_c + \beta_2 f + \beta_3 d + \beta_4 T + \beta_{11} V_c^2 + \beta_{22} f^2 + \beta_{33} d^2 + \beta_{44} T^2 \qquad (3.3)$$

Where, Y = response, i.e. F_c, R_a, tool wear and MRR;

β_0................ $\beta_{44:}$ regression values of the models are to be determined for each of the performance characteristics.

The values of the regression values of the quadratic model are to be determined by:

$$B = (Y^T Y)^{-1} Y^T Z \qquad (3.4)$$

Where B: represents the matrix of parameter estimates; Y: calculation matrix, which includes linear quadratic and interaction terms, Y^T: transpose of Y and Z: matrix of desired performance characteristics.

3.12 MEASUREMENT OF PERFORMANCE CHARACTERSTICS

3.12.1 Surface roughness

The surface roughness was measured by using 'MITUTOYO SURFTEST SJ-301 surface roughness tester shown in Figure 3.8. The roughness tester uses a differential inductance method as s direct technique. The tester consists of a hard needle shape stylus made of diamond. The stylus includes a tip radius of 2 μm and applies a force of 0.75 mN to measure the surface roughness. At three different locations surface roughness (Ra) of the machined surface was measured and the average was taken as the output response. The cutoff length of 0.8 mm was selected and evaluation length of 4 mm was used to measure the surface roughness with a stylus speed of 0.25 mm/s. The Ra and Rz values of TAM machined surface was directly recorded using roughness tester.

3.12.2 Surface topography

The topography of the TAM machined surface was obtained using a 3D laser microscope by using *Olympus* LEST OLS4000 laser confocal microscope available in CMTI, Bangalore as shown in Figure 3.9. The microscope uses a laser scanning to measure the surface profile of the machined components. The microscope can measure surface texture more accurately due to low laser spot diameter of 0.4 μm
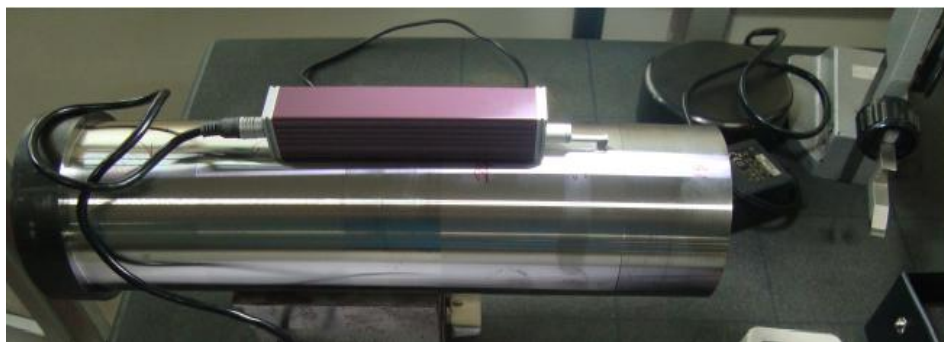
Figure 3.8 Surface roughness tester

Figure 3.9 Laser optical confocal microscope

3.12.3 Metal removal rate

The metal removal rate has been calculated using the weight loss method and computed using equation 3.5.

$$\text{MRR} = \frac{Weight\ loss\ after\ machining}{Time\ taken}\ \text{gm/min} \qquad (3.5)$$

The weight of each sample was measured using precision weighing balance. This weighing balance offers on accuracy of 0.5 g and capacity of 2 kg.

3.12 .4 Microhardness

The microhardness of the hot machines specimens were measured by using OMNI TECH microhardness tester as shown in Figure 3.10. Pyramid shape diamond indenter of 136 angle with a load of 100 gf at a dwell time of 15 sec was used to measure the hardness of the material. The nearby portion of the machined surface was considered as a reference point (0 μm) and it is 10 μm the machined surface because it is very difficult to

measure the microhardness exactly on the machined surface due to improper indentation. At different temperatures and at different zones the hardness was measured and taken as an average. The hardness of 550 Hv for 600 $^{\circ}$C temperature.

Figure 3.10 Microhardness tester

3.12.5 Scanning electron microscope

Scanning electron microscope with Energy dispersive X—ray spectroscopy (EDS) from JEOL as shown in Figure 3.11 was used to study the tool wear, chip morphology and surface morphology and elemental composition of the machined specimens at different temperature. To study the microstructure of the machined specimens were polished on SiC papers with different grades 200, 400,800,1000,1200,2000 and cloth and etched by using etchant (10 gms CuSo4 + 20 ml HNO3 + few drops of distilled water). The scanning electron microscopy instrument had a resolution of at 30 KV. The specimens were loaded properly in the sequence. SEM images at different magnifications were taken. Along with microstructures EDS analysis was carried out for the specimen to know the elemental composition present in the alloy.

Figure 3.11 Scanning electron microscopy

3.12.6 X-ray diffraction (XRD) analysis

The X-ray diffraction analysis were carried out using BRUKER D8 ADVANCE machine it is used to measure the phases present in the hot machined specimens with different temperatures as shown in Figure 3.12. The XRD software the following inputs are: starting angle of scan of 20°, end angle scan of 100°, step size of 0.1 seconds and targeted CuKα. After getting the XRD patterns were analyzed using the software PCPDFWIN to determine the phases present in the machined specimen.

Figure 3.12 X-Ray diffraction

3.12.7 Optical microscope

The *ARTRAY* – 130 ml inverted microscope with *Biovis* image analyzer is used to capture and analyze the image. The optical microscope is used to study the tool wear and microstructure characterization. The specimens are polished and etched by using etchant (10 gms CuSo4 + 20 ml HNO3 + few drops of distilled water).

3.12.8 White layer formation

The white formation is occurred due to the excessive flank wear or cutting conditions workpiece surfaces produced by hot turning can exhibit surface alterations that are known as white layer. The white layer thickness was determined by polishing the cross sectioned specimen of the machined surface by using SiC emery papers with different grades, cloth polishing and etched by using etchant (10 gms CuSo4 + 20 ml HNO3 + few drops of distilled water). The specimen was placed on the scanning electron microscope is used to measure the thickness of the white layer.

3.12.9 Residual stress

X-ray diffraction can be used to measure residual stress using the distance between crystallographic planes, i.e., d-spacing, as a strain gauge. When the material is in tension, the d-spacing increases and, when under compression the d-spacing decreases. Stresses can be determined from the measured d-spacing's. Proto i-XRD instrument was used to measure the strain developed in the machined surface as shown in Figure 3.13

The equipment is initialized for about 15minutes to warm up the system and the X-ray tube is excited to an appropriate level before starting the measurements. The test piece is placed on a suitable fixture & the area where the stress analysis has to be carried out is focused manually in equipment. The measurement is carried out by setting the parameters in accordance with details of the test sample. The gain is set to the optimum level for

better results. The inputs are supplied as required for the test eg., time of exposure, Beta & phi angles, no. of averages etc., and the final measurement is done.
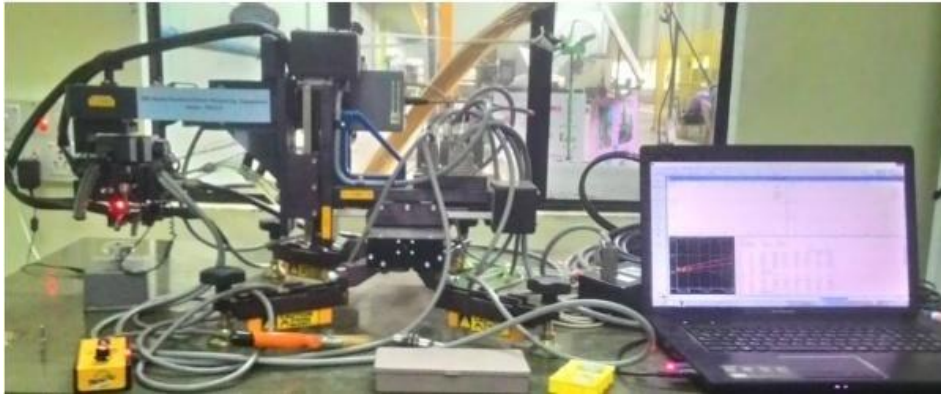
Figure 3.13 Proto i- XRD for residual stress measurement

3.13 SUMMARY

In this chapter, Inconel 718 workpiece material and its properties have been described. TAM experimental setup, experimental procedure has been demonstrated. The research methodology adopted in the current research work has also been described. Finally, the details of the equipments used for measurement of surface roughness, tool wear, microhardness, recast layer, residual stresses, microstructure and surface topography of TAM surface have been described. In case all equipments, measurements were made with more precisely and accurately. Besides, repeatability was obtained in most of the measurements which confirm the minimum deviation.

CHAPTER 4

RESULTS AND DISCUSSION

4.1 INTRODUCTION

The effect of thermally assisted machining parameters on performance characteristics like cutting forces, surface roughness, tool wear and metal removal rate are discussed in the following sections.

The processes parameters and their levels used in the present study are shown in Table 3.7. These parameters were chosen based on literature review and by conducting trail experiments. For performing the experiments and to analyze the process parameters based on Taguchi orthogonal array (OA) L_{27} was selected. To accomplish the objectives of the research work the experimental work was divided in to three phases and is follows

Phase 1: Machining of Inconel 718 using uncoated tool with conventional and thermally assisted machining (TAM).

Phase 2: Machining of Inconel 718 using TiAlN nano multilayer coated carbide tool with TAM.

Phase 3: Machining of Inconel 718 using $TiCN/Al_2O_3/TiN$ triple layer coated carbide tool with TAM.

4.2 EXPERIMENTAL RESULTS

The conventional and thermally assisted machining experiments were performed on Kirloskar lathe machine to study and analyze the effect of input parameters on the responses such as cutting forces, surface roughness, tool wear and metal removal rate. The output parameters with their corresponding S/N ratio values are listed in Table A1 to A4 (See in Appendix) along with three different cutting tools precisely tungsten carbide, TiAlN multilayer and $TiCN/Al_2O_3/TiN$ triple layer coated carbide tools.

Table A1 to A4 depict the attained experimental results of cutting forces, surface roughness, tool wear and MRR with their S/N ratio values for carbide tool. In the present

70

study all the experimental designs, graphs and analysis have been carried out using Minitab-17 statistical software. The Signal to noise ratio factor is used in order to measure the responses to enhance the product and process insensitive to noise factor. This illustrates the degree of predictable responses of product or process in the presence of noise factors. From the attained signal to noise ratio it can be concluded that, the parameters with highest signal to noise ratio yield optimum values with minimum variance. The experimental results and their respective S/N ratio values are represented in Table A2 to A4. The S/N ratio of smaller the better characteristics is incorporated to find the arithmetic mean average surface roughness (Ra), cutting forces and tool wear.

4.3 COMPARISION BETWEEN CONVENTIONAL VS TAM
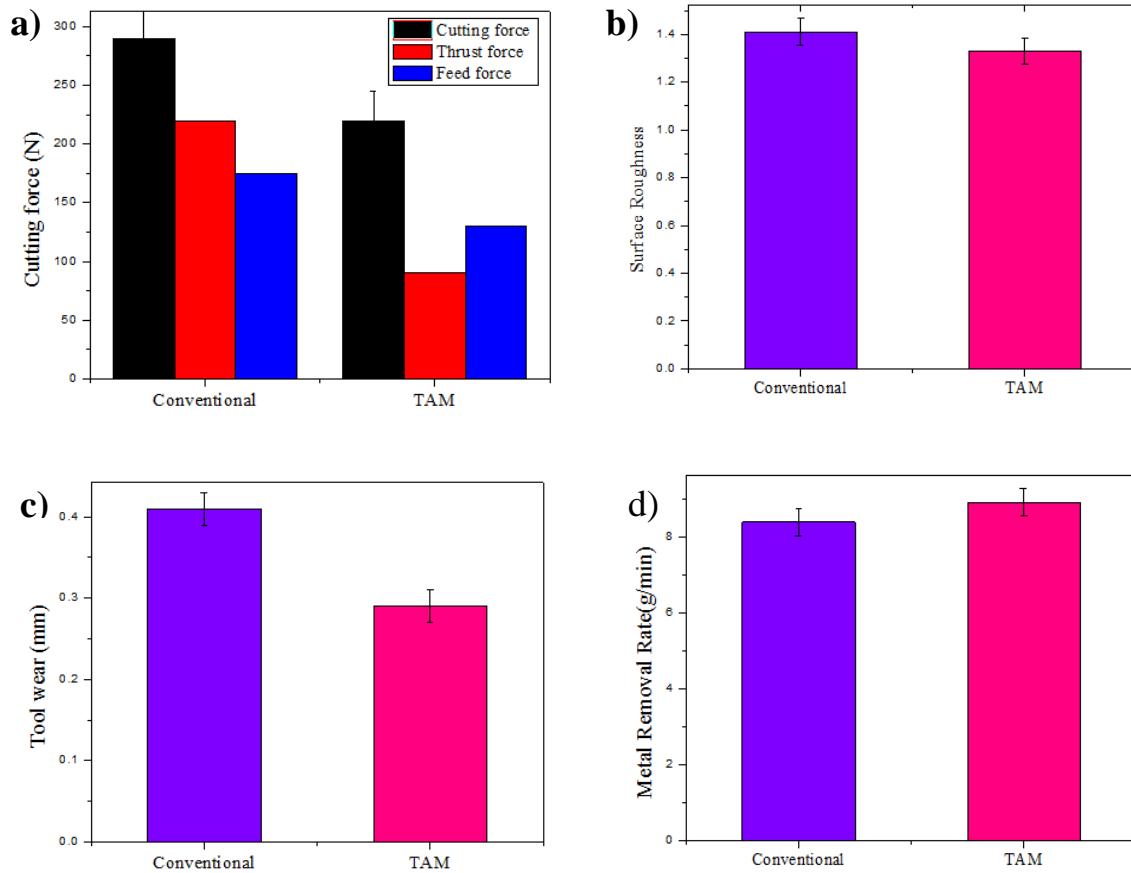
Figure 4.1 Comparisons between Conventional vs TAM of cutting forces, Ra, tool wear and MRR.

Figure 4.1 shows the comparison between conventional machining and thermally assisted machining while turning with Inconel 718 superalloy using uncoated carbide tool. The cutting forces are reduced by around 49 % compared to conventional machining, surface roughness were decreased by 21.8 % , tool wear were decreased by 29 % and metal removal rate is increased by 5.7 %.

4.4 TOOL WEAR MECHANISMS OF CONVENTIONAL VS TAM

TAM Machining (Uncoated tool)   **Conventional machining (Uncoated tool)**
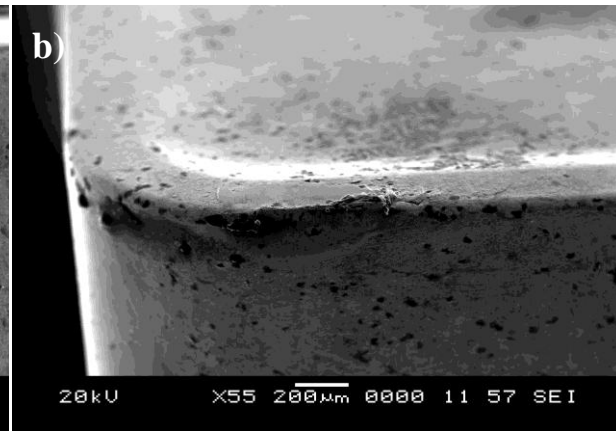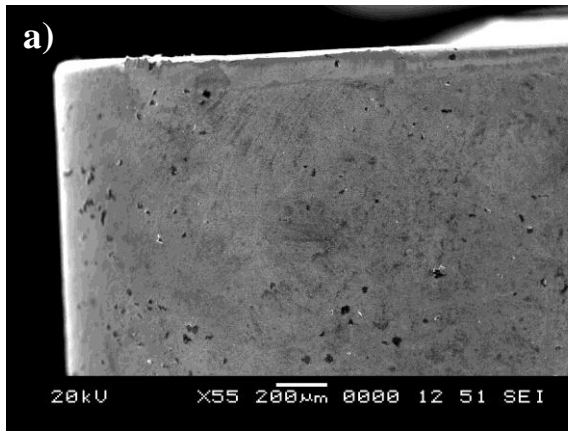
v= 34.08 m/min, f= 0.048 mm/rev d = 0.6 mm t = 600 ^{o}C

v= 34.08 m/min, f= 0.048 mm/rev, d = 0.6 mm   t = 600 ^{o}C
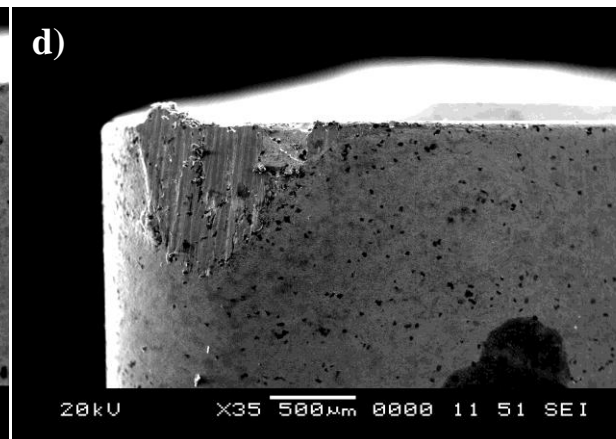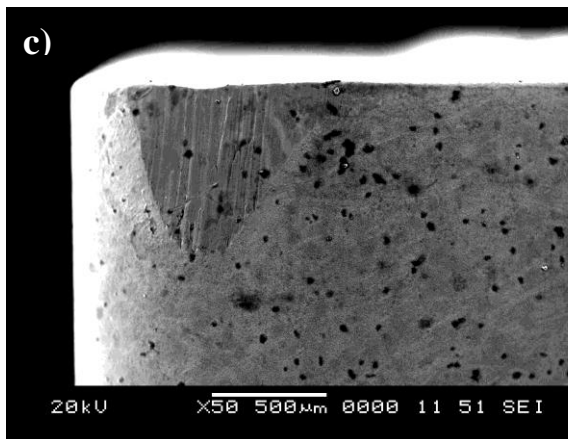
v= 54.97m/min, f = 0.096mm/rev, d=0.4mm, t = 200 ^{o}C

v= 54.97m/min, f = 0.096mm/rev, d=0.4mm, t = 200 ^{o}C

e)	f)
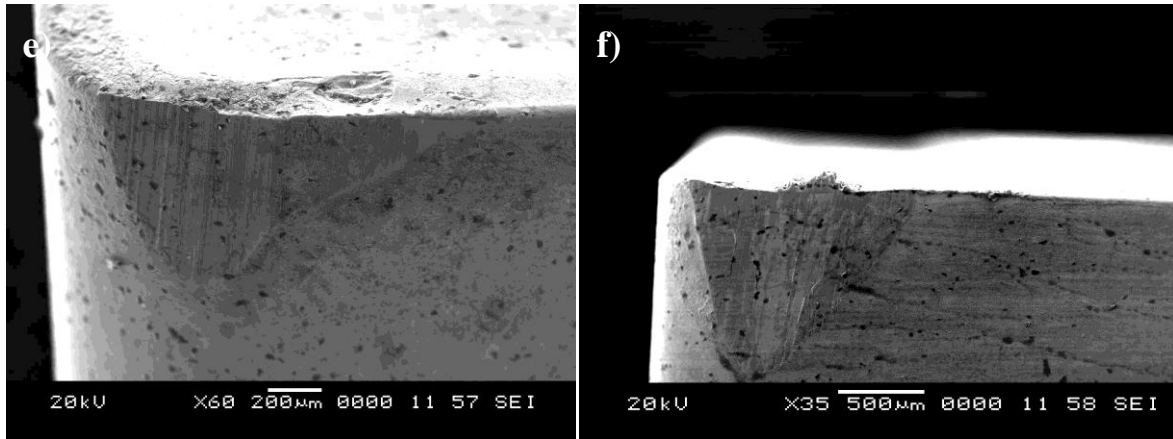
v= 85.21m/min, f =0.143 mm/rev, d=0.6 mm, t =400°C   *v= 85.21m/min, f =0.143 mm/rev, d=0.6 mm,   t =400°C*

Figure 4.2 SEM micrographs of uncoated insert Conventional over hot machining

The tool wear patterns of conventional and thermally assisted machining, this phase mimic the preceding phases wear patterns. The tool wear mechanisms observed in this work are abrasion, adhesion and diffusion. A series of experiments were conducted to analyze these mechanisms at different cutting conditions. The type of wears formed during turning of Inconel 718 is flank wear, chipping and notch. Figure 4.2 illustrate the SEM images of tool wear patterns formed on the flank face of the carbide inserts when turning Inconel 718 workpiece for 4 mins of machining. The different tool wear mechanisms were discussed in the next study.

4.5 EFFECT OF MAIN CUTTING FORCE (F_c), THRUST FORCE (F_t) AND FEED FORCE (F_f)

In order to study the performance of process parameters on main cutting force (F_c), thrust force (F_t) and feed force (F_f), experiments were carried out using L_{27} orthogonal array as shown in Table 3.7 Analysis of variance (ANOVA) is a computational technique used to identify the importance of the process parameters on the output parameters and even to identify the percentage contribution on the output parameters (Ross, 1988 and

73

Table 4.1 Analysis of variance for cutting forces of Inconel 718 machined by uncoated tool.

Source	(DF)	Sum of Square (SS)			Mean squares (MS)			P value			Percentage contribution		
		F_c	F_t	F_f	F_c	F_t	F_f	F_c	F_t	F_f	F_c	F_t	F_f
v	2.00	44570.20	11242.30	11625.60	22285.10	5621.1	5812.80	0.00	0.00	0.00	64.07	65.98	64.75
f	2.00	5695.80	1196.20	1120.20	2847.90	598.08	560.08	0.00	0.00	0.02	8.19	7.02	6.24
d	2.00	1746.40	287.80	292.50	873.20	143.89	146.25	0.06	0.04	0.18	2.51	1.69	1.63
t	2.00	12016.70	3122.90	2818.20	6008.30	1561.4	1409.11	0.00	0.00	0.00	17.28	18.33	15.70
v*f	4.00	3596.40	885.70	1411.70	899.10	221.42	352.92	0.04	0.01	0.03	5.17	5.20	7.86
v*d	4.00	520.30	60.60	125.70	130.10	15.15	31.42	0.61	0.66	0.74	0.75	0.36	0.70
v*t	4.00	338.70	99.10	186.40	84.70	24.77	46.60	0.76	0.47	0.59	0.49	0.58	1.04
Residuals	6.00	1075.80	145.60	373.40	179.30	24.27	62.23						
Total	26.00	44570.20	17040.10	17953.70									

Table 4.2 Analysis of variance for cutting forces of Inconel 718 machined by TiAlN multilayer coated tool.

Source	(DF)	Sum of Square (SS)			Mean squares (MS)			P value			Percentage contribution		
		F_c	F_t	F_f	F_c	F_t	F_f	F_c	F_t	F_f	F_c	F_t	F_f
v	2.00	24746.50	8370.20	8205.50	12373.20	4185.08	4102.73	0.00	0.00	0.00	63.08	66.59	65.29
f	2.00	3146.30	847.50	881.10	1573.20	423.73	440.56	0.01	0.00	0.01	8.02	6.74	7.01
d	2.00	1067.40	229.20	255.00	533.70	114.60	127.49	0.07	0.03	0.14	2.72	1.82	2.03
t	2.00	7137.40	2269.60	1773.80	3568.70	1134.79	886.91	0.00	0.00	0.00	18.19	18.06	14.11
v*f	4.00	1957.80	630.40	1010.00	489.40	157.59	252.51	0.06	0.01	0.03	4.99	5.02	8.04
v*d	4.00	263.80	40.30	78.50	66.00	10.07	19.63	0.71	0.70	0.78	0.67	0.61	0.62
v*t	4.00	185.60	76.50	94.70	46.40	19.13	23.68	0.81	0.44	0.72	0.47		0.75
Residuals	6.00	722.90	106.40	268.30	120.50	17.74	44.71						
Total	26.00	39227.70	12570.00	12566.90									

Table 4.3 Analysis of variance for cutting forces of Inconel 718 machined by TiCN/Al$_2$O$_3$/TiN multilayer coated tool.

Source	(DF)	Sum of Square (SS)			Mean squares (MS)			P value			Percentage contribution		
		F_c	F_t	F_f	F_c	F_t	F_f	F_c	F_t	F_f	F_c	F_t	F_f
v	2.00	27099.1	8404.1	8022.7	13549.6	4202.06	4011.36	0.000	0.000	0.000	63.76	66.16	63.80
f	2.00	3521.8	275.9	811.0	1760.9	137.95	405.50	0.005	0.038	0.024	8.29	2.17	6.45
d	2.00	1015.2	2300.4	198.4	507.6	1150.22	99.19	0.068	0.000	0.240	2.39	18.11	1.58
t	2.00	7403.5	692.3	1949.9	3701.8	173.09	974.96	0.001	0.017	0.003	17.42	5.45	15.51
v*f	4.00	2274.2	61.5	995.6	568.5	15.38	248.89	0.043	0.643	0.049	5.35	0.48	7.92
v*d	4.00	259.9	36.2	113.6	65.0	9.05	28.40	0.702	0.811	0.724	0.61	0.28	0.90
v*t	4.00	230.3	140.2	157.7	57.6	23.37	39.42	0.741		0.606	0.54		1.25
Residuals	6.00	697.8	12701.9	326.0	116.3		54.33						
Total	26.00	42501.8		12574.9									

Phadke, 1989). ANOVA consists of degrees of freedom (DF), sum of squares (SS), mean square (MS), F-ratio (F) and P value. ANOVA was opted to study the significance of process parameters towards the response of cutting forces using uncoated carbide, TiAlN nano multilayer and TiCN/Al$_2$O$_3$/TiN. Table 4.1 shows the analysis of variance of Inconel 718 by using uncoated carbide tool. From Table 4.1 it can be observed that cutting speed (v), feed rate (f) workpiece temperature (t) and interaction effect of cutting speed, feed rate are the significant parameters, while depth of cut (d) was identified it to be as insignificant parameter on main cutting force (F_c). The significance of the individual parameter is decided based on the P-Value. The P-value having less than 0.05 are considered as significant. By calculating the percentage contribution of individual parameters, it shows that cutting speed has a major contribution of 64.07 % followed by workpiece temperature 17.28 %, feed rate 8.19 %, and depth of cut 2.51 % on main cutting force (Fc). The depth of cut having less contribution and considered as less significant.

Table 4.2 shows the analysis of variance for main cutting force (F_c) for Inconel 718 machined by TiAlN multilayer carbide tool. It is observed that cutting speed, feed rate, and workpiece temperature are the significant parameters on the main cutting force (F_c). Depth of cut has no significance on the main cutting force (F_c). In case of TiAlN coated tool the major contribution on the main cutting force (F_c) is cutting speed 63.08 % followed by workpiece temperature of 18.19 %.

Table 4.3 shows the ANOVA for main cutting force (F_c) for Inconel 718 machined by using the TiCN/Al$_2$O$_3$/TiN triple layer carbide tool. It is observed that cutting speed, feed rate and workpiece temperature are the significant parameters on main cutting force (F_c). Depth of cut has no significance on the main cutting force (F_c). In TiCN/Al$_2$O$_3$/TiN coated tool the major contribution on the main cutting force (F_c) is cutting speed of 63.76 % followed by workpiece temperature 15.51 % and feed rate of 6.45 %.

The Figure 4.3 shows the main effect plots for main cutting force (F_c) of Inconel 718 superalloy machined with uncoated carbide tool. From the (Figure 4.3), it can be

concluded that as the cutting force decreases the cutting speed increases. At lower cutting speeds high cutting forces were observed this is due to the low cutting temperature and built up edge formation. Similarly, the higher cutting speeds results in higher cutting temperature in turn reducing the cutting forces, this is due to thermal softening of the workpiece material.

The cutting forces increases as the feed rate increases, this effect is due to large volume of material is to be removed in a same unit time, besides establishing the dynamic effect on the cutting forces. It also leads to corresponding increase in the normal contact stress at the tool chip interface and in the tool chip contact area. Hence cutting forces were found to be increased with the increase in feed rate. The experimental results show that while machining of Inconel 718 superalloy with uncoated carbide tool are slightly higher as compared to TiAN and $TiCN/Al_2O_3/TiN$. It may be due to the influence of tool material composition and thermal properties of the tool. The above results, indicate that, the increase in feed rate in turn increases the cutting force (Fc) thrust force (F_t) and feed force (F_f) for all the cutting tools. From the Figure 4.3 to 4.5, it was observed that as the depth of cut increases the cutting forces increases. This is due to the fact that, increasing depth of cut results in increase in tool workpiece contacts length.

Subsequently, chip thickness becomes significant that causes the growth of the volume of deformed metal and it requires greater cutting forces to cut the chip. The results show a trend that the cutting forces of uncoated cutting tool is higher as compared with TiAlN and $TiCN/Al_2O_3/TiN$ cutting tools. Especially cutting force (F_c) and thrust force (F_t) are dominant followed by the feed force (F_f). The difference between the attained cutting forces is observed in Inconel 718 at higher depth of cut and at higher hardness of the workpiece.

From the Figure 4.3 to 4.5, it was observed that as the workpiece temperature increases the cutting forces decreases drastically. It may be due to the fact that, increase in workpiece temperature results in decrease of shear strength, bulk hardness and microhardness of the material, thus in turn reducing the power required to shear the material. Hence, at lower cutting forces (F_c), thrust force (F_t) and feed force (F_f) in
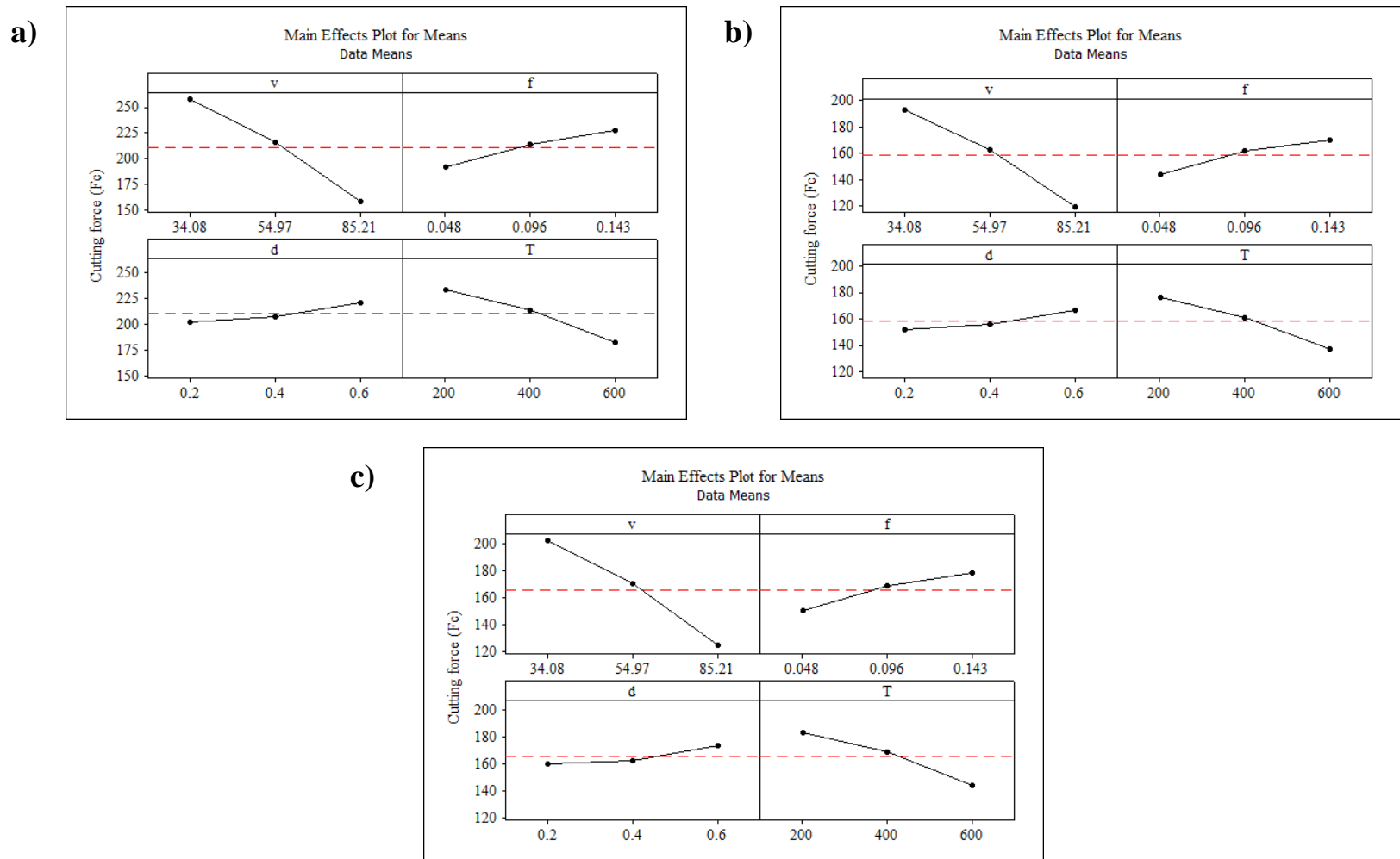
Figure 4.3 Effect of *v, f, d* and *t* on the main cutting force *(Fc)* on Inconel 718 with a) uncoated carbide b) TiAlN multilayer coated carbide and c) TiCN/Al$_2$O$_3$/TiN triple layer coated carbide tool
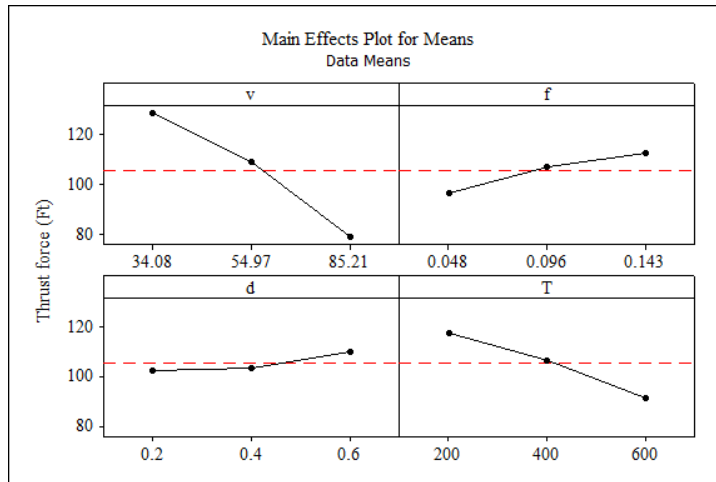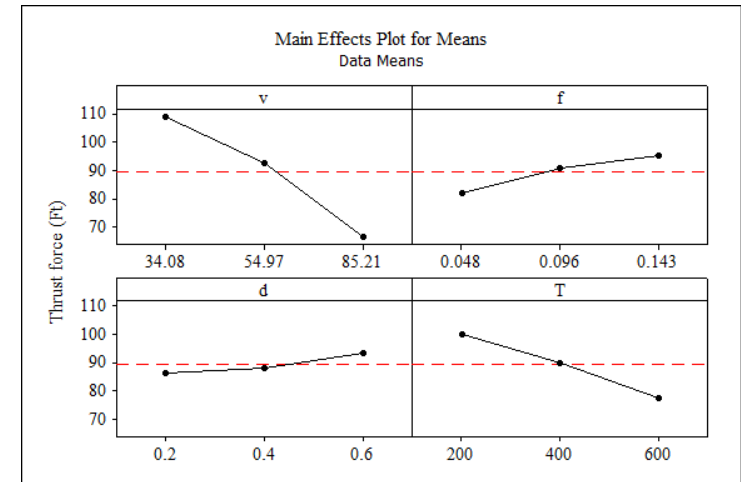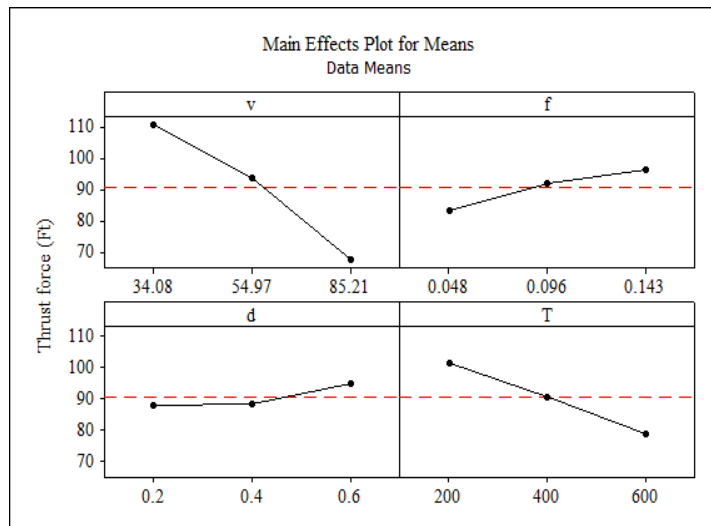
Figure 4.4 Effect of *v, f, d* and *t* on the main thrust force *(Ft)* on Inconel 718 with a) uncoated carbide b) TiAlN multilayer coated carbide and   c) TiCN/Al₂O₃/Tin triple layer coated carbide tool.
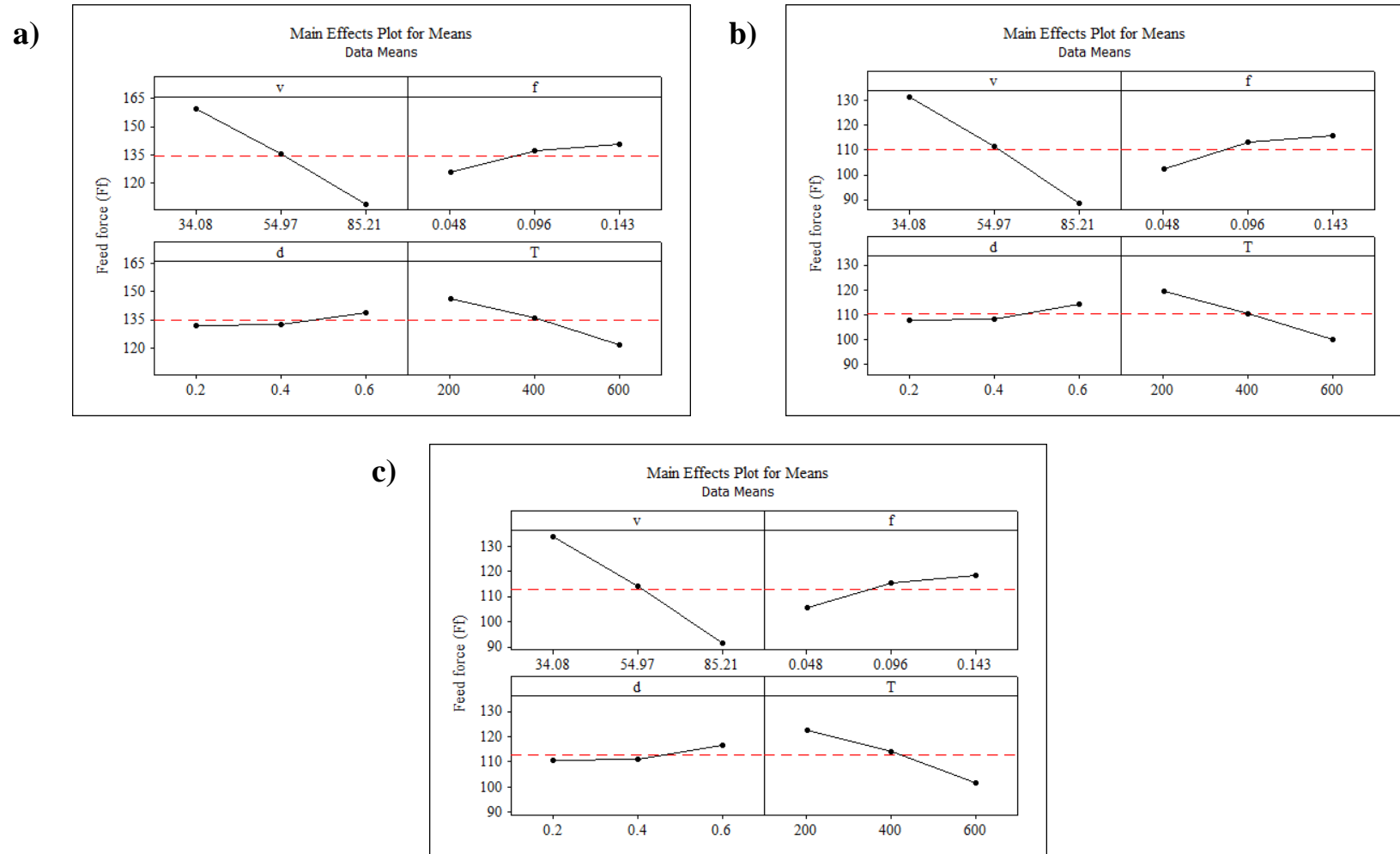
Figure 4.5 Effect of *v, f, d* and *t* on the Feed Force (*F_f*) on Inconel 718 with a) uncoated carbide, b) TiAlN Multilayer Coated Carbide and   c) TiCN/Al₂O₃/TiN Triple layer coated carbide tool

thermally assisted machining of Inconel 718. A similar trend is observed while carrying out the experiments for all the selected cutting tools.

4.6 EFFECT OF PROCESS PARAMETERS ON SURFACE ROUGHNESS (Ra)

To study the individual performance of process parameters on surface roughness (Ra), experiments were carried out using L_{27} orthogonal array as shown in Table A2. In order to study the significance of process parameters towards the response of surface roughness using uncoated carbide, TiAlN nano multilayer, TiCN/Al$_2$O$_3$/TiN ANOVA was performed. Table 4.4 shows the analysis of variance of Inconel 718 by using uncoated carbide tool. From Table 4.4, it can be observed that feed rate (f) and workpiece temperature (t) are the significant parameters and cutting speed (v) and depth of cut (d) are insignificant parameters for surface roughness (Ra). If the attained P-value is less than 0.05, then the parameters are considered as significant parameters else insignificant parameters. By calculating the percentage contribution of individual parameters, it shows that the feed rate has a major contribution of 61.03 % followed by workpiece temperature 16.98 % , cutting speed 1.67 % and depth of cut 0.22 % on surface roughness (Ra). Since, the cutting speed and depth of cut have less contribution, these parameters are considered as insignificant parameters. Table 4.5 shows the analysis of variance for surface roughness for Inconel 718 machined by TiAlN nano multilayer carbide tool. It is observed that workpiece temperature and feed rate are the significant parameters on the surface roughness (Ra). Cutting speed and depth of cut has no significance on the surface roughness (Ra). In TiAlN coated tool the major contribution on the surface roughness is feed rate 61.67 % followed by workpiece temperature 22.55 %.

Table 4.6 shows the analysis of variance for surface roughness for Inconel 718 machined by TiCN/Al$_2$O$_3$/TiN triple layer carbide tool. It is observed that workpiece temperature, feed rate are the significant parameters on the surface roughness (Ra). Cutting speed and depth of cut have no significance on the surface roughness (Ra). In TiCN/Al$_2$O$_3$/TiN coated tool the major contribution on the surface roughness is feed rate 62.15 % followed by workpiece temperature 21.47 %.

Figure 4.6 shows the main effect plots for surface roughness (Ra) of Inconel 718 superalloy machined with uncoated carbide tool. It is observed from the main effect plot (Figure 4.6) that the surface roughness increases with increase in feed rate and depth of cut, and it decreases with increase in cutting speed and workpiece temperature. The cutting speed can be observed to have diminishing effect on surface roughness which can be attributed to increase in cutting zone temperature thereby thermal softening the material, thus causing decrease in surface roughness (Ravi et al., 2014). Considering the feed rate and depth of cut, it is observed that the parameters are complimenting the surface roughness. The feed trend is commonly observed in machining research and the effect is ascribed to the prominent effect of tool profile marks on machined surface resulting in poor surface finish (Pramanik et al., 2003). The effect is due to shift of material towards brittle mode machining at high feed rate. Cutting forces and contact area increases with increase in depth of cut resulting in enhancement of surface deformation thus increasing surface roughness. With increase in workpiece temperature the surface roughness is observed to attain decreasing trend and most significant effect

Table 4.4 Analysis of Variance for Surface roughness (Ra) of Inconel 718
(Uncoated tool)

Source	DF	SS	MS	F	P	Remark	P %
v	2	0.031	0.015	0.29	0.757	In significant	
f	2	4.975	2.487	46.24	0.000	Significant	65.36
d	2	0.137	0.068	1.28	0.344	In significant	
t	2	1.450	0.725	13.48	0.005	Significant	19.05
v*f	4	0.417	0.104	1.94	0.223	In significant	
v*d	4	0.081	0.020	0.38	0.817	In significant	
v*t	4	0.194	0.048	0.91	0.516	In significant	
Residual Error	6	0.322	0.053				
Total	26	7.611					

Table 4.5 Analysis of Variance for Surface roughness (Ra) of Inconel 718
(TiAlN Nano multilayer coated tool)

Source	DF	SS	MS	F	P	Remark	P %
v	2	0.048	0.024	1.86	0.235	In significant	
f	2	2.935	1.467	112.85	0.000	Significant	63.58
d	2	0.281	0.140	10.82	0.010	Significant	6.08
t	2	1.095	0.547	42.12	0.000	Significant	23.72
v*f	4	0.048	0.012	0.94	0.503	In significant	
v*d	4	0.031	0.007	0.61	0.668	In significant	
v*t	4	0.096	0.024	1.85	0.239	In significant	
Residual Error	6	0.078	0.013				
Total	26	4.616					

Table 4.6 Analysis of Variance for Surface roughness (Ra) of Inconel 718
(TiCN/Al$_2$O$_3$ /TiN Triple layer coated tool)

Source	DF	SS	MS	F	P	Remark	P %
v	2	0.064	0.032	1.85	0.237	In significant	
f	2	3.470	1.735	97.80	0.000	Significant	64.10
d	2	0.280	0.140	7.91	0.021	Significant	5.17
t	2	1.232	0.616	34.72	0.001	Significant	22.76
v*f	4	0.079	0.019	1.13	0.426	In significant	
v*d	4	0.034	0.008	0.49	0.746	In significant	
v*t	4	0.142	0.035	2.01	0.212	In significant	
Residual Error	6	0.106	0.017				
Total	26	5.413					
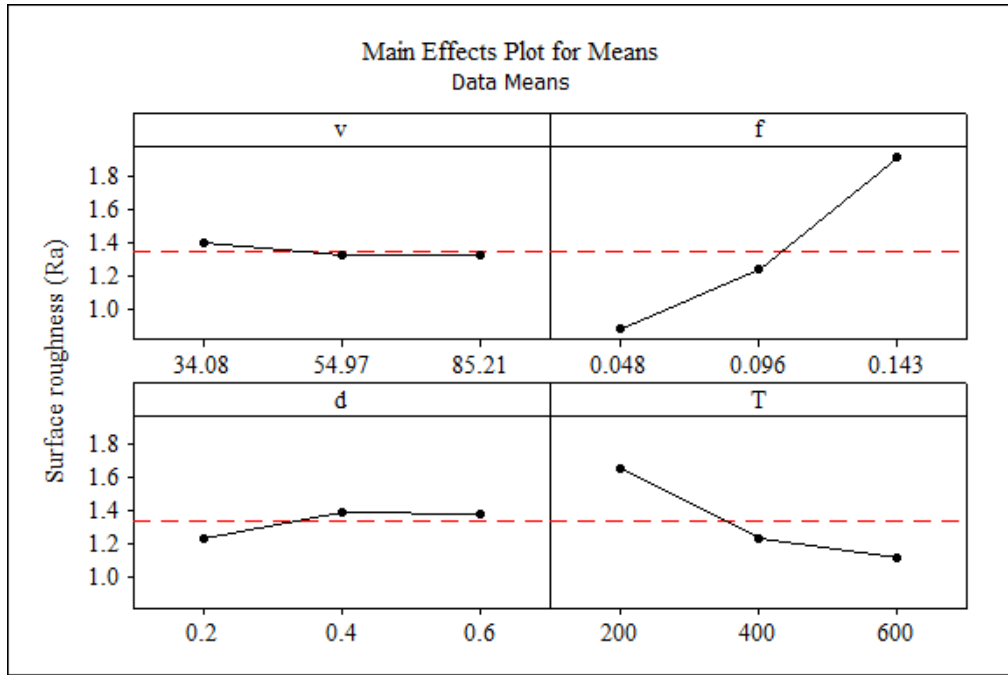
Figure 4.6 Effect of process parameters on surface roughness of Inconel 718 machined with uncoated carbide tool.
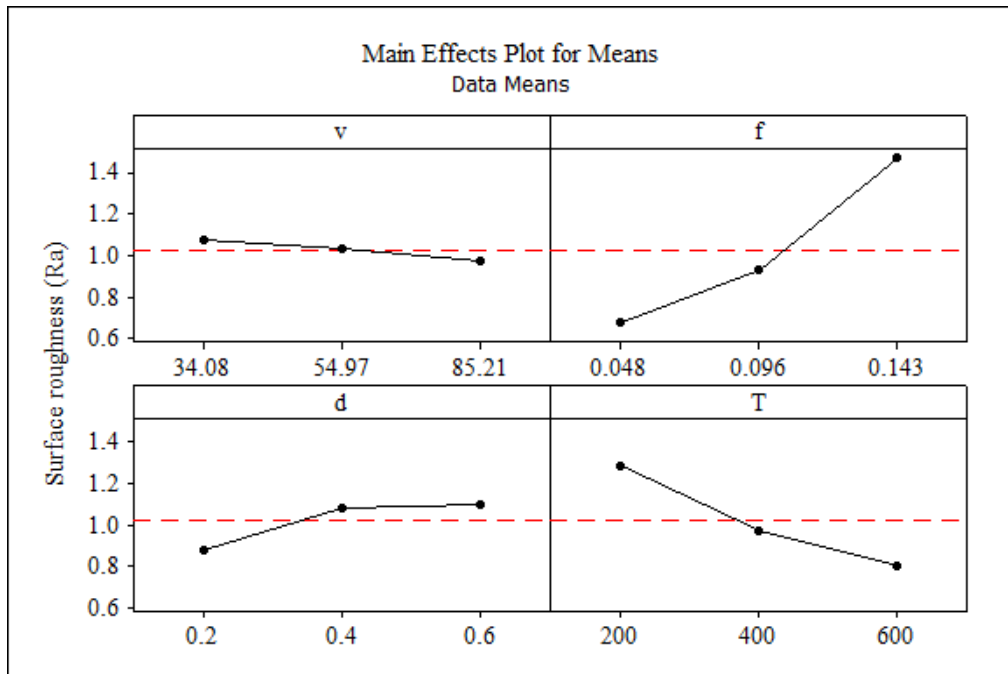
Figure 4.7 Effect of process parameters on surface roughness of Inconel 718 machined with TiAlN multilayer coated carbide tool.

Figure 4.8 Effect of process parameters on surface roughness of Inconel 718 machined with TiCN/Al$_2$O$_3$ /TiN Triple layer coated tool.

after feed rate**.** The reason might be, the reduction in surface roughness is due to reduction in workpiece material hardness leading to smoother removal of chip from the surface because of lower chip rupture stress. The same trend is also observed from the TiAlN nano multilayer coated tool and TiCN/Al$_2$O$_3$/TiN triple layer coated tool as shown in Figure 4.7 and 4.8. Figure 9 shows the machined surface SEM images of three different cutting tools.
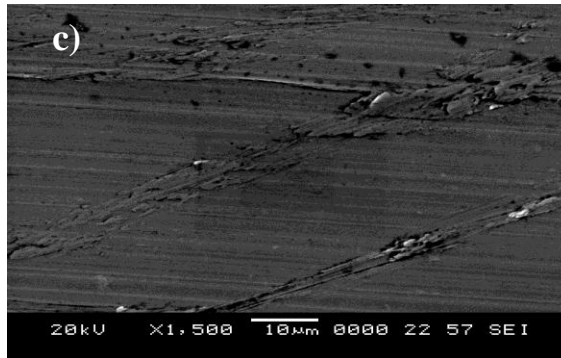
Figure 4.9 SEM Micrographs shows the surface topography TAM of Inconel 718

a) Uncoated carbide tool   b) TiAlN coated carbide tool

c) TiCN/Al$_2$O$_3$/TiN coated carbide tool

4.7 EFFECT OF PROCESS PARAMETERS ON TOOL WEAR

The main purpose of ANOVA is to identify the effect of individual parameters. Table 4.7 to 4.9 shows that analysis of variance with tool wear for Inconel 718 superalloy machined by uncoated, TiAlN multilayer and TiCN/Al$_2$O$_3$/TiN triple layer coated tools. The analysis is carried out for 5 % significance level, i.e., 95 % confidence level.   From Table 4.7 it can be concluded that cutting speed, feed rate, interaction effect of cutting speed and feed rate are the most significant parameters. The depth of cut and workpiece temperature not having much significant effect on the tool wear. Calculated F values are represented in are more the table value (Annexure I): $F_{0.05,2,16} = 3.63$ at 95 % confidence level. From the Table 4.8 and 4.9 major influencing factors are cutting speed followed by feed rate and depth of cut. The cutting speed has 62.99 % contribution on the tool wear and feed rate with 21.66 % by using uncoated carbide tool. The cutting speed has contribution 68.52 % on tool wear by using TiAlN multilayer coated carbide tool. While performing the machining with TiCN/Al$_2$O$_3$/TiN triple layer coated tool, the cutting speed has 62.50 % and feed rate of 16.66 % contributions respectively on the tool wear. Similarly depth of cut, interaction effect of cutting speed and feed rate have less significant effect while performing with uncoated and TiCN/Al$_2$O$_3$/TiN triple layer

coated tools. Similarly in case of the TiAlN multilayer coated carbide tool depth of cut with 3.66 %, interaction effect of cutting speed and feed rate with 5.66 % for machining of Inconel 718.

Figure 4.10 to 4.12 represents the main effect plots for tool wear of Inconel 718 superalloy machining from three different cutting tools. It indicates that the higher value of cutting speed yields in higher tool wear due to the increase in rubbing action between tool and workpiece in turn increasing the cutting speed, by shooting the interface local temperature to a higher value in very short time. This high temperature and stresses induced at the cutting zone leads to thermal softening of tool material and thus enhancing the tool wear. From the main effect plots it was observed that the mean value of tool wear of 0.48 mm is obtained at higher cutting speed by using uncoated tool and 0.28 mm mean value of tool wear was attained by using TiAlN multilayer coated tool. Similarly, mean value of tool wear of 0.32 mm was achieved by using the $TiCN/Al_2O_3/TiN$ triple layer carbide tool during machining Inconel 718.

As seen from the main effect plot of tool wear (Figure 4.10 to 4.12), at lower values of feed rate of the attained tool wear is very less, this is due to the less contact area between tool and the workpiece. In another case, the increase in higher feed rate yields high temperature and stresses at the cutting zone. Thus reducing yield strength of the tool material and enhances wear (Lee and Mathew, 2007).

While the depth of cut has very less influence on tool wear. Higher depth of cut causes high specific contact stress at the tool chip interface and thus has minor effect on average contact temperature (Astakhov, 2004) causing increase in tool wear. As observed from the Figure 4.10 to 4.12, at lower workpiece temperature of 200 $^\circ$C the heat generated between tool and the workpiece is very high which leads to severe tool wear. If further the temperature of the workpiece is increased to 600 $^\circ$C the tool wear decreases this is due to the reduction of shear strength of the workpiece material in the vicinity of the shear zone. Thus leading to reduction in the cutting forces and flank wear and even it leads o the thermal softening of workpiece in turn decreasing the friction between tool and chip, thus reducing the flank wear.

Table 4.7 Analysis Of Variance for Tool wear of Inconel 718
(Uncoated tool)

Source	DF	SS	MS	F	P	Remark	P %
v	2	0.303	0.151	63.59	0.000	Significant	62.99
f	2	0.104	0.052	21.80	0.002	Significant	21.62
d	2	0.003	0.001	0.70	0.532	In significant	0.006
t	2	0.003	0.001	0.80	0.494	In significant	0.006
v*f	4	0.045	0.011	4.74	0.046	Significant	0.09
v*d	4	0.004	0.001	0.49	0.747	In significant	0.08
v*t	4	0.002	0.000	0.24	0.907	In significant	0.004
Residual Error	6	0.014	0.002				
Total	26	0.481					

Table 4.8 Analysis of Variance for Tool wear of Inconel 718
(TiAlN Nano multilayer coated tool)

Source	DF	SS	MS	F	P	Remark	P %
v	2	0.109	0.054	109.87	0.000	Significant	68.52
f	2	0.025	0.012	25.72	0.001	Significant	16.03
d	2	0.005	0.002	5.47	0.044	Significant	3.36
t	2	0.000	0.000	0.59	0.586	In significant	0.36
v*f	4	0.009	0.002	4.54	0.050	Significant	5.66
v*d	4	0.001	0.000	0.63	0.659	In significant	0.78
v*t	4	0.005	0.001	2.67	0.136	In significant	3.33
Residual Error	6	0.003	0.000				
Total	26	0.160					

Table 4.9 Analysis of Variance for Tool wear of Inconel 718
(TiCN/Al$_2$O$_3$ /TiN Triple layer coated tool)

Source	DF	SS	MS	F	P	Remark	P %
v	2	0.090	0.045	152.81	0.000	Significant	62.50
f	2	0.024	0.012	41.21	0.000	Significant	16.66
d	2	0.008	0.004	14.55	0.005	Significant	0.05
t	2	0.001	0.000	3.15	0.116	In significant	0.006
v*f	4	0.007	0.001	6.04	0.027	Significant	0.04
v*d	4	0.004	0.001	3.56	0.081	In significant	0.02
v*t	4	0.006	0.001	5.10	0.039	Significant	0.04
Residual Error	6	0.001	0.000				
Total	26	0.144					
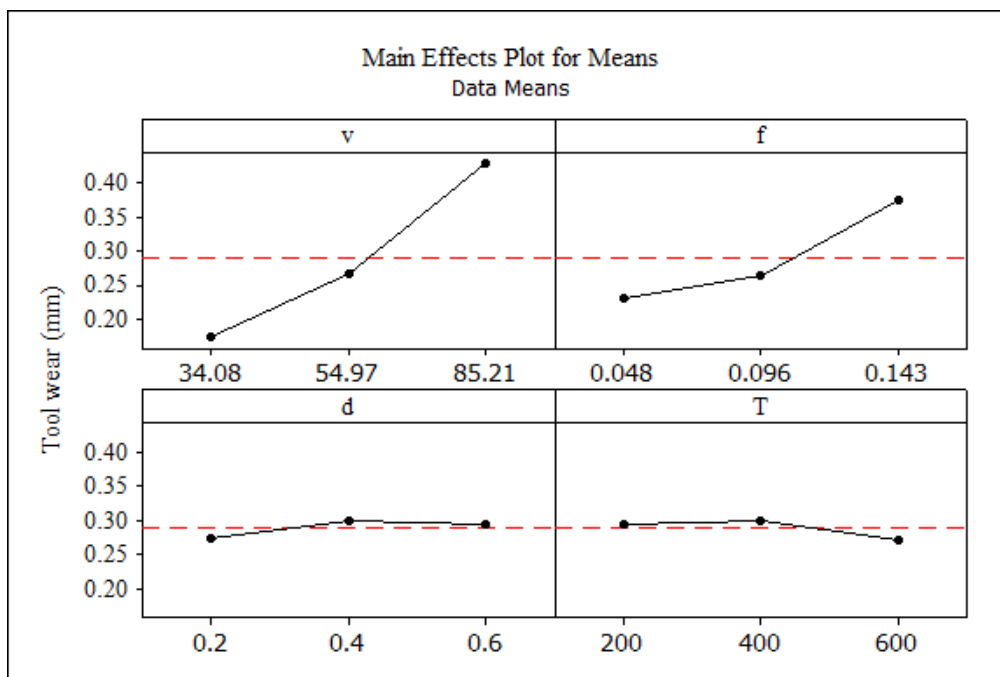
Figure 4.10 Effect of process parameters on tool wear of Inconel 718 machined with uncoated carbide tool.
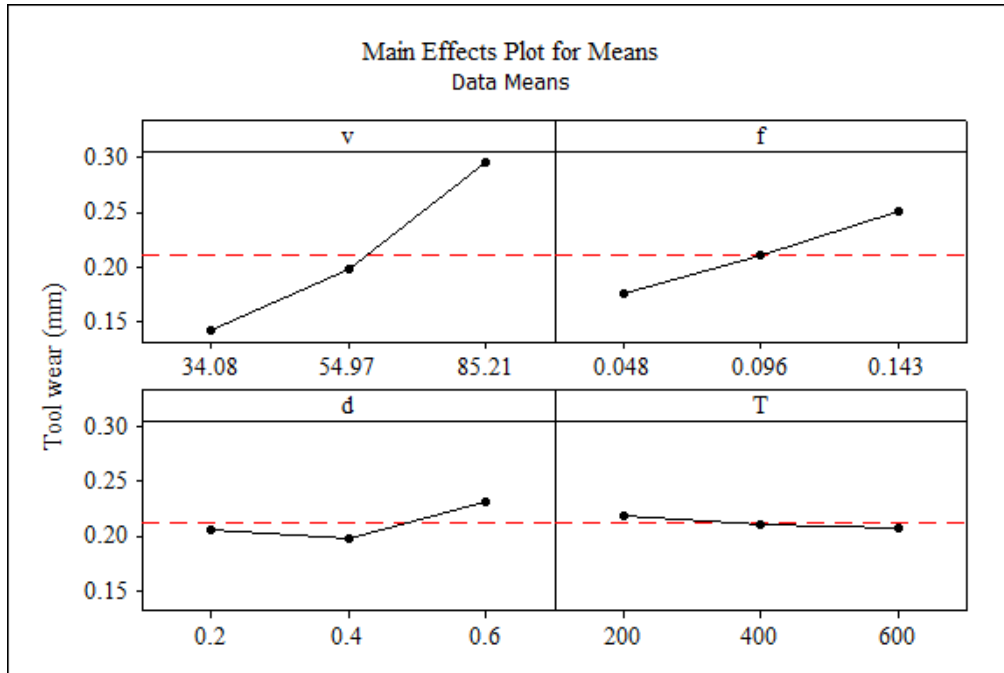
Figure 4.11 Effect of process parameters on tool wear of Inconel 718 machined with TiAlN multilayer carbide tool.
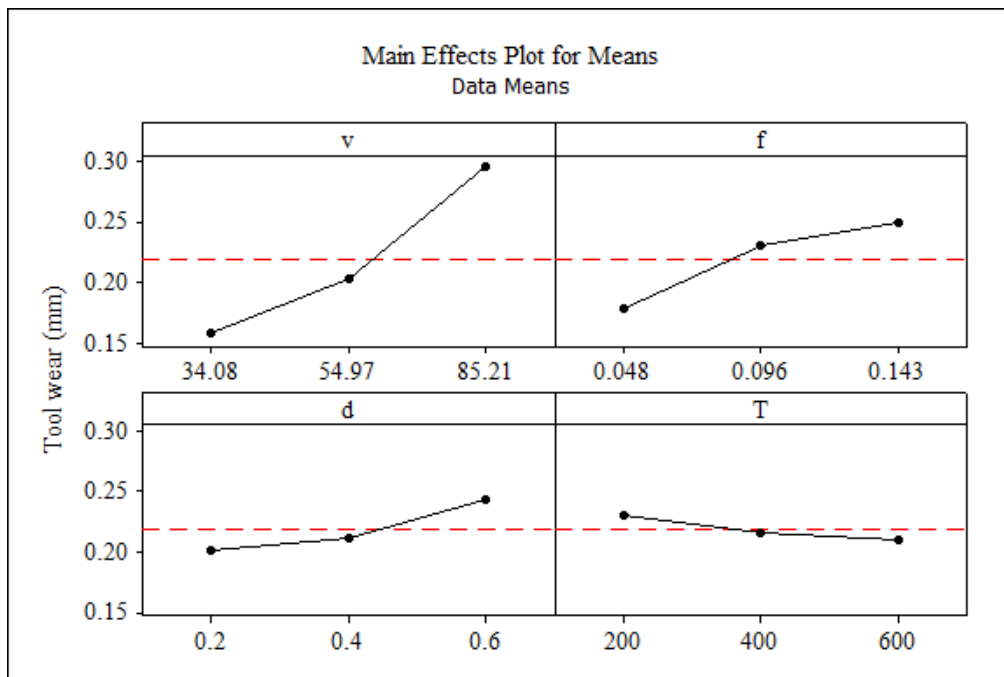
Figure 4 .12 Effect of process parameters on tool wear of Inconel 718 machined with TiCN/Al$_2$O$_3$/TiN triple layer carbide tool.

4.8 EFFECT OF PROCESS PARAMETERS ON MRR

The main purpose of ANOVA is to identify the effect of individual parameters. Table 4.10 to 4.12 shows that analysis of variance with MRR for Inconel 718 superalloy machined by uncoated, TiAlN multilayer and TiCN/Al$_2$O$_3$/TiN triple layer coated tools. The analysis is carried out for 5 % significance level, i.e. 95 % confidence level. From Table 4.10 to 4.12 it can be concluded that cutting speed, feed rate, depth of cut and interaction effect of cutting speed and depth of cut are most significant parameters. The workpiece temperature not having much significant effect on the MRR. Calculated F values are more the table value (Annexure I): $F_{0.05,2,16}$ = 3.63 at 95 % confidence level. From the Table 4.10 to 4.12 major influencing factors is cutting speed, feed rate and depth of cut. The cutting speed with 50.37 % followed by feed rate of 14.49 %, depth of cut of 25.33 % and interaction effect of cutting speed and depth of cut with 7.77 % contributions respectively on the MRR by using uncoated carbide tool. While performing with TiAlN multilayer coated carbide tool the cutting speed with 51.07 %, feed rate of 14.97 %, depth of cut of 24.27 % and interaction effect of cutting speed and depth of cut 7.66 % have respective contributions on MRR. While machining with TiCN/Al$_2$O$_3$/TiN triple layer coated tool, cutting speed 51.01 %, feed rate of 15.24 %, depth of cut of 24.15 % and interaction effect of cutting speed and depth of cut 7.57 % contributions on MRR response. Similarly, interaction effect of cutting speed and feed rate and cutting speed and workpiece temperature have very less significant effect on all the cutting tools. From Figure 4.13 to 4.15 the results shows that cutting speed, feed rate and depth of cut is are more significant parameters, as the speed and feed increases the MRR increases this is due to more volume of chips generated during machining. As depth of cut increases from 0.2 to 0.6 mm MRR increases due to the amount of material is removed during machining. From Figure 4.13 to 4.15 the results shows that workpiece temperature has less significant on metal removal rate, as the workpiece temperature increases the metal removal rate increases due to fact that while heating the material, the chip reduction coefficient reduces with increase in temperature. Hence the machinability of the material improves with increase in temperature

91

Table 4.10 Analysis of Variance for MRR of Inconel 718
(uncoated tool)

Source	DF	SS	MS	F	P	Remark	P %
v	2	440.401	220.201	23.46	0.000	Significant	50.37
f	2	126.758	63.379	64.32	0.000	Significant	14.49
d	2	221.475	110.379	112.73	0.000	Significant	25.33
t	2	2.514	1.257	1.28	0.345	In significant	---
v*f	4	7.823	1.956	1.98	0.216	In significant	---
v*d	4	68.005	17.001	17.25	0.002	Significant	7.77
v*t	4	1.243	0.311	0.32	0.858	Insignificant	---
Residual Error	6	5.913	0.985				
Total	26	874.310					

Table 4.11 Analysis of Variance for MRR of Inconel 718
(TiAlN nano multilayer cutting tool)

Source	DF	SS	MS	F	P	Remark	P %
v	2	434.345	217.173	194.58	0.000	Significant	51.07
f	2	127.327	63.664	57.04	0.000	Significant	14.97
d	2	206.431	103.216	92.48	0.000	Significant	24.27
t	2	1.539	0.769	0.69	0.538	In significant	---
v*f	4	7.691	1.923	1.72	0.263	In significant	---
v*d	4	65.165	16.291	14.60	0.003	Significant	7.66
v*t	4	1.253	0.313	0.28	0.880	Insignificant	
Residual Error	6	6.697	1.116				
Total	26	850.448					

Table 4.12 Analysis of Variance for MRR of Inconel 718
(TiCN/Al₂O₃/TiN nano multilayer cutting tool)

| Source	DF	SS	MS	F	P	Remark	P %
v	2	431.575	215.788	195.38	0.000	Significant	51.01
f	2	128.956	64.478	58.38	0.000	Significant	15.24
d	2	204.326	102.163	92.50	0.000	Significant	24.15
t	2	1.608	0.804	0.73	0.521	In significant	---
v*f	4	7.668	1.917	1.74	0.260	In significant	---
v*d	4	64.099	16.025	14.51	0.003	Significant	7.57
v*t	4	1.114	0.279	0.25	0.898	Insignificant	---
Residual Error	6	6.627	1.104				
Total	26	845.973					100
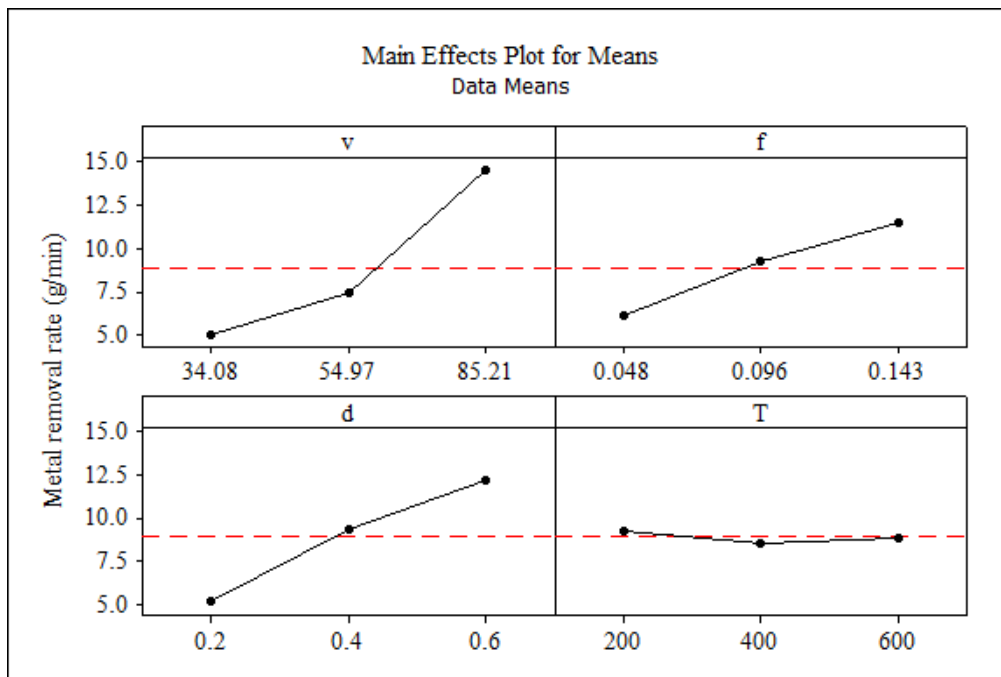
Figure 4.13 Effect of process parameters on metal removal rate of Inconel 718 machined with uncoated carbide tool.
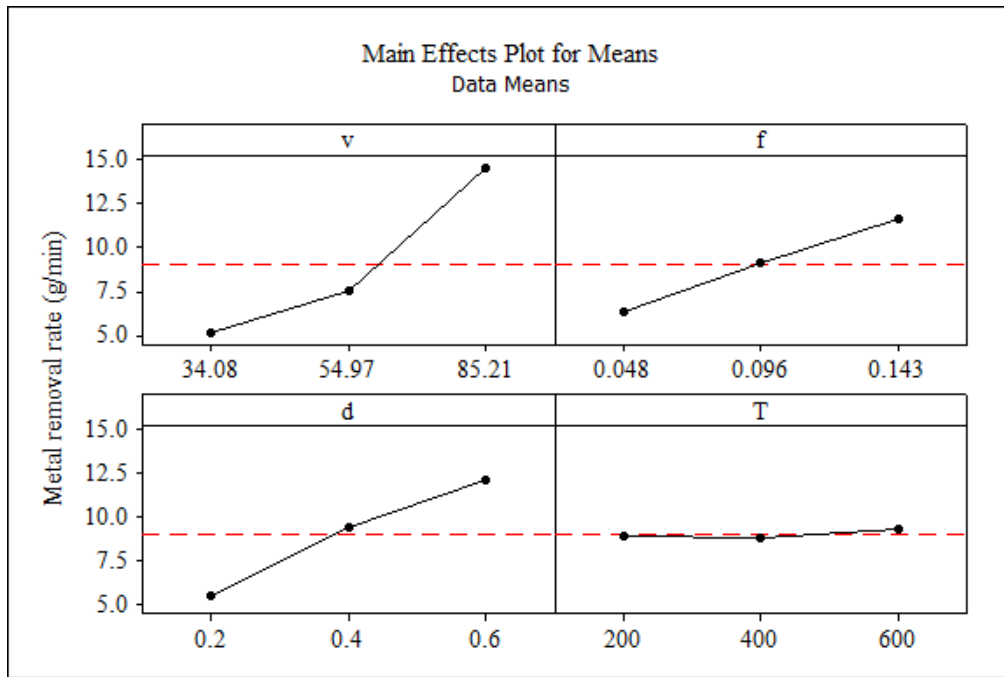
Figure 4.14 Effect of process parameters on metal removal rate of Inconel 718 machined with TiAlN multilayer carbide tool.
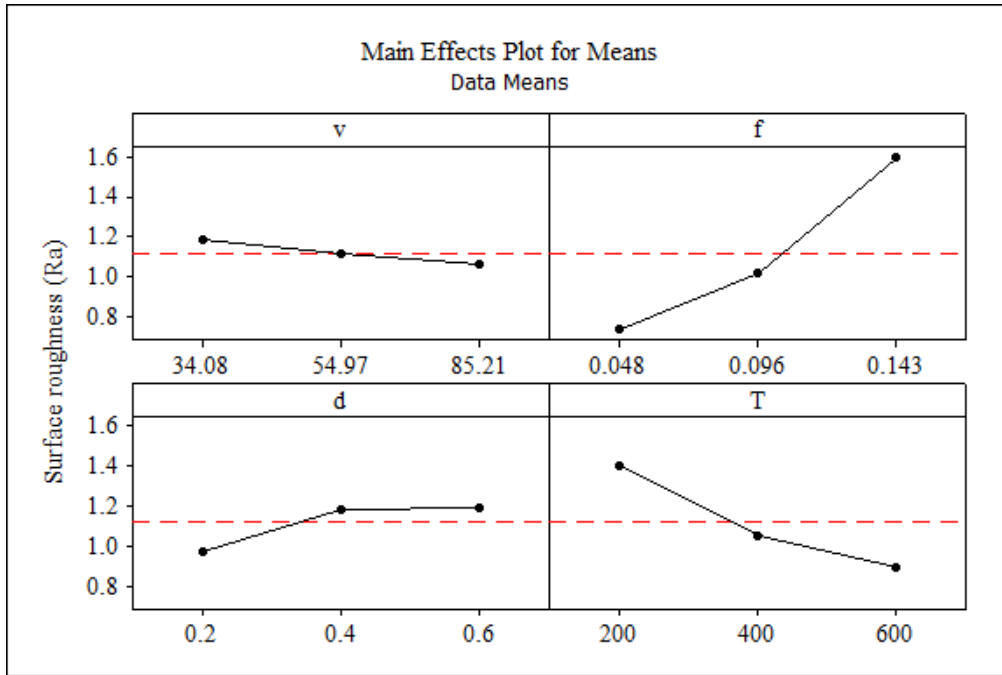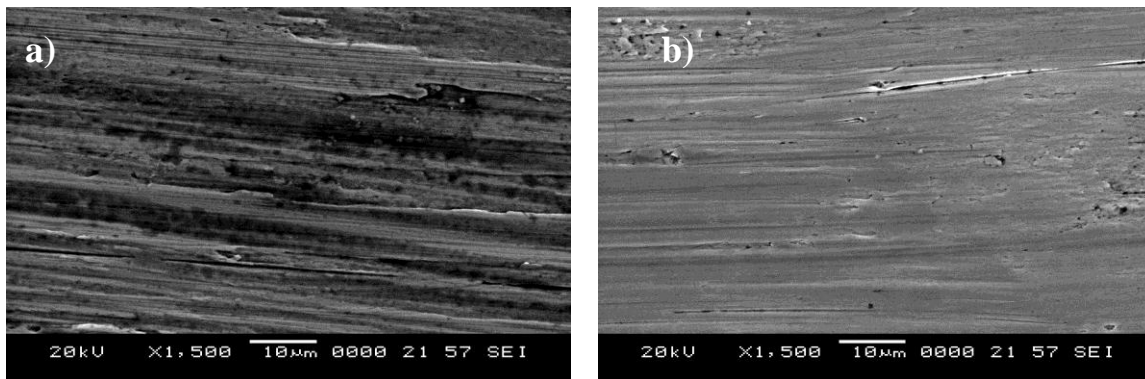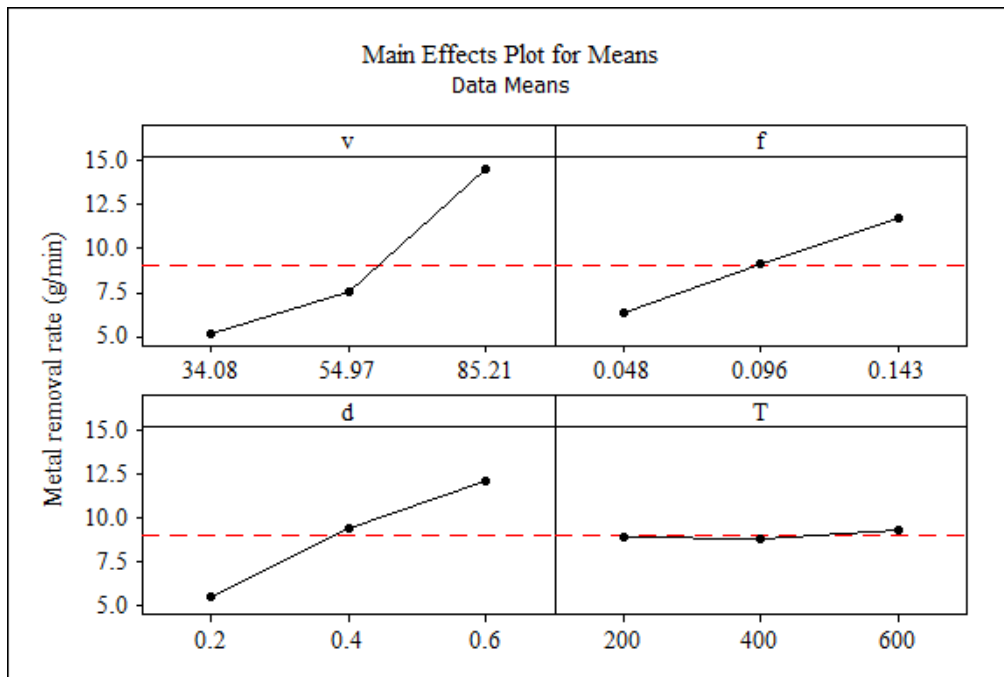

Figure 4.15 Effect of process parameters on metal removal rate of Inconel 718 machined with TiCN/Al$_2$O$_3$/TiN triple layer carbide tool .

4.9 TOOL WEAR MECHANISMS

Tool wear is a phenomenon caused due to mechanical and chemical process. Tool wear basically differs the tool from its original shape during machining, thus resulting steady loss of tool material. The wear mechanism for a particular tool failure mode can vary based on the cutting parameters (feed rate, depth of cut, cutting speed, and workpiece temperature), geometry of tool used, and material types. During machining there are different wear mechanisms which take place mainly attrition (adhesion), abrasion (abrasive), oxidation wear and diffusion wear (Trent and Wright 2000). Abrasion wear prevails at low cutting speeds and at low tool-chip interface temperature when sliding conditions prevail. It is caused by hard particles or asperities at the tool workpiece interface during the relative motion between the tool surface and the workpiece surface (Liu et al., 2011). This mechanical wear causes severe wear on rake, flank face and depth of cut notch. As the cutting speed increases abrasive wear increases (Lima et al., 2005). Adhesion wear occurs when tool material is removed from the tool surface when the adhesive junction in the tool material or coating breaks. The tool rake surface can deteriorate fast during adhesive wear. If the cutting speed is further increased, the adhesion wear effect can be reduced. Chemical wear occurs at a high temperature which causes diffusion of material from tool surface to chip and vice versa. The contact conditions can change fast because of chemical diffusion that can lead to tool failure (Wang et al., 2002). Oxidation wear were observed due to the presence of air, high temperature and high cutting speed. Chemical reaction can observed at tool-work interface which causes weakened the cutting tool.

In this study, TAM machining of Inconel 718 superalloy with uncoated carbide, TiAlN PVD multilayer coated carbide and $TiCN/Al_2O_3/TiN$ CVD triple layer coated carbide tools were conducted at different machining conditions. The coated carbide inserts, have a multilayer coating (Ti,Al,N) on tungsten carbide substrate. The coating produced by physical vapor deposition (PVD) process can with stand high temperatures. The extraction of aluminium from the TiAlN lattice leads in formation of oxide layer of Al_2O_3. The performance of this protective layer is further enhanced by the high hot

hardness and oxidation resistance properties (due to the formation of an intermediate layer comprised of titanium, aluminum, oxygen, and nitrogen during machining). The TiCN/Al$_2$O$_3$/TiN coating by chemical vapour deposition process (CVD), TiN for heat resistance and with low coefficient of friction, TiCN for wear resistance and thermally stable and Al$_2$O$_3$ for heat and crater wear resistance. The combined top coating and gradient substrate provide extremely good behavior during dry machining (Park et al., 2010). To study the wear mechanism on the flank, nose (corner) and rake surface, a series of turning tests were performed at constant time of 4 minutes, where each experiment was starting from a fresh insert corner. The type of wear will be analyzed using optical microscopy and SEM analysis.

4.9.1 Wear mechanism at low machining conditions
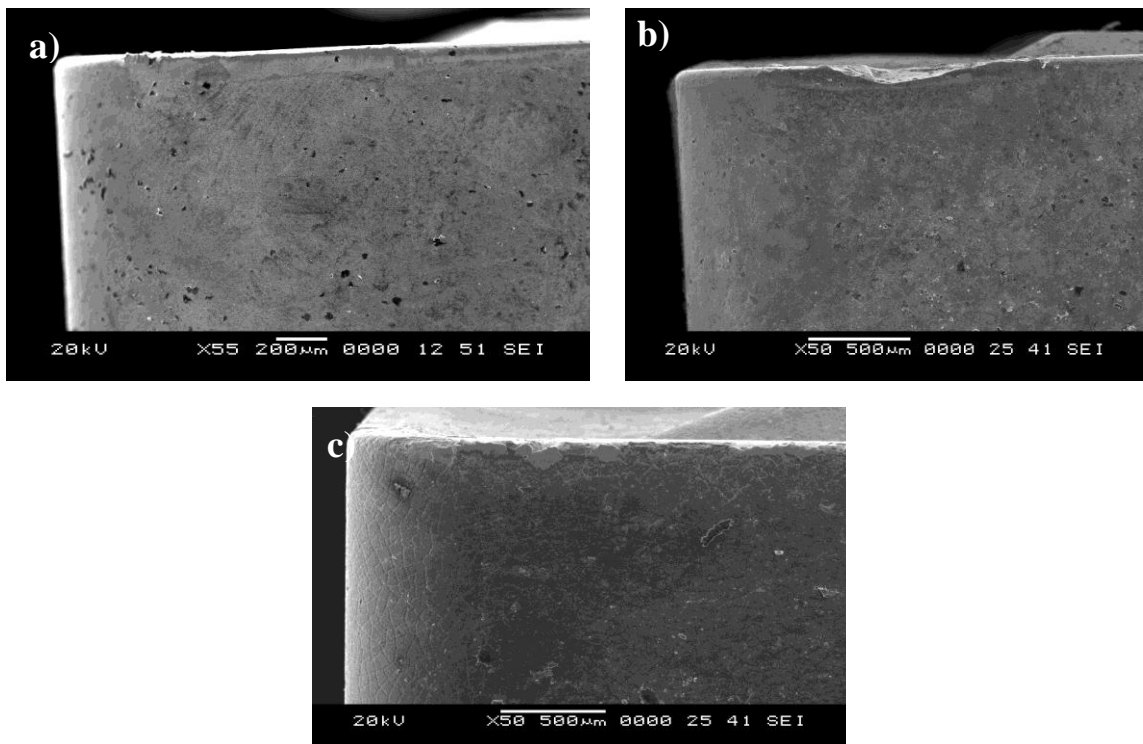
Figure 4.16 SEM images at v = *34.08 m/min, f= 0.048 mm/rev, d= 0.2 mm* and *t = 200 ^{o}C* a) uncoated b) TiAlN c) TiCN/Al$_2$O$_3$/TiN cutting tools.

96

Figure 4.16 shows the worn surfaces of uncoated carbide tool in the machining of Inconel 718 superalloy for cutting time of 4 min. The SEM examination showed that tool material has been removed on the flank face of the cutting tool. It can be observed that the smooth and clean abrasive grooves on the worn area shows that tool were uniformly abraded. These grooves are oriented along the speed direction. The latter seems to be the results of high abrasive wear. Grooves usually appear at the beginning of the machining and never disappear. It indicates that abrasive wear was the main mechanisms of wear which results in the formation of abrasive marks on the cutting tool. Similar phenomenon was observed by (Bhatt et al., 2010).

From the above discussion it is clear that wear mechanisms occurred initially. At low cutting speed of 34.08 m/min, feed rate 0.048 mm/rev, depth of cut 0.2 mm and workpiece temperature 600 ^{o}C tool wear mechanisms observed were abrasive wear and adhesive wear on flank face of on all the cutting tools. The abrasive wear is occurred due to the hard carbide particles and impurities present within the workpiece material, such as carbon nitride and other oxide components, as well as, built-up fragments. The adhesive wear is due to the high temperature and pressures were developed at the cutting zone, which causes welding to occur between the clean fresh surface of the chip and the rake face. The common tool wear mechanism was observed for all the three tools was flank wear. In TiCN/Al$_2$O$_3$/TiN tool has observed another tool wear approach was observed; flaking of the cutting tool, the depth of cut notch wear is also observed on the tool.

4.9.2 Wear mechanism at medium machining conditions

The tool wear mechanisms studied at medium cutting speed at 50 m/min, feed rate at 0.096 mm/rev, depth of cut at 0.4 mm and workpiece temperature at 400 ^{o}C. Figure 4.16 shows the tool wear mechanisms of all the three cutting tools. The tool wear mechanisms observed for all the three cutting tools is similar to low cutting speeds. But in case of TiCN/Al$_2$O$_3$/TiN cutting tool, a diffusion wear mechanism and extreme chipping of the cutting edge was identified (Abhay Bhatt et al.,2010). The reason for the cause of the extreme chipping is due to the tangling of the chips. The tangling of the chips in turn

increases the vibration level. In Inconel 718 at higher cutting speeds, the uncoated cutting tool did not perform at greater
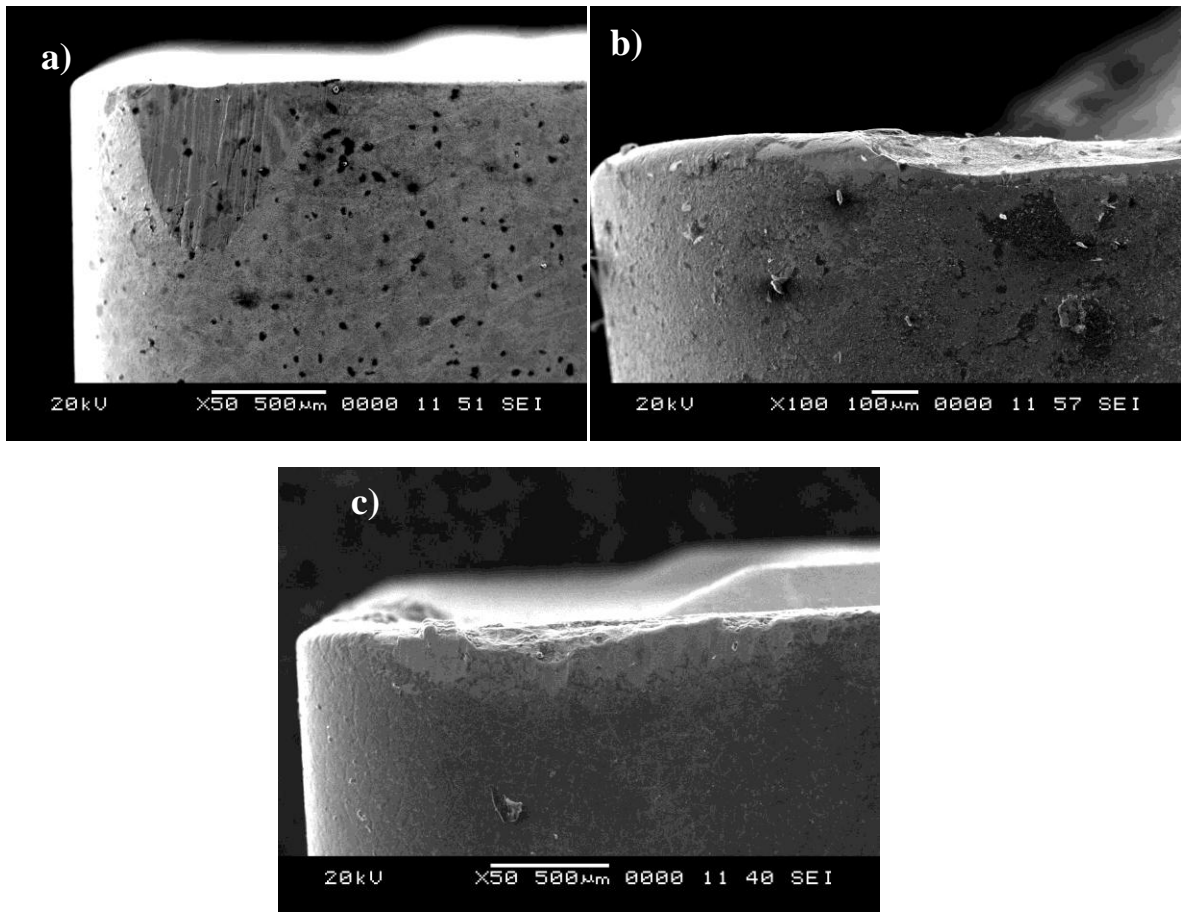
Figure 4.17 SEM images at *v= 50 m/min, f= 0.096 mm/rev, d= 0.2 mm and t = 400 ^{o}C*
a) uncoated b) TiAlN c) TiCN/Al$_2$O$_3$/TiN cutting tools.

excellence due to the plastic deformation of the cutting edge and thermal softening of the cobalt binder phase. However, the TiAlN coated tool was able to with stand the levels of temperature and stresses resulted at the cutting speed of 34.58 m/min and feed rate in the range of 0.048–0.143 mm/rev. The reason for excellence performance of TiAlN is due to the formation of the protective layer (oxide layer of Al$_2$O$_3$) which is formed when the aluminium get extracted from lattice of TiAlN and get exposed to air. The other factor that led to the high performance of the TiAlN coating is the incidence of compressive

residual stresses and their beneficial ability in retarding abrasive wear and depth of cut notching.

4.9.3 Wear mechanism at higher machining conditions

The tool wear mechanism also investigated at higher cutting speeds 85 m/min feed rate at 0.143 m/min, depth of cut at 0.6 mm and workpiece temperature at 600°C. The SEM images of all the three tools are shown in Figure 4.18. As expected that tool wear was high at higher cutting speeds. Again, for all the three tools abrasive, adhesive wear was observed.
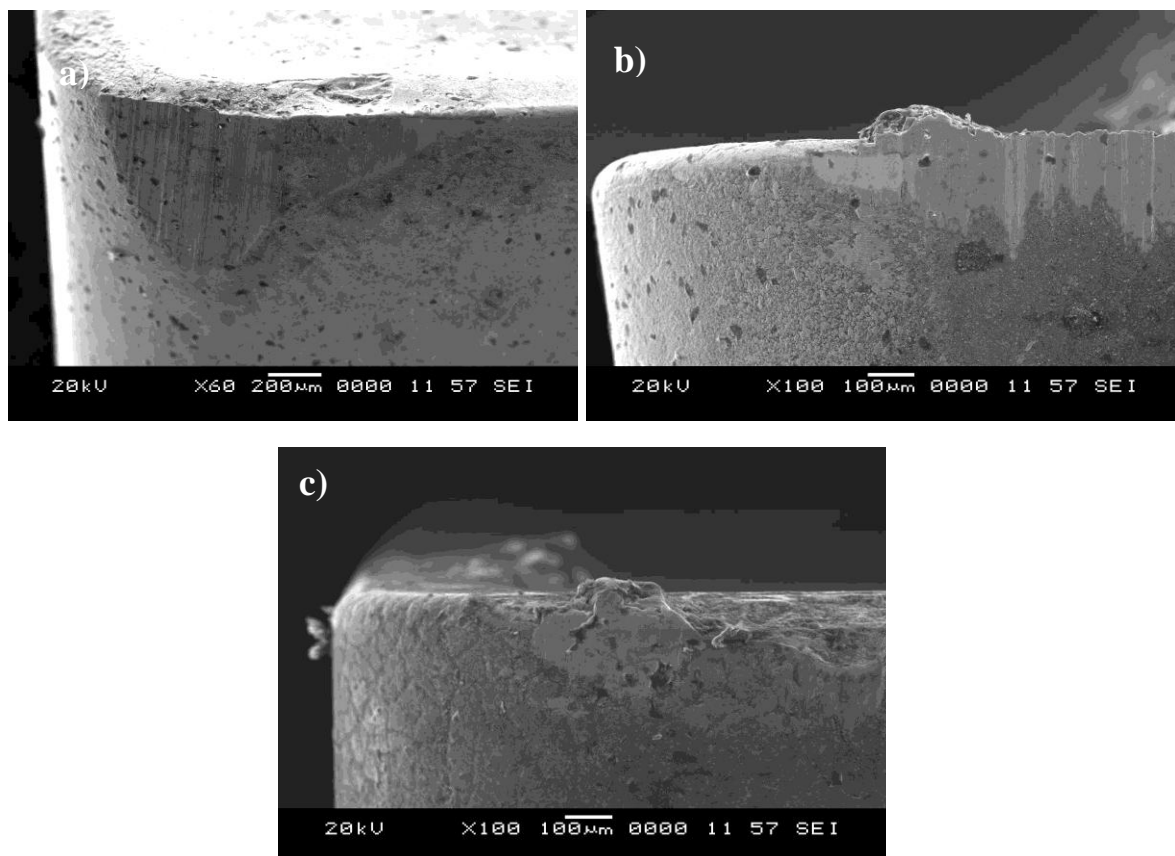
Figure 4.18 SEM images at *v= 85 m/min, f= 0.143 mm/rev, d= 0.6 mm and t = 600 ^{o}C* a) uncoated b) TiAlN c) TiCN/Al$_2$O$_3$/TiN cutting tools

Based on the earlier observation the flank wear was the main tool failure mode, it was resulted due to the low cutting speeds. The TiAlN inserts led to the tangling of the chips in turn increasing of the vibration level. The diffusion wear mechanism a crater wear was observed by utilizing the $TiCN/Al_2O_3/TiN$. But as compared to all the tools in the study TiAlN yielded in good results with all the cutting speeds.

4.10 COMPARISION OF CUTTING TOOL INSERTS ON CUTTING FORCES, SURFACE ROUGHNESS, TOOL WEAR AND MRR
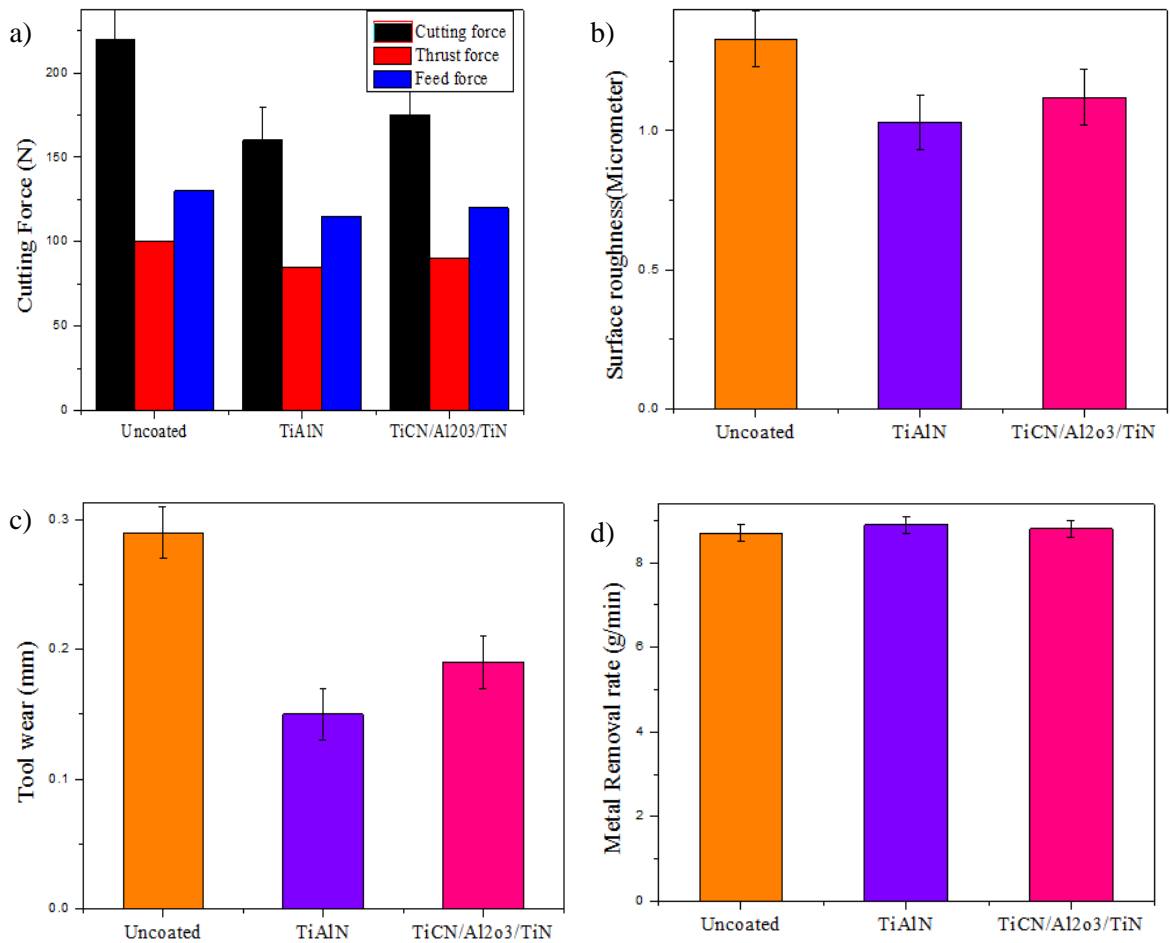
Figure 4.19 Comparison of cutting tool on cutting forces, surface roughness, tool wear and MRR.

Figure 4.19 shows the comparison made between the three different cutting tools on cutting forces, surface roughness, tool wear and MRR for uncoated, TiAlN and

TiCN/Al$_2$O$_3$/TiN coated carbide tools with similar machining conditions. The bar chart plotted as per the mean values of the experimental data. Compared to uncoated and TiCN/Al$_2$O$_3$/TiN coated tool the main cutting force is less in TiAlN nano multilayer coated carbide tool. The reason is that TiAlN coated tools have high hardness and wear resistance compared to other tools these causes less tool wear, improved chip flow with a low friction coefficient results in generation of low cutting forces. Figure 4.19 (b) shows the surface roughness of Inconel 718 superalloy by uncoated, TiAlN and TiCN/Al$_2$O$_3$/TiN coated carbide tool. Compared to uncoated and TiCN/Al$_2$O$_3$/TiN carbide tool the surface roughness is improved in TiAlN nano multilayer coated carbide tool. The surface roughness of the workpiece is mainly affected by the machining process parameters and the tool properties. Figure 4.19 (c) shows the comparison between three different tools such as uncoated, TiAlN, TiCN/Al$_2$O$_3$/TiN. Similar effect was observed in tool wear. Figure 4.16 (d) shows the metal removal rate of Inconel 718 superalloy by three cutting tools. All cutting tools have similar effect on metal removal rate.

4.11 SUMMARY

The effect of process parameters on cutting forces, surface roughness, tool wear and MRR of machined components by TAM of Inconel 718 superalloy have been investigated experimentally. The experiments were conducted as per L$_{27}$ OA to explore the effects of machining parameters such as cutting speed, feed rate, depth of cut and workpiece temperature on the proposed performance characteristics. Also, in this study, the influence of uncoated carbide tool on the performance of TAM on cutting forces, Ra, MRR, tool wear was compared with TiAlN multilayer, TiCN/Al$_2$O$_3$/TiN triple layer coated tool. Based on the experimental results and discussion, the following conclusions were being drawn:

- Cutting forces in TAM were observed to be less compared to conventional machining; Surface roughness was improved remarkably in TAM by about 21.8 % reduction in surface roughness was observed in TAM compared to conventional machining.

- Tool wear was improved by 29 %, and MRR was improved by 5.9 % in TAM compared to conventional machining.

- Cutting speed, feed rate, depth of cut and workpiece temperature have greater influence on cutting force; whereas feed rate and workpiece temperature are most significant process parameters on surface roughness. Similarly, cutting speed, feed rate and depth of cut have greater influence on tool wear and MRR during machining of Inconel 718 superalloy using uncoated, TiAlN multilayer coating and TiCN/Al$_2$O$_3$/TiN triple layer coated cutting tools.

- TiAlN multilayer coated tool is better suitable tool to machine Inconel 718 superalloy than uncoated and TiCN/Al$_2$O$_3$/TiN triple layer coated tool due to smooth surface finish, tool wear and without compromising the MRR. In addition from the SEM microstructures proves TiAlN multilayer coated tool produces less micro cracks, melted droplets and craters on the machined surface compared to TiCN/Al$_2$O$_3$/TiN tool.

CHAPTER 5

ONE FACTOR AT A TIME APPROCH

5.1 INTRODUCTION

Conventional plan of experiments were conducted to study the individual effect of process parameters on the responses. Each parameter of five levels selected to study the effect on the output responses. This chapter illustrates the effect of cutting speed, feed rate, depth of cut and workpiece temperature on the cutting force, tool wear, MRR and surface integrity. The cutting speed, feed rate, depth of cut and workpiece temperature are the most significant factor on surface roughness, heat effected zone, compositional changes on the machined surface and even the microhardness was analyzed on the machined surface.

5.2 PLAN OF EXPERIMENTS

For the thermally assisted machining experiments, the process parameters and the best cutting tool were selected based on the previous study. Cutting speed, feed rate, depth of cut and workpiece temperature were considered to study the individual effect on the output responses such as cutting force, surface roughness, tool wear, MRR, residual stress and the microhardness. The parameters for 5 different levels were considered and the considered range of the parameters are as follows cutting speed from 18 m/min to 90 m/min , feed rate from 0.048 to 0.143 mm/rev and depth of cut from 0.2 to 0.6 mm and workpiece temperature from 200 $^{\circ}$C to 600 $^{\circ}$C. The TiAlN multilayer coated tool were selected as cutting tool to machine Inconel 718 based on the earlier studies. The levels of the parameters are depicted in Table 5.1. The fixed parameters were selected the middle level of each parameter as shown in Table 5.2.

Table 5.1 Thermally assisted machining process parameters and their levels

Symbol	Control parameters	Level – I	Level - II	Level – III	Level – IV	Level - V
v	Cutting speed	18	34	52	72	90
f	Feed rate	0.048	0.071	0.096	0.119	0.143
d	Depth of cut	0.2	0.3	0.4	0.5	0.6
T	Workpiece temperature	200	300	400	500	600

Table 5.2 Constant process parameters during thermally assisted machining

Control parameters	Level
Cutting speed (m/min)	52
Feed rate (mm/rev)	0.096
Depth of cut (mm)	0.4
Workpiece temperature (^{o}C)	400

5.3 ANALYSIS OF CUTTING FORCE

Figure 5.1 shows the effect of thermally assisted machining process parameters on cutting forces. Figure 5.1 (a) shows the influence of cutting speed on cutting force with constant parameters of feed rate 0.096 mm/rev, depth of cut 0.4 mm, and workpiece temperature 400 ^{o}C. It has been observed that as cutting speed increases from 18 m/min to 90 m/min the cutting force decreases drastically by 47.66 %. This effect is mainly due to the high temperature developed at higher cutting speeds which intern increase the shear plane angle leads to softening of the workpiece, and reduction of chip thickness resulting lower cutting force (Lima et al. 2005). From Figure 5.1 (b) as the given values of feed rate increases the cutting force increases linearly by 101.66 %, due to increase in feed rate contact area between tool tip and workpiece which in turn increases the plastic deformation, results in decreasing the cutting force. At lower feed rate the resistance to

104
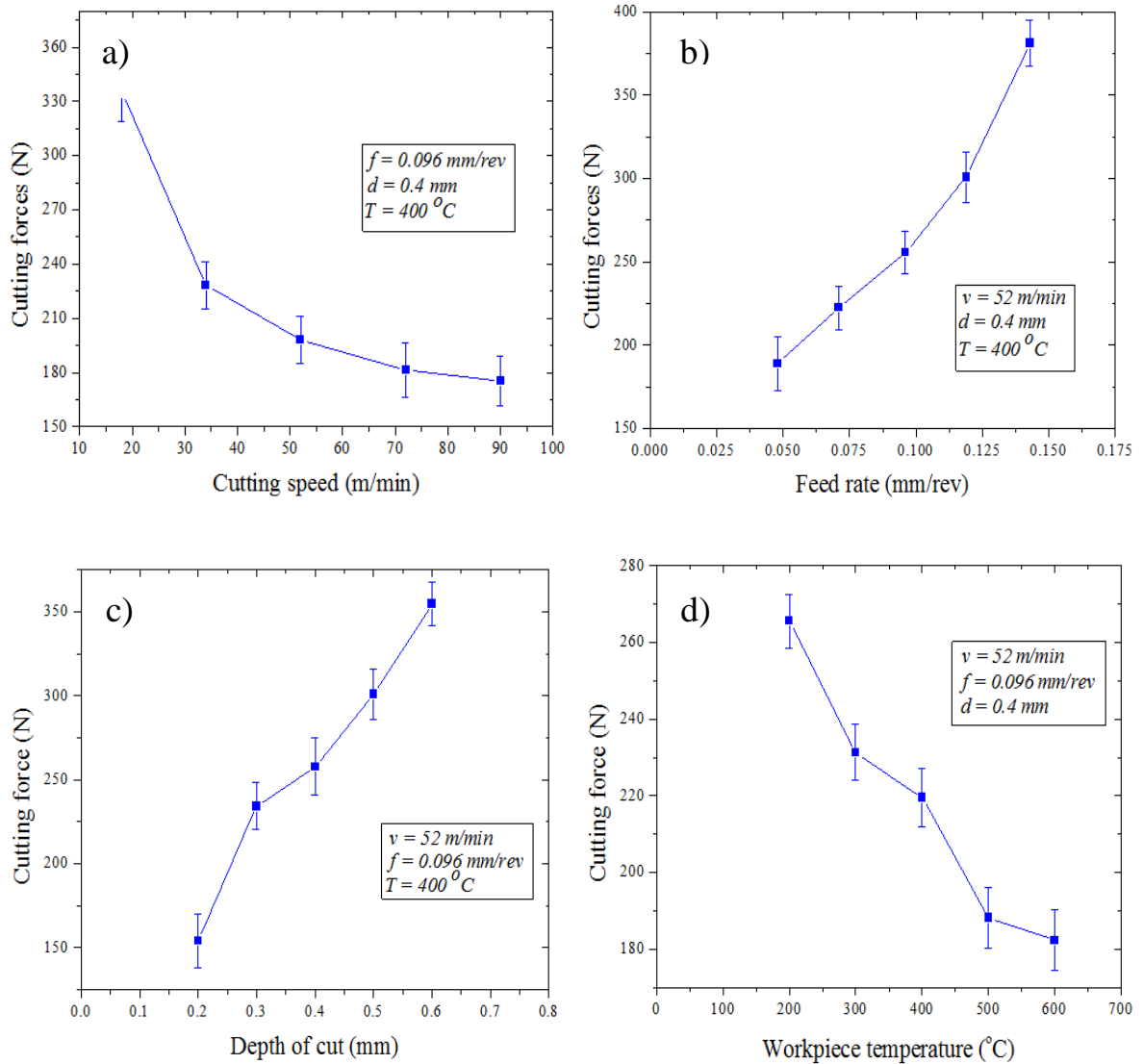
Figure 5.1 Effect of TAM parameters of on cutting forces.

tool in the direction of feed rate is very less, on the other hand, as the feed rate increases the workpiece material offers high resistance in the direction of cutting tool, which leads to increasing in cutting force. As shown in Figure.5.1 (c) with increase in the depth of cut, the cutting forces increases by 130.30 %. From the Figure 5.1 (d) it is observed that as workpiece temperature increases cutting force decreases by 31.36 %. This significant effect is mainly due to the reduction of yield strength of the machining workpiece resulting in less cutting force generation.

5.4 ANALYSIS OF SURFACE ROUGHNESS
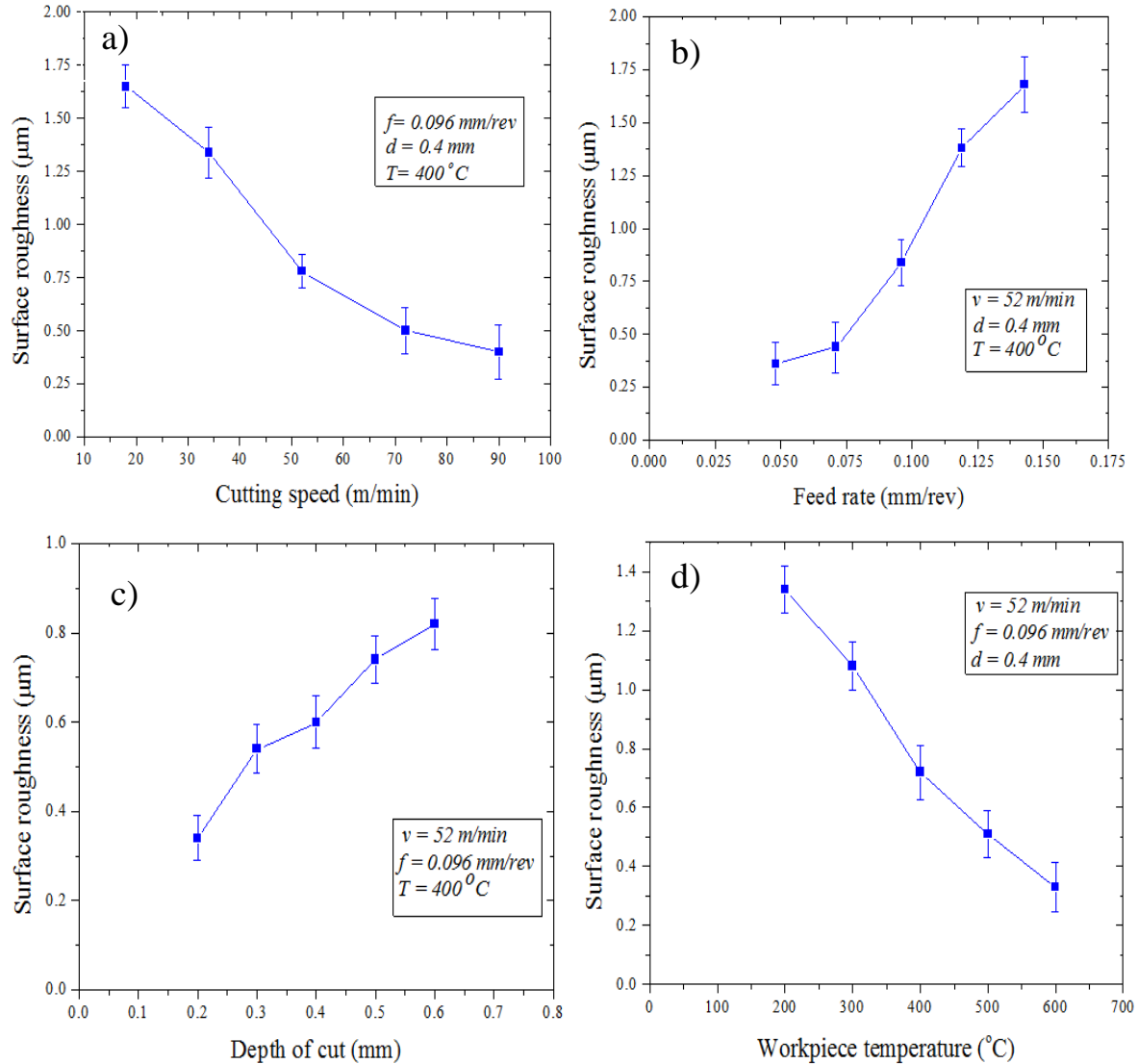
Figure 5.2 Effect of TAM parameters of Surface roughness

The surface roughness of thermally assisted machining of Inconel 718 mainly depends on the machining conditions and mechanical properties. Figure 5.2 (a) depicts the effect of cutting speed on surface roughness with constant parameters of feed rate 0.048 mm/rev, depth of cut 0.4 mm and workpiece temperature 600 $^{\circ}$C variation of surface roughness against cutting speed. It is observed that with the increase in cutting speed from 18 to 90 m/min, the surface roughness is sharply decreased from 1.37 μm to 0.41 μm by 72.99 %.

The probable reason might be as the cutting speed increases the heat generation at the cutting zone increases, leads thermally softening of the workpiece material and thus reduces the surface finish. Figure 5.2 (b) shows the variation of surface roughness against feed rate. As the feed rate increases the surface roughness value also increases by 266.66 %. This is due to with increased feed rate, the thrust force increases, leads to generating more heat and vibration thereby resulting higher surface roughness (Suresh, Basavarajappa and Samuel 2012). Figure. 5.2 (c) depicts that as increased surface roughness by 141.17 % trend was observed due to restructuring of surface flaws and discontinuities with increase in depth of cut. As seen from the Figure. 5.2 (d) as the workpiece temperature increases the surface roughness decreases by 75.37 % can be observed and can be attributed to these three mechanisms. (i) Reduction in cutting forces indirectly reducing the chatter vibration (Thandra and Choudhury 2010). (ii) Continuous chip formation instead of discontinuous chip formation. (iii) Reduction in the tendency to form built up edge.

5.5 ANALYSIS OF TOOL WEAR

Flank wear is mostly used to estimate the tool condition. It normally occurs on the relief face or flank on the tool cutting edge. Flank wear occurs due to the presence of abrasive particles present in the workpiece material. The tool wear on Inconel 718 superalloy of thermally assisted machining mainly depends on the process parameters. Figure 5.3(a) depicts the effect of cutting speed on flank wear with constant parameters of feed rate 0.096 mm/rev, depth of cut 0.4 mm, and workpiece temperature 400 ^{o}C. The tool flank wear is increased with the increase in cutting speed by 166.66 %. Flank wear is observed to be higher at higher cutting speeds. With the increase in cutting speed, the rubbing action between the tool and the workpiece is faster and high cutting temperatures generated even though at the less contact time. This effective absorption of high cutting temperatures generates close to the cutting edge. From this cutting condition, the strength of the cutting tool reduced when the rubbing action over the surface. Figure 5.3 (b) and 5.3 (c) illustrate that as feed rate and depth of cut increases the flank wear also increases by 154.54 % and 250 %, the
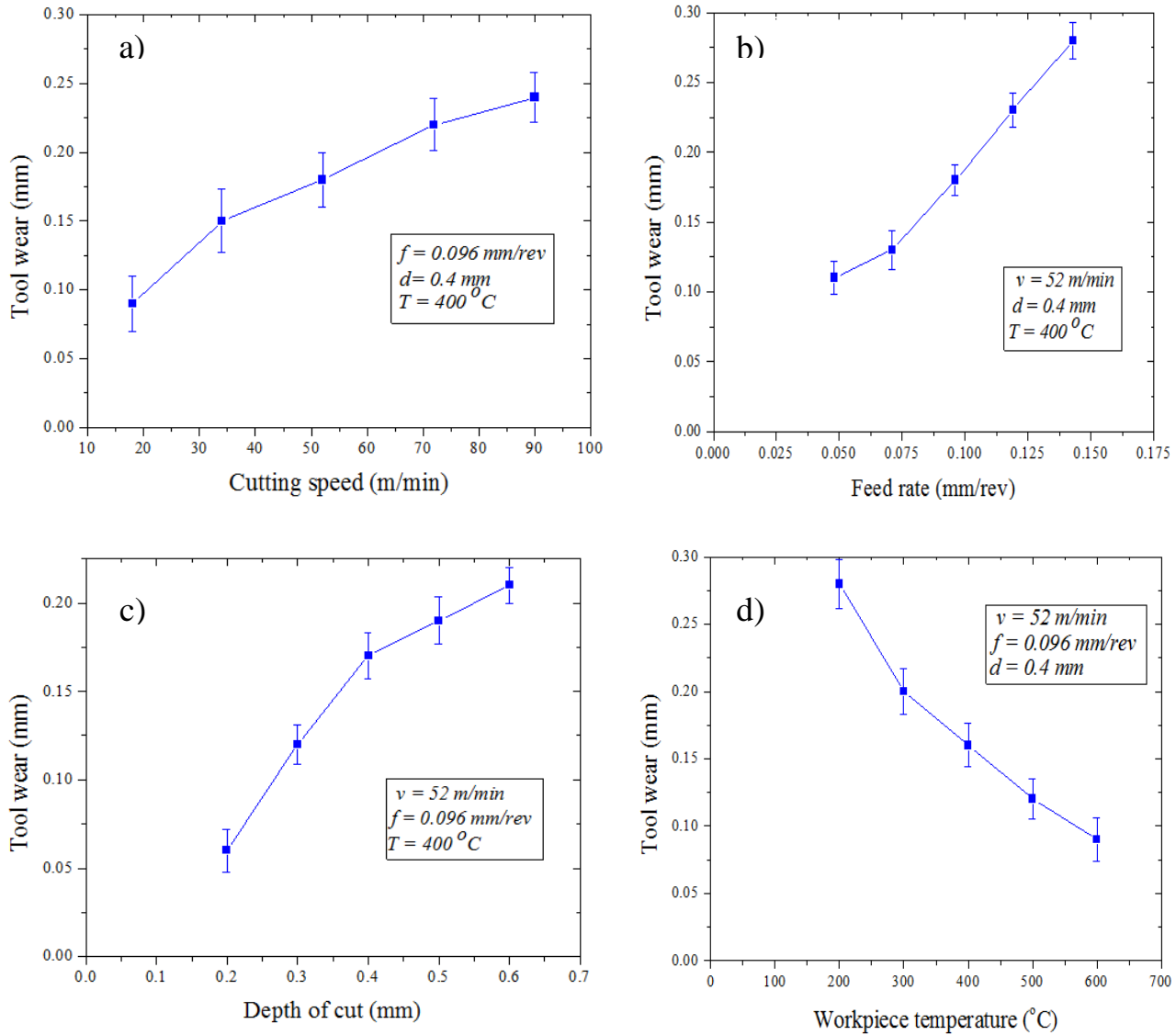
Figure 5.3 Effect of TAM parameters on tool wear.

reason behind that increase in cutting forces which weakens the cutting tool. High cutting temperatures, high stresses generated at rake and flank face close to the nose area probably caused the yield strength of the tool to reduce flank wear. Figure 5.3(d) depicts that as workpiece temperature increases from 200 $^\circ$C to 600 $^\circ$C the flank wear decreases by 67.85 %. This may be due to the fact that flank wear decreases, which is

majorly due to reduction of shear strength of workpiece material due to heat causing less friction at tool-chip interface causing a significant decrease in flank wear.

5.6 TOOL WEAR MECHANISMS

During thermally assisted machining of Inconel 718, there are different types of wear observed, namely abrasive wear, adhesive wear, chemical wear and diffusion wear.

Figure 5.4. shows SEM micrographs of cutting tools after TAM operation at different cutting parameters. Experiments were performed at low and high levels of each process parameter and the remaining parameters kept constant as shown in Table 5.2. In this study at low cutting speed 18 m/min the tool surface was very smooth and very less amount of wear debris were observed on tool surface, the tool wear mechanism observed were mainly abrasive wear. Due to the presence of hard abrasive, carbide particles present in the workpiece material and plucked-off particles from the tool substrate found responsible for abrasive wear (Sobiyi et al. 2015) as shown in Figure 5.4(a). Further at higher cutting speed 90 m/min, abrasive wear, adhesive wear and chipping of the flank wear were observed in Figure 5.4(b). On the other side at low feed rate 0.048 mm/rev, the tool wear is low because the contact area between tool and workpiece is very less and also the temperature is not so high to plastically deform the workpiece material at low level causes adhesion shown in Figure 5.4(c). At high feed rates 0.143 mm/rev, abrasive, adhesive wear and excessive chipping were observed. The adhesive wear is formed due to the high temperatures generated at the tool- work interface, which leads to welding occur between chip and tool. Due to frequent formation and diminishing of adhered particles lead to fluctuation of cutting forces causes excessive chipping on the tool surface. It also causes crack between tool coating and tool substrate and then the PVD coating is cut by the workpiece and peel off as cutting process is going on, as shown in Figure 5.4(d). According to Figure 5.4 (e and f) depth of cut has less effect on tool wear. In low depth of cut 0.2 mm the tool wear mechanism observed was abrasive and adhesive wear. In higher depth of cut 0.6 mm the tool flank wear was increasing due to contact

109
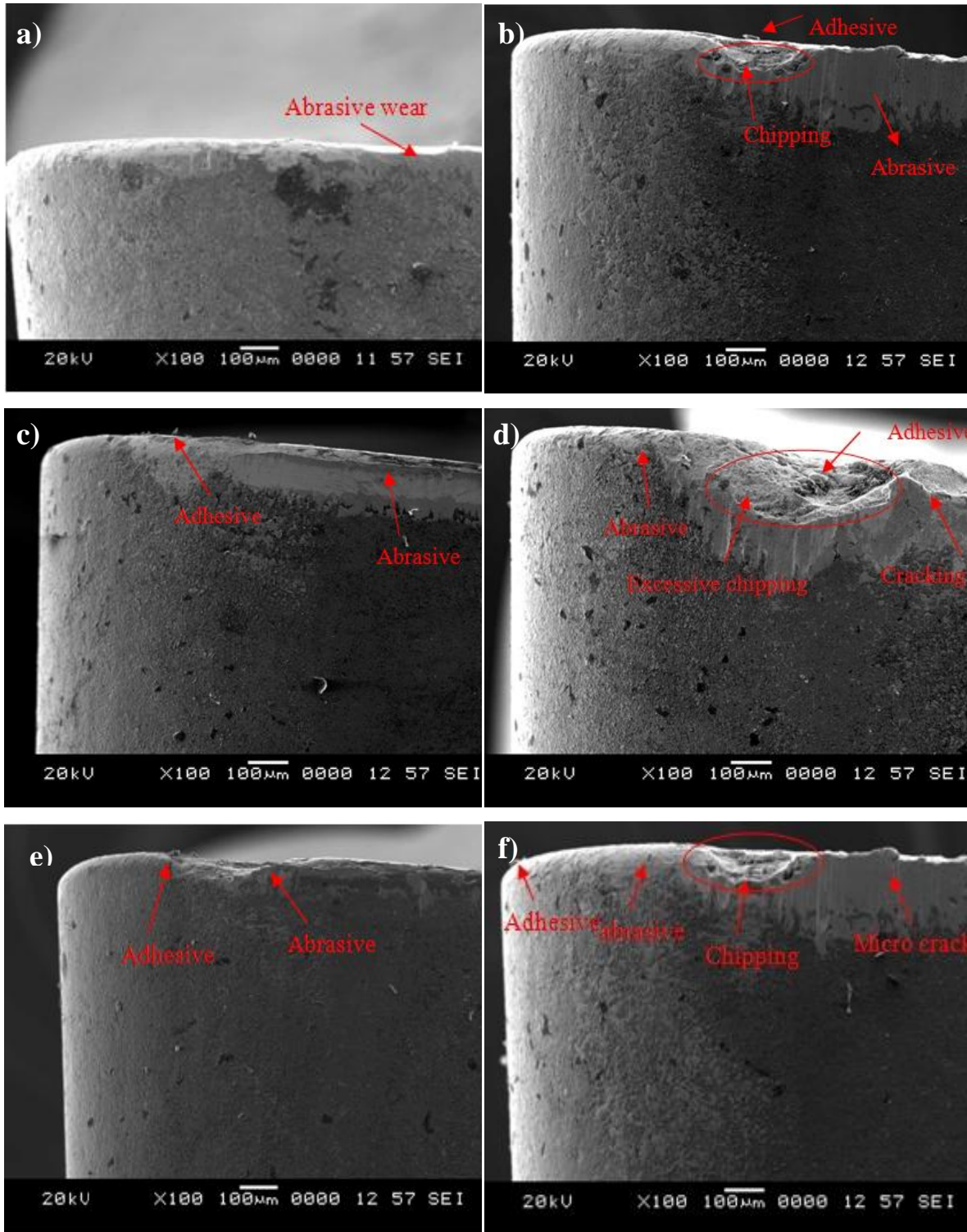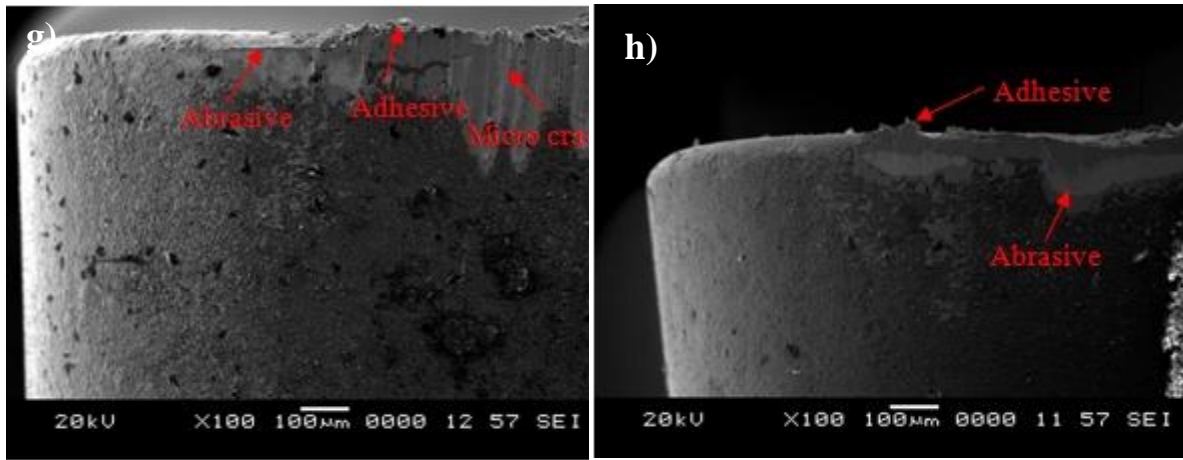
Figure 5.4 SEM images of tool flank wear at

a) cutting speed at 18 m/min   b) cutting speed at 90 m/min c) feed rate at 0.048 mm/rev

d) feed rate at 0.143 m/min   e) depth of cut at 0.2 mm   f) depth of cut at 0.6mm

g) workpiece temperature at 200 ^{o}C   h) workpiece temperature at 600 ^{o}C

between tool and workpiece is increasing. From Figure 5.4 (g) at low workpiece temperature 200 ^{o}C the tool flank wear is increasing due to the adhesive layer built up edge formation on the tool surface. This layer is formed due to the high temperatures generated at the tool and the workpiece during machining.   Also, at high temperature, the transmit of elements between tool and workpiece is penetrate to the tool causes diffusion wear and thermal fatigue cracks (Lima et al., 2005). It was observed that in Figure 5.4 (h) at a high workpiece temperature 600 ^{o}C the flank wear was very less. This effect is due to heating of the workpiece causes reduction of shear strength at the cutting zone, leading to reduction of cutting forces and flank wear. The other reason might be due to heating workpiece become soft and friction between tool and chip reduces, reduction of thrust force leading to reduced flank wear. Similar discussion were found elsewhere (Ren & Liu 2016 ; Anderson et al., 2006).

5.7 SURFACE TOPOGRAPHY

The surface topography of thermally assisted machining of Inconel 718 machined

surface has been shown in Figure 5.5. Experiments were performed at low and high levels of each process parameter and the remaining parameters kept constant as shown in Table 4. Figure 5.5(a) shows that at low cutting speed 18 m/min the intensity of the peaks are high larger and deeper crater on the machined sample leads to poor surface finish, better smoothness and fine surface can be obtained at higher cutting speeds 90 m/min, because as the speed increases the cutting temperature increases at the cutting zone that causes thermal softening of the material causes less surface roughness. According to Figure 5.5(b) it is evident that the intensity of the peaks is less on the machined surface at high cutting speeds 90 m/min, hence good surface were observed. Then by comparing the average surface roughness of the machined workpiece at cutting speed of 18 m/min and 90 m/min, the difference of 0.96 μm has been found which indicates that cutting speed significant effect on average surface roughness. Similarly, by comparing the average surface roughness of machined workpiece at a feed rate of 0.048 mm/rev and 0.143 mm/rev, the difference of 1.17 μm has been observed that feed rate has another great influence process parameter affecting surface quality of the machined workpiece.

Figure 5.5 (e) shows the smooth surface of the machined surface at low depth of cut 0.2 mm because of contact between tool and workpiece is very less. But at higher depth of cut 0.6 mm the surface roughness increases due to restructuring of surface flaws and discontinuities were observed as shown in Figure 5.5(f). From the Figure 5.5(e, and f) it is evident that the depth of cut has negligible effect on surface roughness. From Figure 5.5(g) it was observed the at low workpiece temperature 200 ^{o}C the surface roughness is increasing because of cutting forces and chatter vibrations. On the other hand, at high workpiece temperature 600 ^{o}C the smoother and better surface roughness were observed as shown in Figure 5.5(h). Because, due to high temperature softening of the material effects low cutting forces, mechanism of chip changes from discontinuous to continuous leads to smooth surface roughness.

g)

h)
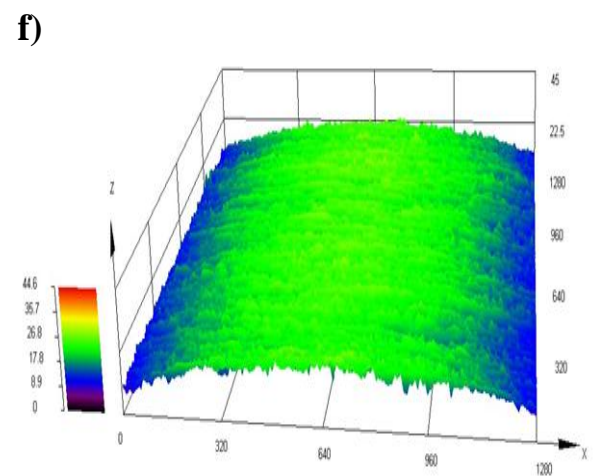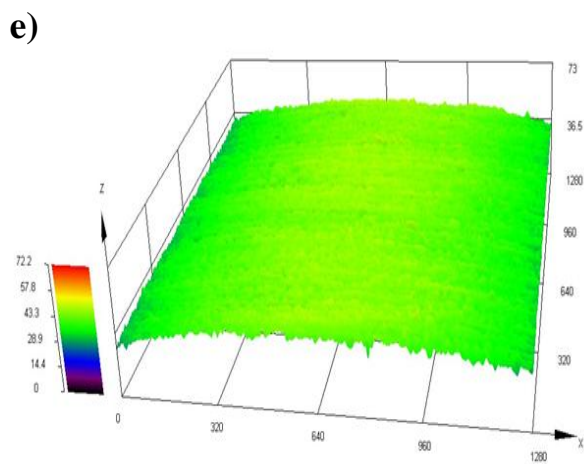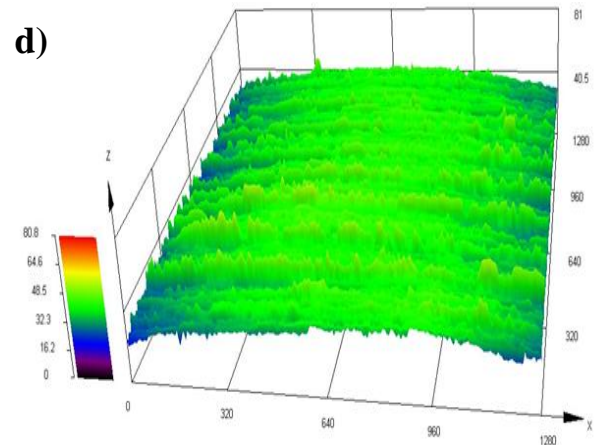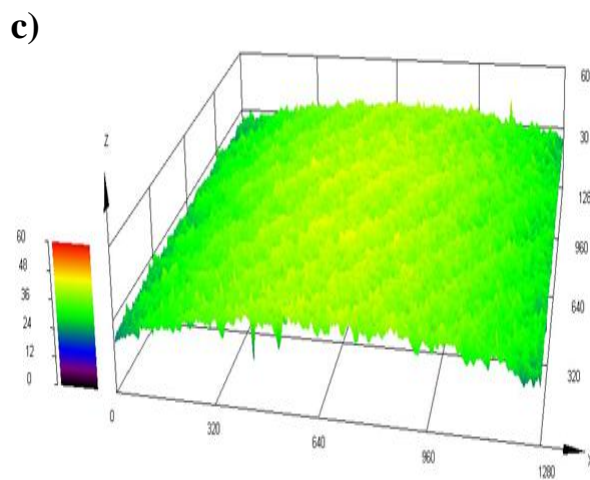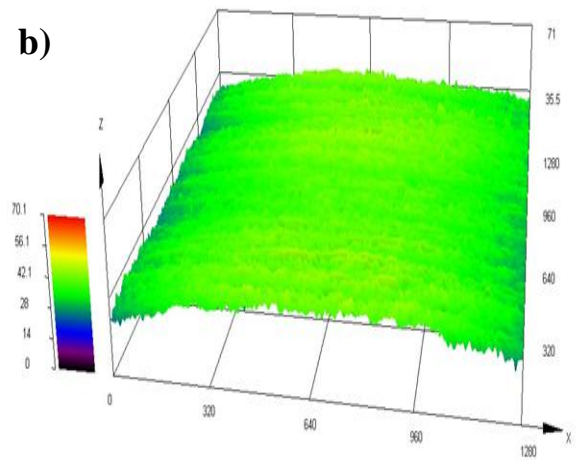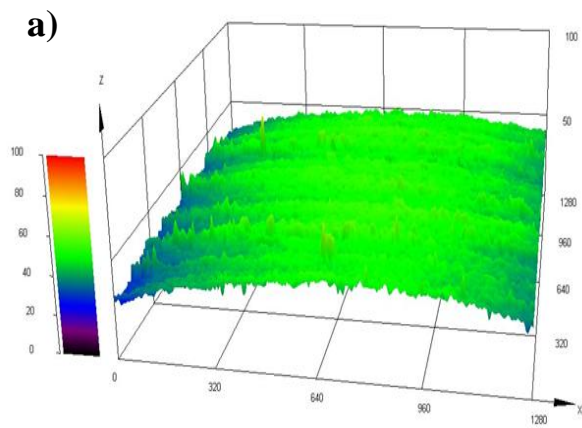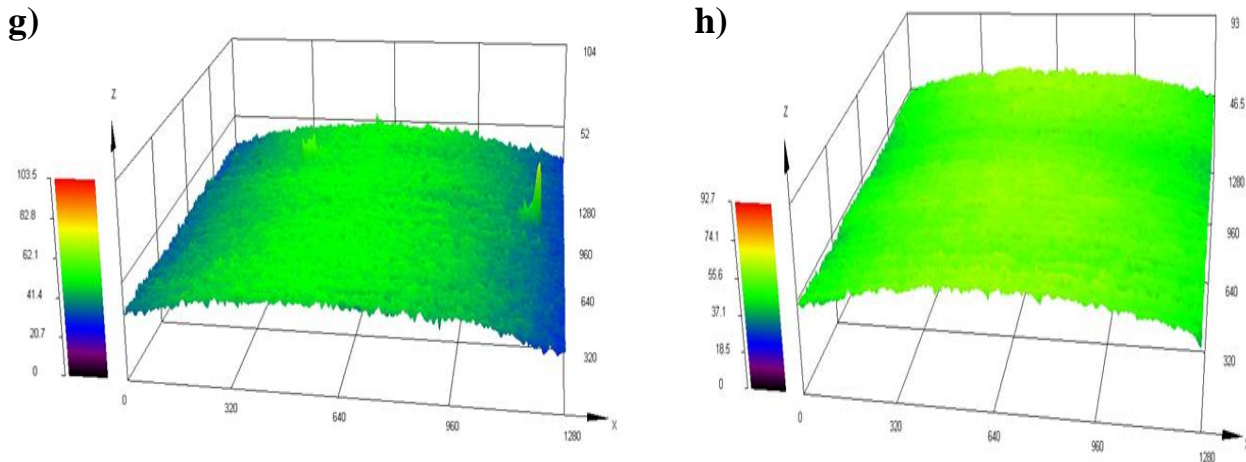
Figure 5.5 Surface topography of TAM surface

a) cutting speed at 18 m/min   b) cutting speed at 90 m/min   c) feed rate at 0.048 mm/rev
d) feed rate at 0.143 m/min   e) depth of cut at 0.2 mm   f) depth of cut at 0.6 mm
g) workpiece temperature at 200 $^{\circ}$C   h) workpiece temperature at 600 $^{\circ}$C

5.8 SURFACE DEFECTS

Figure 5.6. shows the material side flow on the machined surface during turning of Inconel 718 superalloy using TiAlN multilayer coated carbide tool at different machining conditions. The general topography of machined surface consists of long straight grooves in direction parallel to the cutting speed. These grooves are caused by the micro roughness of cutting edge and flank wear topography. Examination of the machined surface using SEM reveals the dependence of surface topography on cutting conditions employed. Cutting tool wear and chip morphology have great influence on material side flow. Thus, it helps to study the significant machining parameters influencing on the machinability of material. Experiments were performed at low and high levels of each process parameter and the remaining parameters kept constant as shown in Table 5.2. Figure 5.6 (a and b) at low cutting speed the detachment of segments of the workpiece from the machined surface leaving cavities. The severity of surface damage is high at low cutting speed; this effect is due to high tool wear at low speeds

114
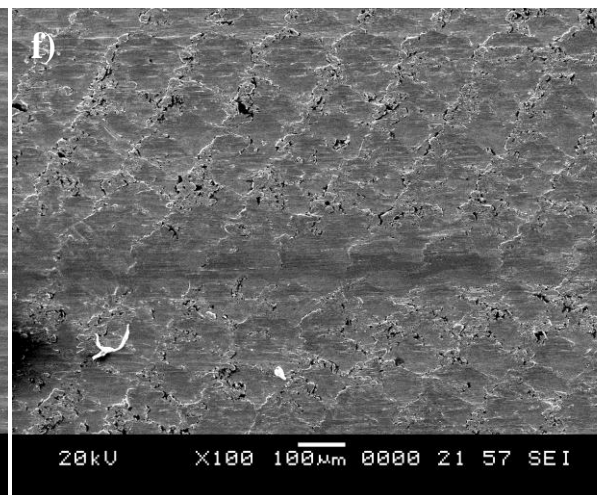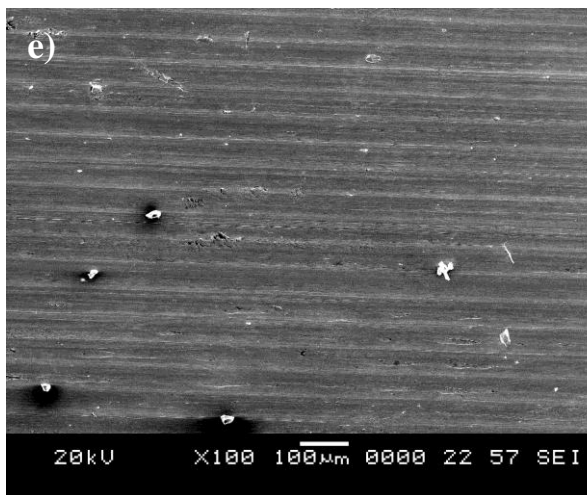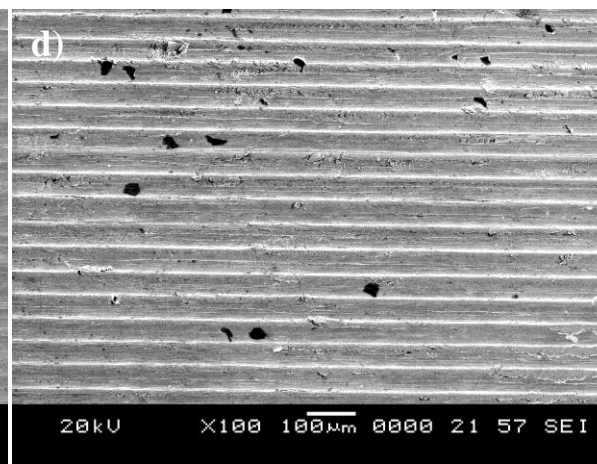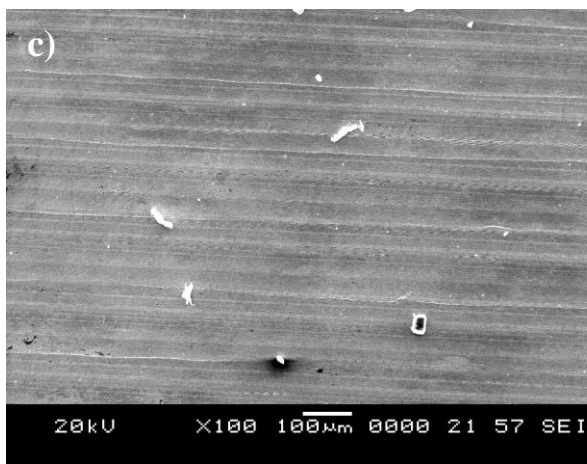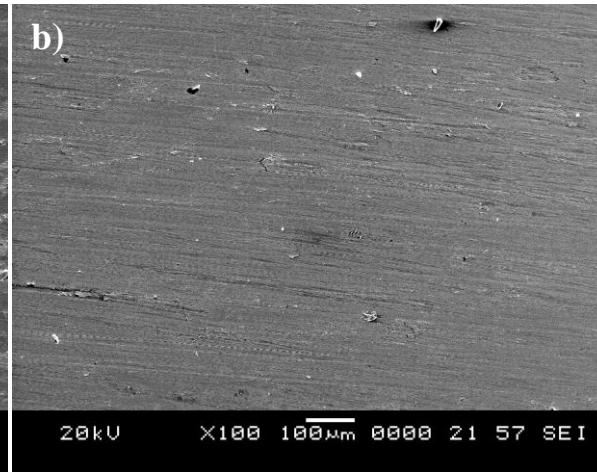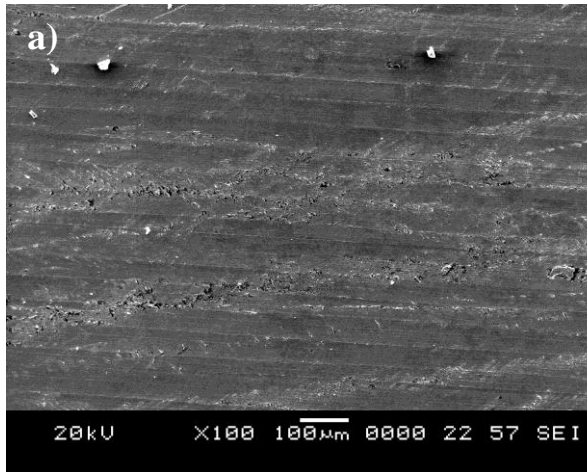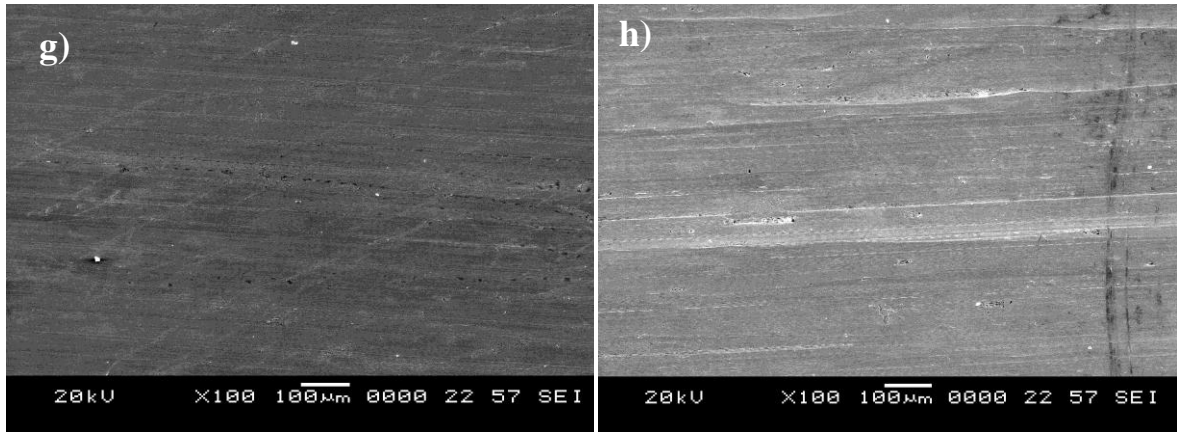
Figure 5.6 SEM images of surface produced during turning of thermally assisted machining

a) cutting speed at 18 m/min   b) cutting speed at 90 m/min   c) feed rate at 0.048 mm/rev

d) feed rate at 0.143 m/min   e) depth of cut at 0.2 mm   f) depth of cut at 0.6mm

g) workpiece temperature at 200 ^{o}C   h) workpiece temperature at 600 ^{o}C

As the cutting speed increases high temperatures developed at the machining zone that leads to thermal softening of the workpiece material the subsurface structure produced large carbide particle forced to deform in the vicinity of the surface, due to high cutting temperature micro cracks beneath the machined surface, such type of surface damage will affect the product quality. Figure.5.6 (c and d) The results reveal that, lower feed rate have significant effects on material side flow during machining of Inconel 718. The reason may be the minimum chip thickness value depends on lower feed rate. The material side flow is observed in the area of the feed marks where plastically deformed material is ploughed aside, when the chip thickness was less than the minimum chip thickness. Thus, below a minimum chip thickness value the material to be cut was ploughed on the workpiece. Further at high feed rate the extensive straight well defined groves parallel to the direction of relative work tool motion can be observed. These grooves were more frequently due to high tool wear. It can be seen that as the tool wear progress the surface roughness increases and segments of the workpiece are detached from below the surface, leaving deep

116

grooves and cavities. It indicates that the increase in the surface roughness can be attributed to the existence of large grooves and material side flow on machined surface. Figure.5.6 (e and f) at lower and higher depth of cut, the material side flow is facilitated by the trailing edge notch and also built up layer on the cutting edge. These grooves are observed more frequently as the tool wear land increases and promote severe material side flow on the machined surface. Figure.5.6 (g and h) at low workpiece temperature the grooves produced on the machined surface this effect is due to increased tool wear resulting ploughing large part of uncut chips. At higher workpiece temperature the quality machined surface were observed the reason might be less tool wear and continuous chips.

5.9 SUBSURFACE DEFECTS
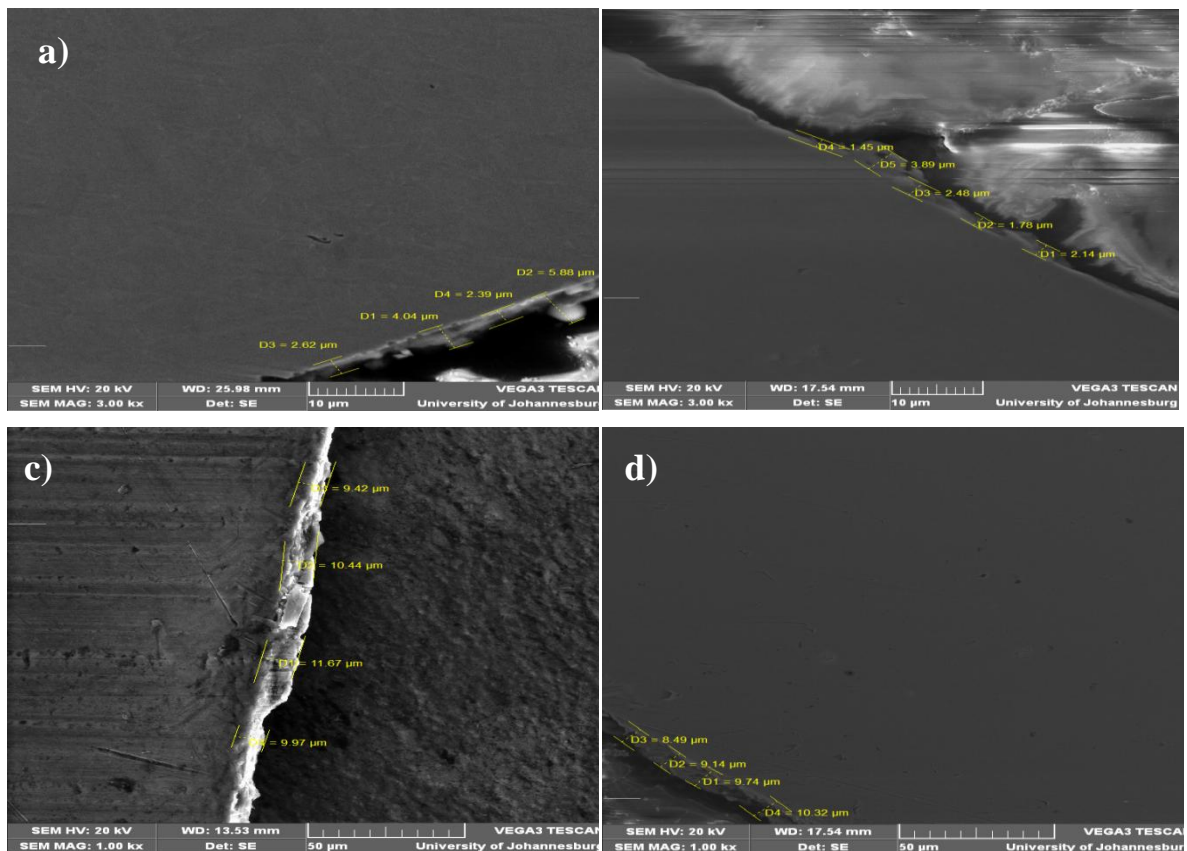
Figure 5.7 SEM images of machined surface of Inconel 718 at different workpiece temperatures (a) Room temperature (b) 200 ^{o}C (c) 400 ^{o}C (d) 600 ^{o}C

White layer is a micro-structural condition where the grain structure of a metal is extremely refined. This condition may occur on the machined surface of hard turned parts, especially when aggressive machining parameters are applied or worn cutting tool is used. In industry, when white layer exists, it is typically less than 10μm thick and is removed by another finishing process, such as super finishing (Dawson, 2002).

The typical method for observing white layer involves chemically etching the cross-section of a sample in order to visually emphasize the microstructure. When a specimen is etched and observed using optical microscope, white layer appears white. White layer is usually accompanied by 'dark layer' underneath it, although dark layer may appear without white layer. As the name implies, dark layer appears darker than the bulk material after etching. Figure 5.7. shows SEM images of white layer in machined surface of Inconel 718 superalloy using TiAlN multilayer coated carbide tool at different workpiece temperatures.

5.10 CHIP MORPHOLOGY

Figure 5.8. shows the chip morphology of thermally assisted machining of Inconel 718 at different cutting conditions. The SEM images evident that continuous ribbons like chips are formed. The analysis shows that due to thermal softening effect chips produced by the TAM shows a tendency to shear localization and large strain in the primary shear zone. At low cutting speed 18 m/min, loose arc type chips, twisted appearance is observed as shown in Figure.5.8(a), owing to the swirling distribution of solidified structure inside the segment resulting twist in the chips, but very minor cracks were observed on the outer surface of the chip. As the cutting speed increases straight strip continuous saw tooth chips, sharper and thicker chips were observed. This effect is mainly due to the wider plastic deformation occurs around the shear band during chip formation, and also chip cracking and chip burning due to high cutting temperature Figure.5. 8(b). From Figure. 5.8 (c) at low feed rate 0.043 mm/rev it can be observed that thickness of the chip at primary and secondary zone, and shear bond angle decreases. However, at higher feed rate 0.143 mm/rev chips produced much larger deformed material in the primary shear

zone compared to lower feed rate. The heat generated at the cutting zone also increases when the feed rate increases, hence continuous saw tooth chips are observed. From Figure. 5.8 (d) at low depth of cut 0.2 mm the chips produced are twisted and curl saw tooth type due to the less contact length between the tool-chip and also the heat generation of the primary shear zone and the tool. As higher depth of cut 0.6mm the chips produced are continuous saw type. The un deformed and slipping surface of the chip and segmented chips were noted at low temperature 200 ^{o}C as shown in Figure. 5.8(g). As the workpiece temperature increases 600 ^{o}C the chip produced are continuous straight strip chip. The material undergoes heavy compression during segmentation and the superior deformability of the material near the free surface due to heating enables it to be deformed plastically.
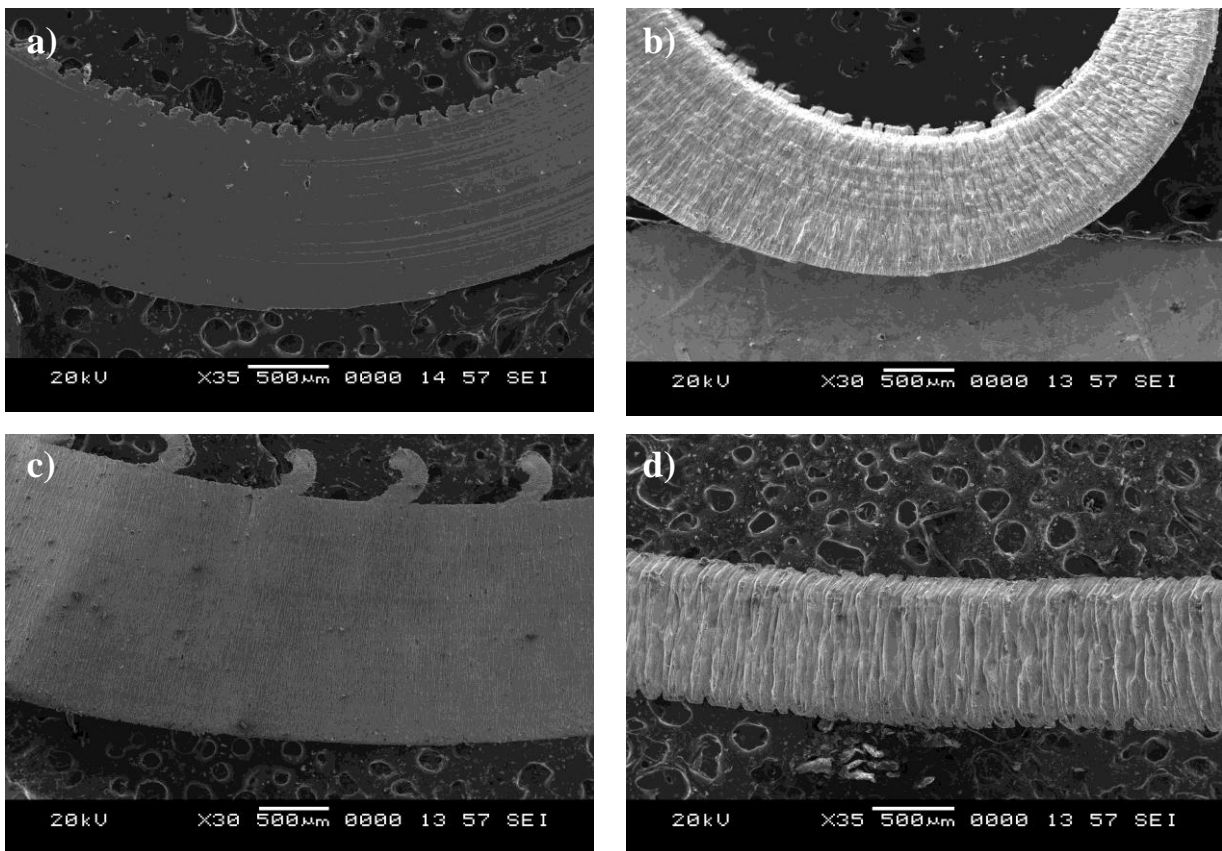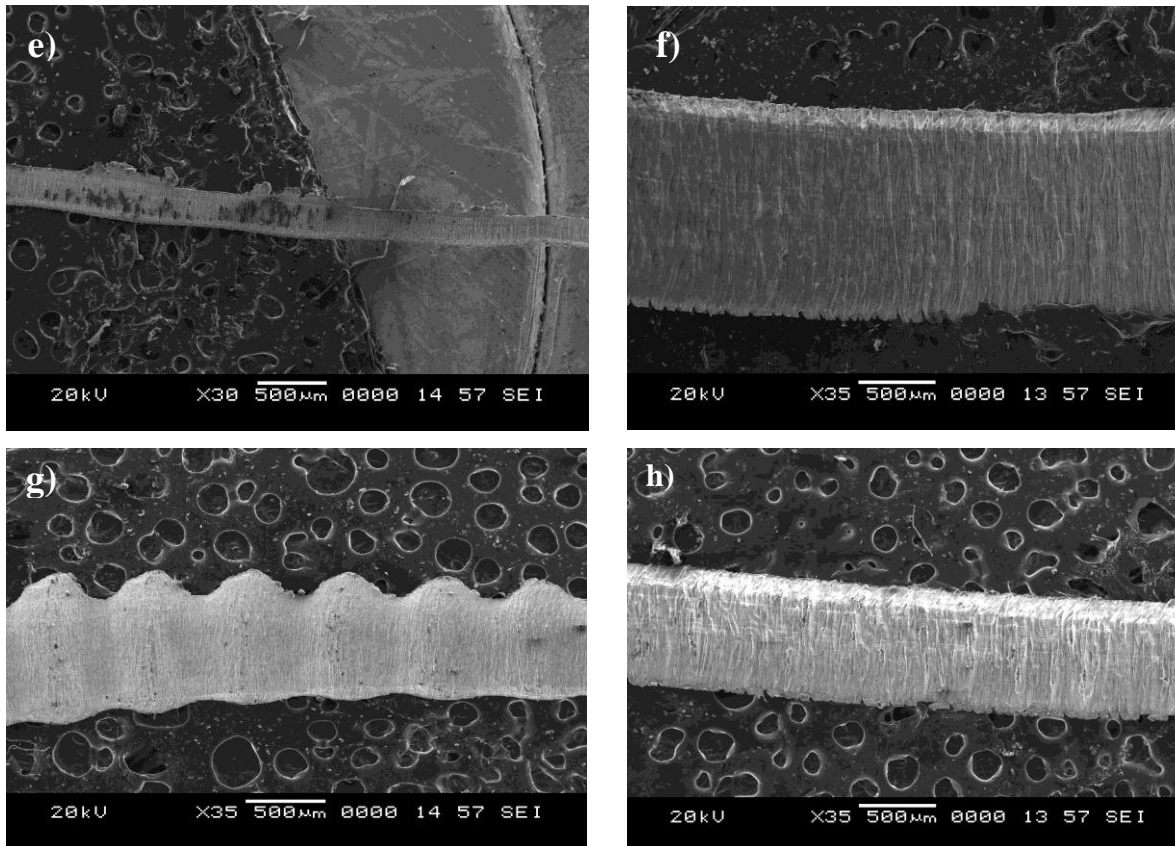
Figure 5.8 SEM images of chip morphology at different machining conditions

a) cutting speed at 18 m/min   b) cutting speed at 90 m/min   c) feed rate at 0.048 mm/rev

d) feed rate at 0.143 m/min   e) depth of cut at 0.2 mm   f) depth of cut at 0.6mm

g) workpiece temperature at 200 ^{o}C   h) workpiece temperature at 600 ^{o}C

5.11 MICROHARDNESS

The microhardness of the machined samples of Inconel 718 by thermally assisted machining was measured at different workpiece temperatures 200 ^{o}C, 300 ^{o}C, 400 ^{o}C, 500 ^{o}C and 600 ^{o}C keeping other parameters constant as shown in Figure. 5.10. The nearby portion of the machined surface was considered as a reference point (0 μm) because it is very hard to measure the microhardness precisely on the machined surface due to improper indentation. Microhardness of TAM Inconel 718 was observed to be high in the near surface layer, and then it was found to decrease rapidly. As the

workpiece temperature increases the microhardness value increases. The probable reason might be, as the temperature increases grain refinement occurs on the machined surface, this lead to smaller grain size and in turns increases the hardness on the surface and subsurface of the machined parts.
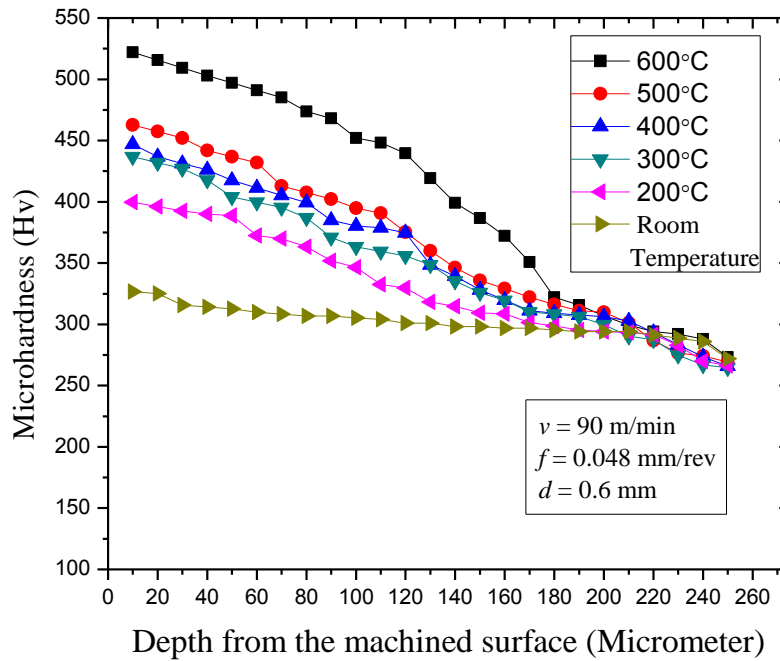
Figure 5.9 Subsurface hardness profiles of thermally assisted machined components

5.12 X – RAY DIFFRACTION (XRD)

The machined samples were examined using X- ray diffraction (XRD). The peaks were observed at 43.06 ^{o} (111), 50.79 ^{o} (200) and 74.67 ^{o} (220). The peaks reveal that presence of γ-Ni matrix precipitates with face-centered cubic (FCC) crystal structure. The intermetallic phases such as γ-NiCr, γ' Ni_3Al and γ'-Ni_3Nb are precipitated in the γ-Ni matrix. By comparing the XRD peaks broadening and intensity ratio between different workpiece temperatures from 200 ^{o}C to 600 ^{o}C, a qualitative evaluation of the metallurgical changes was done as shown in Figure 5.11. There are neither phase

121

changes, nor broadening of the peaks that were observed at different machining conditions. It shows that the temperature generated in the cutting zone was not considerable enough to cause the possible phase transformation
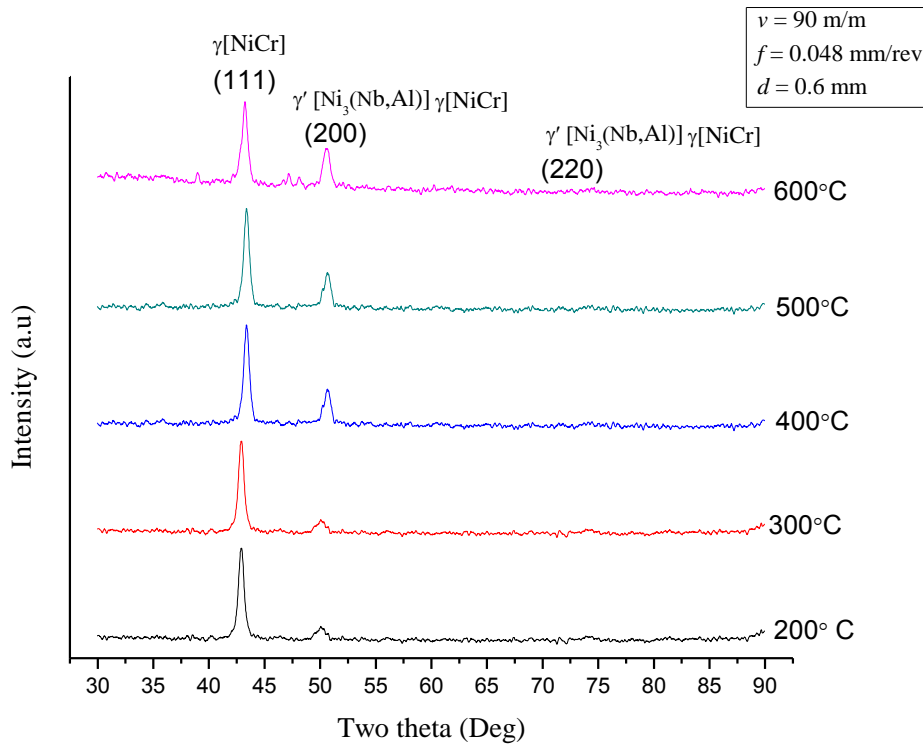
Figure 5.10 XRD analysis to observe the phase transformation of the machined surfaces at different workpiece temperatures such as 200,300,400,500 and 600 ^{o}C

5.14 RESIDUAL STRESSES

To evaluate the degree of residual stress induced in the machined surface by TAM, X-ray diffraction measurement was performed. In this study the effect of workpiece temperature on residual stress were evaluated. From Figure 5.12 it was observed that the tensile residual stresses were produced on the machined surface for varying workpiece temperature from 200 ^{o}C to 600 ^{o}C. At higher workpiece temperature the yield strength of the material will reduce and the material becomes soft, this leads to reduction of residual stresses.
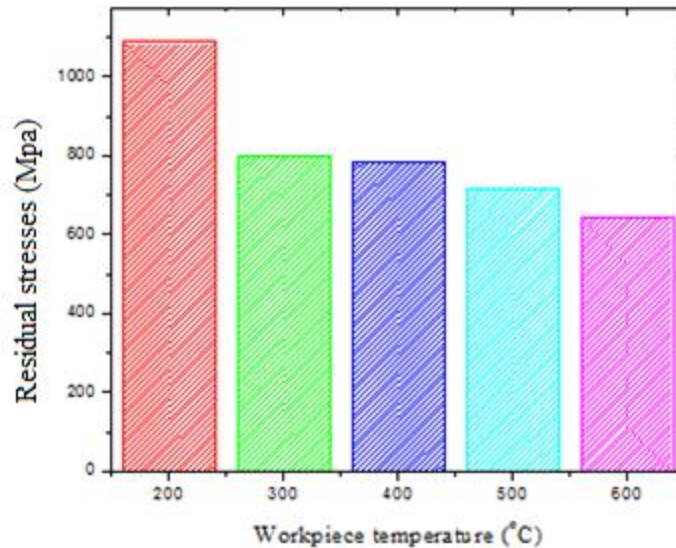
Figure 5. 11 Surface residual stresses distribution of Inconel 718 for varying workpiece temperature.

5.15 SUMMARY

Based on the experimental investigation, the influence of cutting speed, feed rate, depth of cut and workpiece temperature on the TAM performance characteristics was evaluated.

- The cutting force and surface roughness increases with increased feed rate and depth of cut, decreases with increased cutting speed and workpiece temperature for Inconel 718 superalloy.

- At high cutting speed, the type of wear observed in thermally assisted machining was abrasive, adhesive, diffusion, and micro chipping.

- The microhardness increases as the workpiece temperature increases, hence TAM improves the performance of the product.

- The XRD results of thermally assisted machining reveals that there are neither phase changes, nor broadening of the peaks that were observed at different machining conditions.

CHAPTER 6

MODELLING AND OPTIMIZATION

6.1 INTRODUCTION

In this chapter modelling and optimization of the process parameters were performed by using central composite rotatable design (CCRD). The CCRD matrix helps to conduct all possible combinations of levels and process parameters. The analysis of cutting forces, surface roughness, tool wear and MRR was performed using analysis of variance (ANOVA). The developed mathematical models have been optimized the process parameter by using particle swarm optimization.

6.2 EXPERIMENTATION

Response surface methodology (RSM) a combination of both statistical and mathematical technique used for analysis and design of experiments. This technique is obliging for modeling and analysis of parameters, in which response of interest is affected by a several variables and the reason is to optimize this response. A five level four factor central composite rotatable design (CCRD) was employed to develop the response models using RSM. In the current work 30 experiments were carried out which consists of 16 factorial points, 8 axial points and 6 center points, the TAM experiments were performed with TiAlN cutting insert to study the interaction effect between the cutting parameters and given output parameters as listed in Table 6.1. The range of control factors was selected based on previous study so as to achieve better responses. The experiments are carried out to identify the interaction effect between input and output parameters.

6.3 INFLUENCE OF PROCESS PARAMETERS ON RESPONSES

The four chosen parameters have influence on the machining performance. The significance of the parameters is found out by the analysis of variance (ANOVA). By the

Table 6.1 Process parameters with the Experimental design and their results

Run order	Cutting speed (m/min)	Feed rate (mm/rev)	Depth of cut (mm)	Workpiece temperature (^{o}C)	Cutting force (N)	Surface roughness Ra (μm)	Tool wear (mm)	MRR (g/min)
1	52	0.071	0.3	300	216.58	1.36	0.09	2.15
2	104	0.071	0.3	300	190.12	0.79	0.12	10.625
3	52	0.119	0.3	300	242.06	1.64	0.12	4.25
4	104	0.119	0.3	300	168.92	1.47	0.24	13.375
5	52	0.071	0.5	300	208.18	1.4	0.1	5
6	104	0.071	0.5	300	124.46	0.98	0.14	12.625
7	52	0.119	0.5	300	227.76	1.69	0.15	7.5
8	104	0.119	0.5	300	126.42	1.55	0.26	17.129
9	52	0.071	0.3	500	171.5	0.84	0.07	4.25
10	104	0.071	0.3	500	178.12	0.5	0.16	11.34
11	52	0.119	0.3	500	167.96	1.2	0.14	6.625
12	104	0.119	0.3	500	158.92	0.95	0.24	15.342
13	52	0.071	0.5	500	163.23	0.89	0.09	6.96
14	104	0.071	0.5	500	165.16	0.63	0.18	12.95
15	52	0.119	0.5	500	199.52	1.28	0.15	7.98
16	104	0.119	0.5	500	162.12	0.98	0.2	16.559
17	26	0.095	0.4	400	218.46	1.4	0.07	4.125
18	130	0.095	0.4	400	196.12	1.24	0.28	24.161
19	78	0.047	0.4	400	178.36	0.69	0.09	4.75
20	78	0.143	0.4	400	197.96	1.6	0.17	11.419
21	78	0.095	0.2	400	159.74	0.92	0.14	5.5
22	78	0.095	0.6	400	144.06	0.98	0.17	8.77
23	78	0.095	0.4	200	166.6	1.58	0.19	8.272
24	78	0.095	0.4	600	162.63	0.72	0.14	9.35
25	78	0.095	0.4	400	149.78	1.1	0.16	6.84
26	78	0.095	0.4	400	172.35	0.94	0.18	6.14
27	78	0.095	0.4	400	161.65	0.84	0.19	5.845
28	78	0.095	0.4	400	151.21	0.93	0.18	6.321
29	78	0.095	0.4	400	168.25	0.99	0.17	6.12
30	78	0.095	0.4	400	152.35	0.94	0.16	8.36

Table 6.2 ANOVA analysis for cutting forces.

Source	Sum of squares	DF	Mean square	F-value	Prob>F	Percentage contribution
Model	19883.79	10	1988.38	12.71	< 0.0001	
V	5619.08	1	5619.08	35.92	< 0.0001	24.58
f	237.7	1	237.7	1.52	0.2327	
d	921.2	1	921.2	5.89	0.0254	
t	887.07	1	887.07	5.67	0.0279	
$V*f$	889.38	1	889.38	5.69	0.0277	
$V*d$	877.79	1	877.79	5.61	0.0286	
$V*t$	3805.96	1	3805.96	24.33	< 0.0001	16.64
$d*t$	1303.03	1	1303.03	8.33	0.0095	
$V*V$	4268.61	1	4268.61	27.29	< 0.0001	18.6
$f*f$	1586.26	1	1586.26	10.14	0.0049	
Residual	2972.01	19	156.42			
Lack of Fit	2511.71	14	179.41	1.95	0.2379	
Pure Error	460.3	5	92.06			
Cor Total	22855.79	29				

Table 6.3 ANOVA analysis for surface roughness

Source	Sum of squares	DF	Mean square	F-value	Prob>F	Percentage contribution
Model	2.92	6	0.49	53.3	< 0.0001	
V	0.32	1	0.32	35.03	< 0.0001	10.22%
f	1.12	1	1.12	122.98	< 0.0001	35.78%
t	1.18	1	1.18	129.71	< 0.0001	37.69%
$V*V$	0.23	1	0.23	24.9	< 0.0001	7.34%
$f*f$	0.06	1	0.06	6.59	0.0172	
$t*t$	0.06	1	0.063	6.95	0.0148	
Residual	0.21	23	0.009126			
Lack of Fit	0.17	18	0.009631	1.32	0.4090	
Pure Error	0.037	5	0.007307			
Cor Total	3.13	29				

Table 6.4 ANONA analysis for tool wear

Source	Sum of squares	DF	Mean square	F-value	Prob>F	Percentage contribution
Model	0.068	4	0.017	32.15	< 0.0001	
V	*0.046*	*1*	*0.046*	*86.59*	*< 0.0001*	56.00%
f	*0.021*	*1*	*0.021*	*39.59*	*< 0.0001*	25.92%
d	*9.38E-04*	*1*	*9.38E-04*	*1.77*	*0.1957*	
t	*3.38E-04*	*1*	*3.38E-04*	*0.64*	*0.4326*	
Residual	0.013	25	5.31E-04			
Lack of Fit	*0.013*	*20*	*6.27E-04*	*4.27*	*0.0571*	
Pure Error	*7.33E-04*	*5*	*1.47E-04*			
Cor Total	0.081	29				

Table 6.5 ANOVA analysis for metal removal rate.

Source	Sum of squares	DF	Mean square	F-value	Prob>F	Percentage contribution
Model	651.18	7	93.03	110.29	< 0.0001	
V	462.02	1	462.02	547.75	< 0.0001	68.98%
f	54.6	1	54.6	64.73	< 0.0001	8.15%
d	26.64	1	26.64	31.58	< 0.0001	3.99%
t	5.52	1	5.52	6.54	0.0179	
*V*V*	99.31	1	99.31	117.73	< 0.0001	14.82%
*f*f*	3.81	1	3.81	4.51	0.0452	
*t*t*	8.48	1	8.48	10.05	0.0044	
Residual	18.56	22	0.84			
Lack of Fit	14.31	17	0.84	0.99	0.5573	
Pure Error	4.24	5	0.85			
Cor Total	669.74	29				

regression analysis, mathematical model has been developed to identify the effect of process parameters on the machining performance, such as MRR and surface roughness. The performance of the model was confirmed with the help of analysis of variance (ANOVA) (Tables 6.2 to 6.5). In this technique, all the proposed models are computed and found that "Prob > F" is less than 0.05 which indicates that the model is significant. For all the computed models, correlation coefficient (R^2) values are close to unity which shows the adequacy of the fitted regression models. Responses for all the models are delineating that "Pred R-Squared" values are reasonable accidence with the "Adj R-Squared" values. The proposed model satisfies the accuracy ratio (> 4). Moreover, the diagnostic graph confirms the competence of the ideal model for the actual system, showing the numerical assumption fits the analytic data is admirable.

6.4 EFFECT OF PROCESS PARAMETERS ON RESPONSES

The 3D surface graphs for cutting force, surface roughness, tool wear, and MRR is represented in Figure 6.1 to 6.4. From Figure 6.1 (a, b) shows that the cutting forces decreases with increase in cutting speed and workpiece temperature, and increases with increase in feed rate and depth of cut. The event has been attributed as the cutting speed increases more heat were developed at the machining zone which intern increase the shear plane angle leads to thermally softening of the workpiece and reduce the chip thickness resulting lower cutting force. However, as the feed rate increases the cutting force increases due to increases the contact length. As the workpiece temperature increases the cutting force decreases due to reduction of yield strength of the material ensuing less cutting force.

From Figure. 6.2 (a, b) shows that surface roughness significantly decreases as the rise of cutting speed and depth of cut. The possible reason behind this is temperature generation at the cutting zone increases as cutting speed and depth of cut increases this leads to thermally softening of the material, less cutting forces were generated resulting fewer
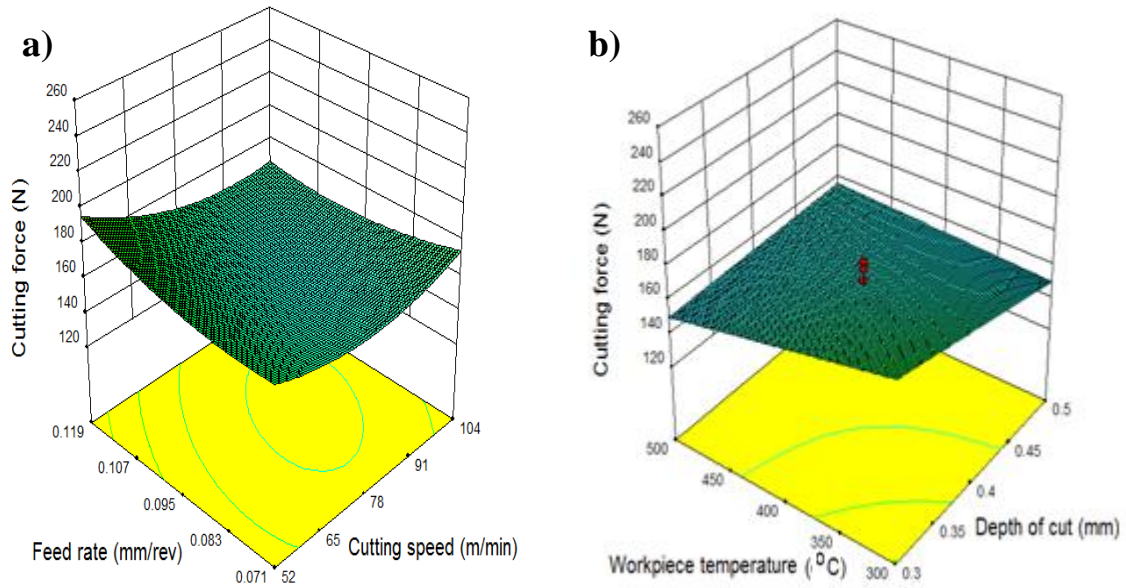
Figure 6.1 Effect of cutting parameters on Cutting force
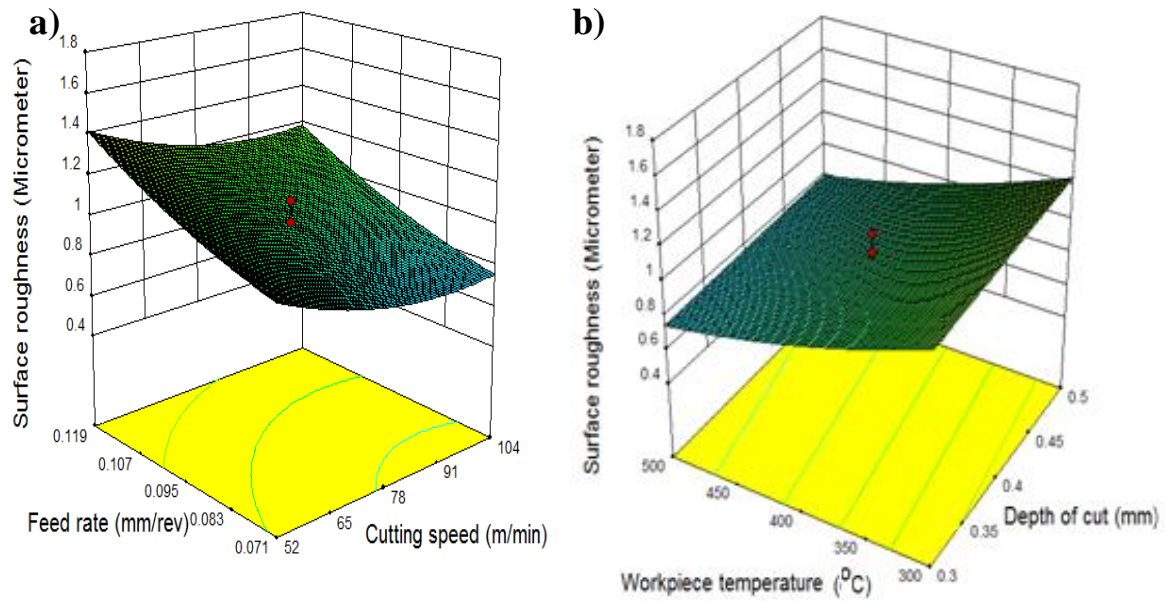
Figure 6.2 Effect of cutting parameters on Surface roughness
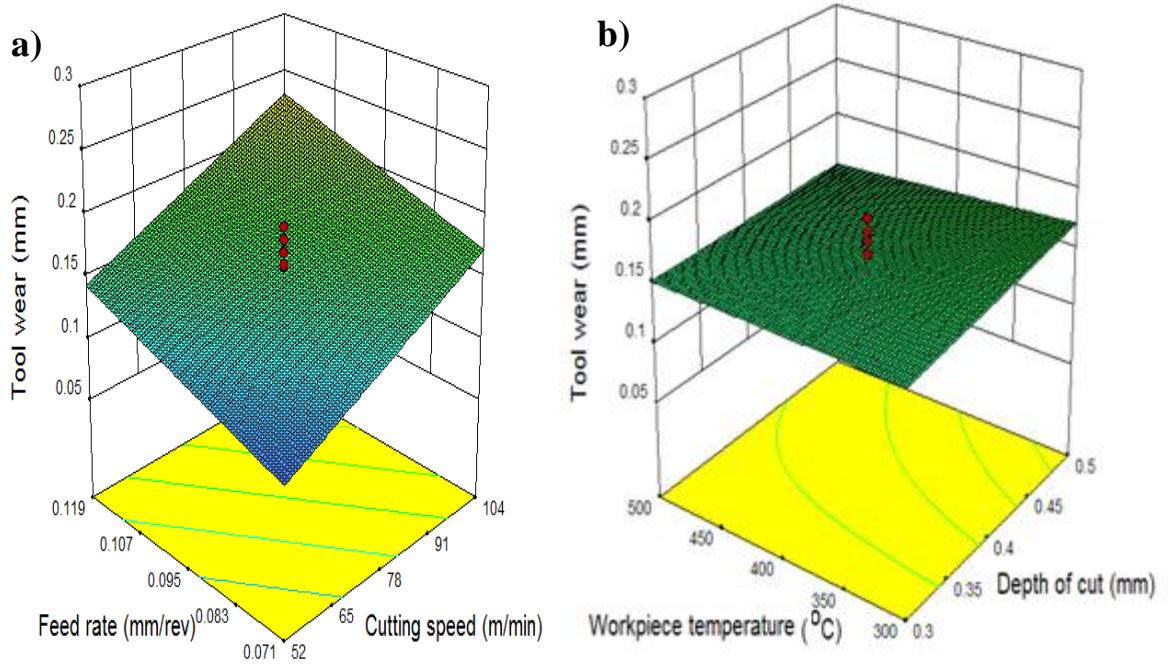
Figure 6.3 Effect of cutting parameters on Tool wear
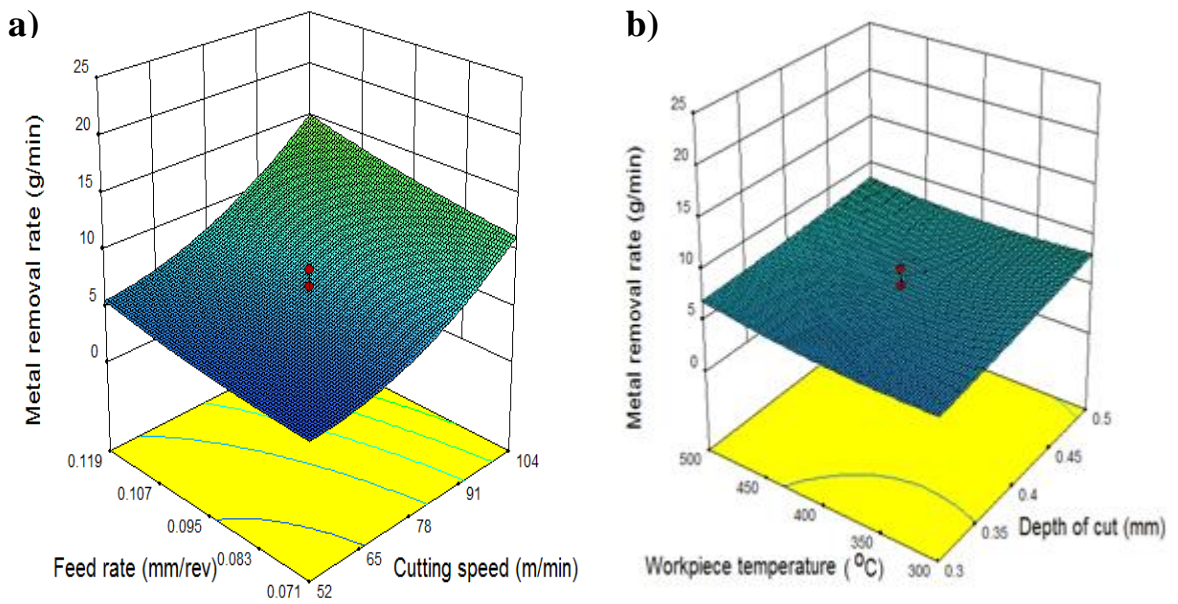
Figure 6.4 Effect of cutting parameters on MRR

tool marks on the machined surface. The thrust force increases with an increase in feed rate, it is well-known fact that feed rate is inversely proportional to surface roughness. As the workpiece temperature increases the surface roughness decreases this effect is due to reduction in workpiece material hardness leading to smoother removal of chip from the surface because of lower chip rupture stress (Upadhyay et al., 2012).

From Figure 6.3 (a, b) represents that an increasing trend was observed for flank wear with the rise in cutting speed, feed rate and depth of cut. The basic reason is that as cutting speed, feed rate and depth of cut increases, the rubbing action between tool and workpiece rises, friction between the tool and workpiece increases hence high temperature were generated at the cutting zone this led to high flank wear. On the other hand, as the workpiece temperature rises, the flank wear decreases, the reason might be as the workpiece temperature increases the shear strength of the material decreases causing less friction at tool-chip interface leading to less tool wear. It was observed during TAM condition, the temperature developed at the machining zone leads to diminution of temperature at the chip-tool interface and thus reduces the built-up edge formation.

Finally from Figure 6.4 (a, b) MRR sharply increases as the cutting speed, feed rate depth of cut and workpiece temperature rises. The reason behind this is as the speed and feed rate increases more volume of chips were generated during machining, as the depth of cut rises the more amount of material is removed during machining. Therefore, as the workpiece temperature increases the metal removal rate increases due to fact that while heating the material the chip reduction coefficient reduces with increase in temperature. Hence the machinability of the material improves with increase in temperature.

Chips samples were collected at different machining conditions (shown in Figure 6.5) and it was observed that there are two types of chips namely the small loose arc type chips and long ribbon type chips were formed during the machining of Inconel 718 under TAM condition. It was found that when cutting speed at 52 m/min, feed rate at 0.071 mm/rev, depth of cut at 0.3 mm and workpiece temperature at 300 $^{\circ}$ C, loose arc type chips were produced. The chips coming out from the machining zone are curled along the

normal plane and then hit the principle flank face of the cutting insert, which fracture in to tiny loose arc shapes. Moreover, the scanning electron microscope was used to study
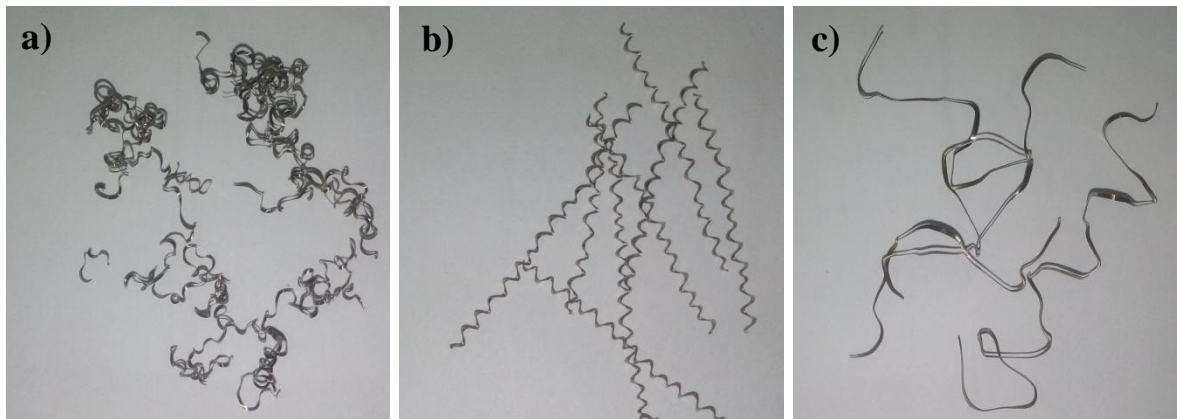
Figure 6.5 Chip samples collected at

(a) Cutting speed at 52 m/min, Feed rate at 0.071 mm/rev, Depth of cut at 0.3 mm and Workpiece temperature at 300 ^{o}C

(b) Cutting speed at78 m/min, Feed rate at 0.047 mm/rev, Depth of cut at 0.4 mm and Workpiece temperature at 400 ^{o}C

(c) Cutting speed at104 m/min, Feed rate at 0.119 mm/rev, Depth of cut at 0.5 mm and Workpiece temperature at 500 ^{o}C.
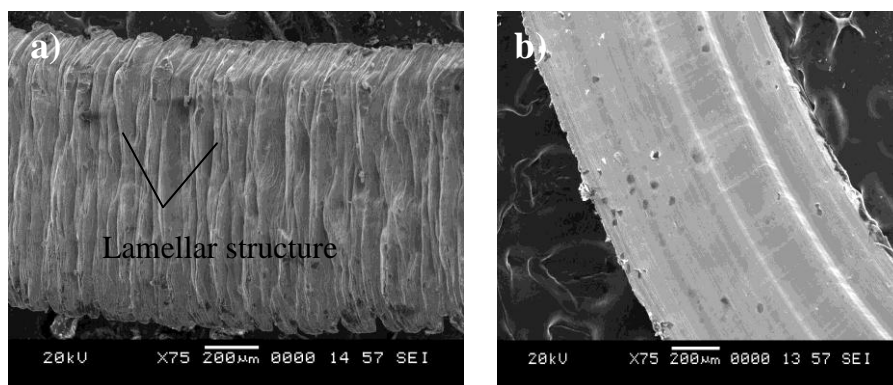
Figure 6.6 Surface topography of the chips a) Cutting speed at 52 m/min, Feed rate at 0.071 mm/rev, Depth of cut at 0.3 mm and Workpiece temperature at 300 ^{o}C

(b) Cutting speed at104 m/min, Feed rate at 0.119 mm/rev, Depth of cut at 0.5 mm and Workpiece temperature at 500 $^{\circ}$C

the lamella structures at the surface of the chip. Figure 6.6 (a) it was noticed that owing to the swirling distribution of solidified structure inside the segment resulting twist in the chips, but very negligible cracks were observed on the outer surface of the chip. When cutting speed at 104 m/min, feed rate at 0.119 mm/rev, depth of cut at 0.5 mm and workpiece temperature at 500 $^{\circ}$C, long ribbon type chips are produced. Due to thermal softening of the workpiece material leads to increase the length of the chip. As demonstrated in Figure 6.6 (b) at higher temperatures the material undergoes heavy compression during segmentation and the superior deformability of the material near the free surface due to heating enables it to be deformed plastically. It was observed that at TAM condition, the temperature developed at the machining zone leads to diminution of temperature at the chip-tool interface and thus eliminates built-up edge formation.

6.5 REGRESSION ANALYSIS

The regression analysis was performed to obtain a correlation between the input and output response parameters. The model was further used in PSO to optimize the multi-objective variables such as cutting forces, tool wear, MRR and Ra. The quadratic method is used to fit the model and to analysis the experimental data. The regression was developed for cutting forces, tool wear, MRR and Ra for Inconel 718 material. The regression equation for cutting forces, tool wear, MRR and Ra are presented in equation (6.1), (6.2),(6.3) and (6.4).

$$F_c = 621.09954 - 3.51368V - 1400.23356f - 200.72292d - 0.88446t - 11.94812Vf$$
$$- 2.84880Vd + 5.9319 \times 10^{-3}Vt + 0.90244\ d\ t + 0.018122V^2 + 12964.8166\ f^2$$

(6.1)

$$Ra = 3.25248 - 0.021444\ V - 6.27511\ f - 1.40856 \times 10^{-4}V^2 + 80.45015\ f^2 + 4.75893$$
$$\times 10^{-6}\ t$$

(6.2)

$$VB_{max} = 0.072758 + 1.72993 \times 10^{-3}V + 1.23264\ f + 0.062500\ d - 3.7500 \times 10^{-5}\ t \quad (6.3)$$

$$MRR = 9.43365 - 0.17938V_c - 58.75719\,f + 10.53583d - 0.039226\,t + 2.94452 \times 10^{-3}\,V_c^2$$
$$+\,640.00496\,f + 5.50268 \times 10^{-5}t^2 \qquad (6.4)$$

Table 6.6 ANOVA results of regression analysis related to equation

Responses	R^2	R^2 - Adj
Cutting force	87.00%	80.15%
Surface roughness	93.29%	91.54%
Tool wear	83.72%	81.12%
MRR	97.23%	96.35%

The significance of the developed mathematical models has been tested through the analysis of variance (ANOVA) and coefficient of determination (R^2) and is presented in Table 6.6 which clearly indicates the adequacy of the developed models. The residual analysis has also been employed to check the accuracy of the developed models. The normal probability plots for cutting force, surface roughness, tool wear and MRR are shown in Figures 6.7, where in the residuals closely follow the straight lines, clearly indicating that the errors are normally distributed.

The significance of the developed mathematical models has been tested through the analysis of variance (ANOVA) and coefficient of determination (R^2) and is presented in Table 6.6 which clearly indicates the adequacy of the developed models. The residual analysis has also been employed to check the accuracy of the developed models. The normal probability plots for cutting force, surface roughness, tool wear and MRR are shown in Figures 6.7, where in the residuals closely follow the straight lines, clearly indicating that the errors are normally distributed.

The adequacy of the model has also been investigated by the examination of residuals (Montgomery 2008, Garg et al. 2012). The residuals are the difference between the respective observed values and predicted values these are examined using normal probability of the residual plot. Figure 6.7 represents the normal probability of the

residuals for cutting force, surface roughness, tool wear and MRR which indicate that residual points of all the models were close to the same straight line, which shows that errors were normally distributed. It reveals that model is adequate and it can be used to navigate the design space.
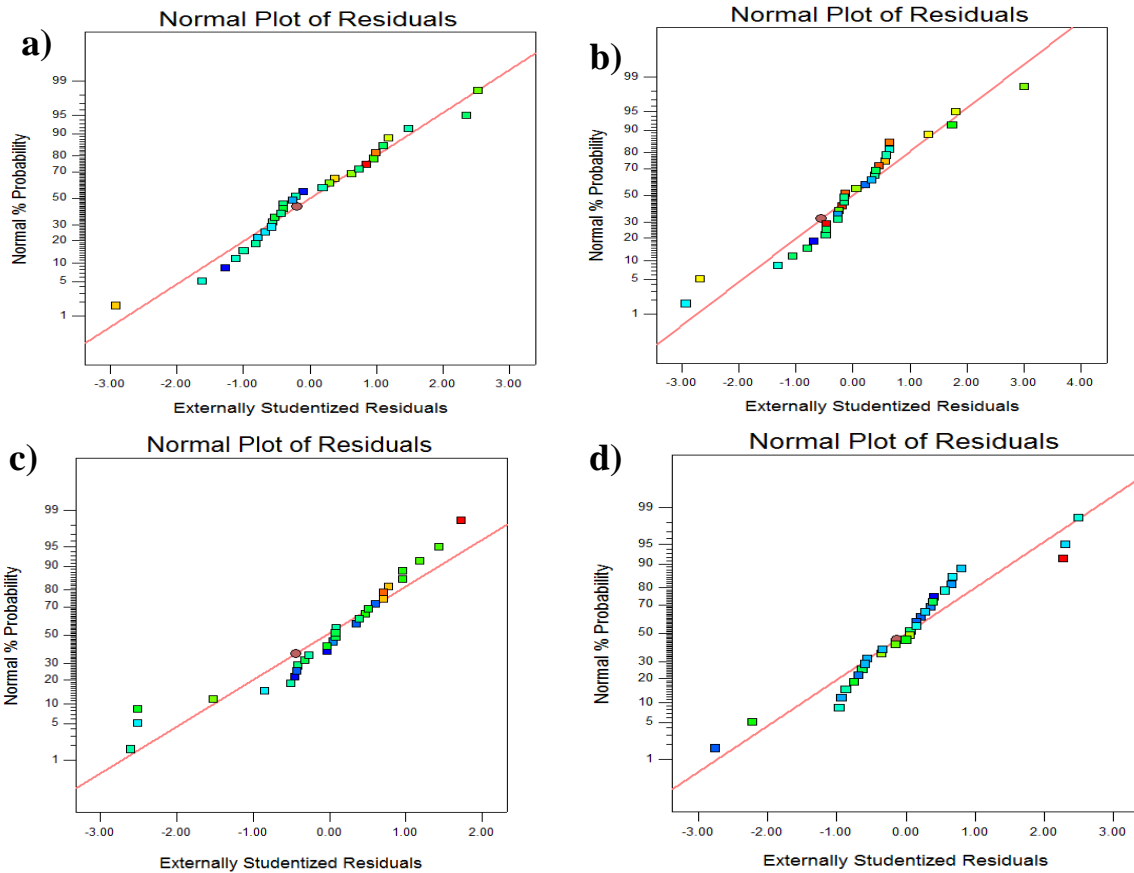
Figure 6.7 Normal probability plots of residuals for a) cutting force b) surface roughness c) tool wear d) MRR

6.6 OPTIMIZATION TECHNIQUES

Nowadays, optimization algorithms have received a wide scope by the engineering design arena and the industrial sector. Many research issues are optimization problems and are conflicting in nature. To solve the conflicting objective optimization problems, one has often used approximate methods which return near optimal solutions in a

relatively shorter time. Algorithms of these types are called as heuristics as they use specific knowledge to solve problems in order to build or improve solutions. Optimization concern to the finding best optimum results for the given objective functions. Finding an optimal solution may be for the minimization or maximization problems. In the physical system, finding an optimal solution for a single objective function is called the single objective optimization. Apart from the gradient and heuristic approach stochastic search principles such as evolutionary algorithms and simulated algorithm are the examples of such algorithm.

If finding an optimal solution for more than one objective functions called multi objective optimization. In most optimization problem involves multiple objectives. A multi objective function problem has number of objective functions which are to be minimized or maximized. All the objectives are important; a solution is may be extreme for one objective, in that situation compromise of other objective is required. Optimization is technique to obtain best results for the given problems under given constraints.

6.7 EVOLUTIONARY ALGORITHMS

Evolutionary algorithms (EAs) are imitative of natural evolutionary principles to constitute search and optimization procedure. Genetic algorithm (GA) is evolutionary algorithm and was introduced by John Holland (1975). These algorithm functions are to selection of the fittest to produce better approximation to solutions.

Particle swam optimization algorithm (PSO) is a relatively new approach in modern heuristics for optimization, is one of the evolutionary protocol methods. PSO was first developed by Eberhart and Kennedy (1995) (Kennedy and Eberhart, 1995) for continues function optimization. There are several stochastic algorithms such as genetic algorithms, differential evolution, Tabu search, simulated annealing, ant colony optimization and particle swarm optimization. These algorithms are used to find optimal solution for different objective function. The basic concept of PSO is originated from the food hunting behavior of birds. It was found that the intelligent swarming behavior, flocks of birds would always suddenly change the direction, scatter and

gather. Behaviour of birds is also unpredictable but always consistent as whole, with individuals keeping the most suitable distance. Every swarm of PSO is a solution in the solution space. It adjusts the flight according to its own and its companion flying experience.

6.8 BACKGROUND OF PSO

Optimality of solution is based on the one or several criteria that are usually a problem and user dependent. Constraints can be posed by the user or the problem itself, thereby reducing the number of prospective solutions. If the solution fulfils all the constraints, it is called the feasible solution. Among all the feasible solution the global optimization problem concerns the detection of the optimum one. However, this is not always necessary. Indeed, there are cases where sub optimal solutions are acceptable depending on their quality compared to optimal one. This is usually described as local optimization, although the same terms have been used to describe the local search in a strict vicinity of the search space. A mathematical modeling phase precedes the optimization procedure with all underlying constraints. The building blocks of candidate solutions are translated into numerical variables and solutions are represented as numerical vectors. Moreover a proper mathematical function is to build such that it's global minimizes that are points where its minimum value is attained which corresponds to optimal solutions of the original problems. This function called the objective function and detection of its global minimize is the core subject of global optimization. Instead of minimizing an optimization problem it can be maximization by inverting the sign of the objective function. Algorithm of PSO is moderately simple and its implementation is, therefore straight forward and easy. PSO has been found to be very effective in all variety of applications, being able to produce good results with less computational time (quick convergence) and low cost (Kennedy, 2010)

6.9 PSO OPTIMIZATION OF TAM PROCESS PARAMETERS

PSO coding structure is to be defined and the initial population is distinct. The computation with particle swarm with particle swam intelligent operators is used to evaluate fitness with respect to the objective function. General flow chart of PSO algorithm is shown in Figure 6.8.

Terminology used in PSO algorithm

Terms used in PSO algorithm are listed here:

Particle: Individual in the group of swarms. A potential solution is represented each swarm in the problem.

Swarm: Population of the algorithm.

Pbest (personal best): Personal best position of a given particle, so far. That is, the position of the particle that has provided the greatest success. Pk in equation 6.5 represents best position (Pbest) individual until iteration k.

Gbest (Global best): Position of the best particle of the entire swarm. Gk in equation 6.5 represents best position of the group until iteration k.

Leader: Particle that is used to guide another particle towards better regions of the search space.

*Velocity (vecto*r): This vector drives the optimization process, that is, it determines the direction in which a particle needs to "fly" (move), in order to improve its current position.

Inertia weight (w): It is employed to control the impact of the previous history of velocities on the current velocity of a given particle and denoted by w.

Learning factor: Represents the attraction that a particle has towards either its own success or that of its neighbors. Two learning factors used: C1 and C2, where C1 is the cognitive learning factor and it represents the attraction that a particle has towards its own success and C2 is the social learning factor and represents the attraction that a

particle has toward the success of its neighbors. Both, C1 and C2 are constants (González et al., 2012).

The PSO algorithm searches in parallel using a group of individuals similar to other Artificial intelligence based heuristic optimization techniques. An individual in a swarm approaches to the optimum or a quasi-optimum through its present velocity, previous experience, and the experience of its neighbors.
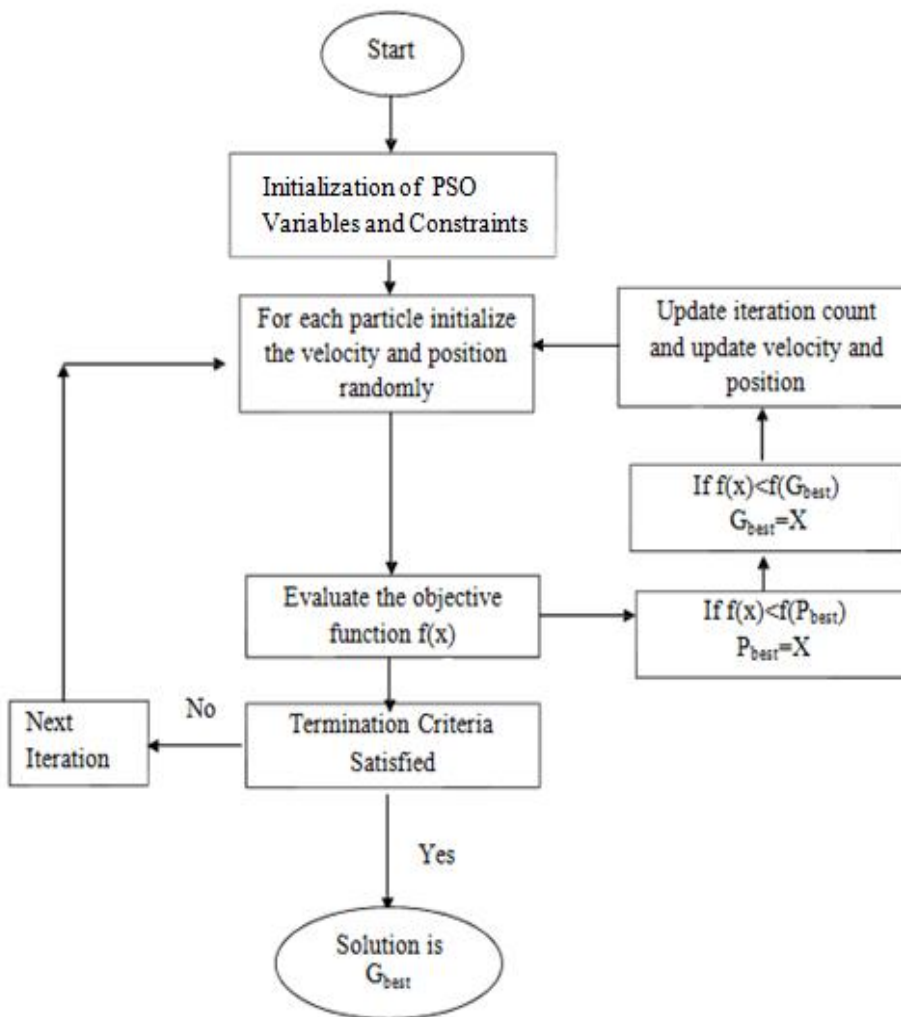
Figure 6.8 Generalized flow chart of PSO

In a physical n-dimensional search space, the position and velocity of individual i are represented as the vectors $X_i = (x_{i1}........x_{in})$, and $V_i = (v_{i1}..........v_{in})$ respectively, in the PSO algorithm. Let $Pbest_i = (x_{i1}^{pbest} .... x_{in}^{pbest})$ and $Gbest_i = (x_{i1}^{Gbest} ....x_{in}^{Gbest})$, respectively, be the best position of individual and its neighbors' best position so far. Using the information, the updated velocity of individual i is modified under the following equation in the PSO algorithm (Chen et al., 2007).

$$V_{k+1} = wv_k^i + c_1 rand_1 * (P_k^{besti} - X_k^i) + c_2 rand_2 * (G_k^{besti} - X_k^i) \text{-----------------(6.5)}$$

Where V_k^i = velocity of individual iteration;

W = weight parameter;

C_1 C_2 = weight factors;

$rand_1$, $rand_2$ = Random numbers between 0 and 1;

X_k^i = Position of individual at iteration k;

P_k^{besti} = Best position of individual until iteration k;

G_k^{besti} = Best position of group until iteration k.

The steps involved in PSO algorithms are:

1. Initialize an array of particles with random positions and velocities on D dimensions (parameters to be optimized i.e A, B and C).

Set constants C_1, C_2.

    (a) Initialize the particle position $X_0^i = X_{min} + rand (X_{max} - X_{min})$ ---- (6.6)

    (b) Initialize the particle velocity $V_0^i = X_{min} + rand (X_{max} - X_{min})$ -----(6.7)

Set k=1

2. Evaluate the desired maximization function (F_k^i),

    (a) If $F_k^i \leq F_{best}^i$ then $F_{best}^i = F_k^i$, $P_k^i = X_k^i$ -----------(6.8)

    (b) If $F_k^i \leq F_{best}^g$ then $F_{best}^g = F_k^i$, $P_k^g = X_k^i$ -------------- (6.9)

(c) If stopping condition is satisfied then go to step 3.

3. Update particle velocities V_{k+1}^i

$V_{k+1} = wv_k^i + c_1 \text{rand}_1 * (P_k^{besti} - X_k^i) + c_2 \text{rand}_2 * (G_k^{besti} - X_k^i)$ --------------(6.5)

4. Update particle position X_{k+1}^i

$$X_{k+1}^i = X_k^i + V_{k+1}^i$$ -------------------------- (6.10)

5. Evaluate the objective function (F_k^i)

    (a) If $F_k^i \leq F_{best}^i$ then $F_{best}^i = F_k^i$, $P_k^i = X_k^i$ ----------------(6.11)

    (b) If $F_k^i \leq F_{best}^g$ then $F_{best}^g = F_k^i$, $P_k^g = X_k^i$ ---------------- (6.12)

    (c) If stopping condition is satisfied then go to step 7, otherwise go to step 5.

6. Increment K

7. Go to next iteration.

8. Terminate.

Accordingly in the current approach individual particle (swarm) represents a possible solution to fitness function. Initially a random set of 20 populations is created for the particles to be optimized (A, B and C). The velocity and position updates based on swarm and personal influence was first depicted pictorially by (Hashim et al. 2012) and is shown in Figure 6.9. Later a new parameter called inertia weight 'w' is added into the original PSO algorithm. A large inertia weight facilitates a global search, while a small inertia weight facilitates local search (Shi and Eberhart, 1998). In equation (6.1), particle velocities on each dimension is clamped to a maximum velocity V max , so that if the sum of the three parts on the right side exceeds a constant value specified by the user, then the velocity on that dimension is assigned to be $\pm$ vmax . Here r1 and r2 represent the uniform random numbers range between 0 and 1 (Yiqing et al., 2007).
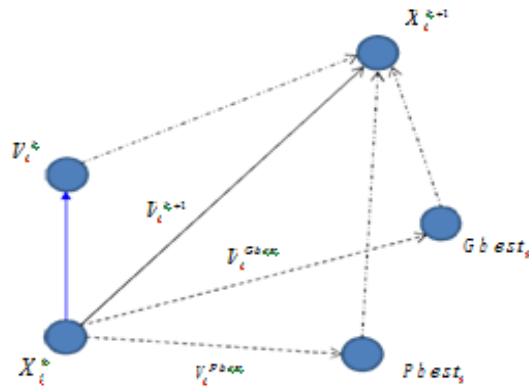
Figure 6.9 Mechanism of velocity and position updates in Particle Swarm

Where

X_k^i = Current position;

X_i^{k+1} = Current position;

V_i^k = Current velocity;

V_i^{k+1} = Modified velocity;

V_i^{best} = Velocity best on Pbest$_i$

V_i^{Gbest} = Velocity best on Gbest$_i$

Table 6.7 Minimum and Maximum values of TAM process parameter

Code	Parameter	Minimum	Maximum
A	Cutting speed (m/min)	28	130
B	Feed rate (mm/rev)	48	62
C	Depth of cut (mm)	20	80
D	Workpiece temperature (^{o}C)	200	600

The present study considers simultaneously multi objective optimization of cutting force, surface roughness, tool wear and metal removal rate which are

143

conflicting in nature. In order to convert the first objective (cutting force), it is to be modified. The objective functions used for evaluation of fitness values are given (Garg et al., 2012). All the objectives were minimized as follows.

Objective   (1) = cutting force (Fc)

Objective   (2) = Surface roughness (Ra)

Objective   (3) = Tool wear

Objective   (4) = MRR

Figure 6.10 illustrates the PSO flow chart to optimize the process parameters of TEM for cutting force, surface roughness, tool wear and metal removal rate as objective functions. The second order regression models for cutting force, surface roughness, tool wear and metal removal rate are obtained from the design expert 10 statistical software, by using equations 6.1, 6.2, 6.3 and 6.4 respectively. These regression models are used for multiobjective optimization using PSO as fitness functions. The PSO algorithm was applied in MATLAB, and the Table 6.9 indicated the minimum and maximum values of TAM process parameters were used as constraints to evaluate the objective functions. The Figure 6.10 illustrates the flow chart of PSO.

Fitness evaluation function for Inconel 718 superalloy is described in the Figures 6.10. Table 6.7 shows the multiobjective performance with respect to input machining process parameters for PSO.

The process parameters play an important role in receiving good convergence characteristics of PSO for Inconel 718 superalloy, the set obtained for 100 iterations as shown in Figure 6.11. Sixteen solutions out of 100 set of iterations along with the corresponding parameter setting is shown in the Table 6.8 for Inconel 718. In this sixteen optimal points are considered have been reported in the Table 6.8 and Based on the surface component requirements the best solution can be selected. PSO optimal process parameters can be used as handy technology guidelines for optimal machining of Inconel 718 superalloy.
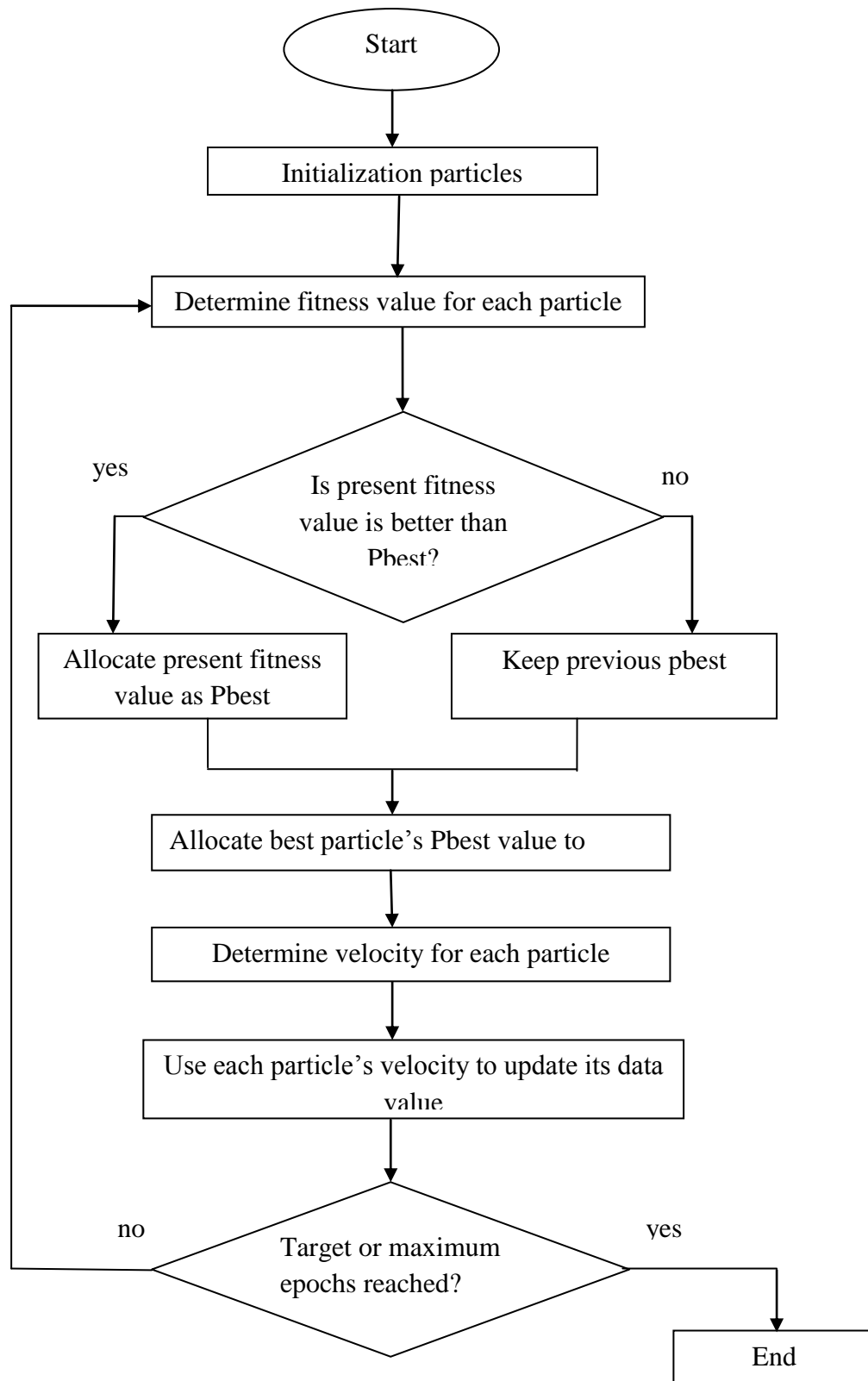
Figure 6.10 Flow chart for PSO design
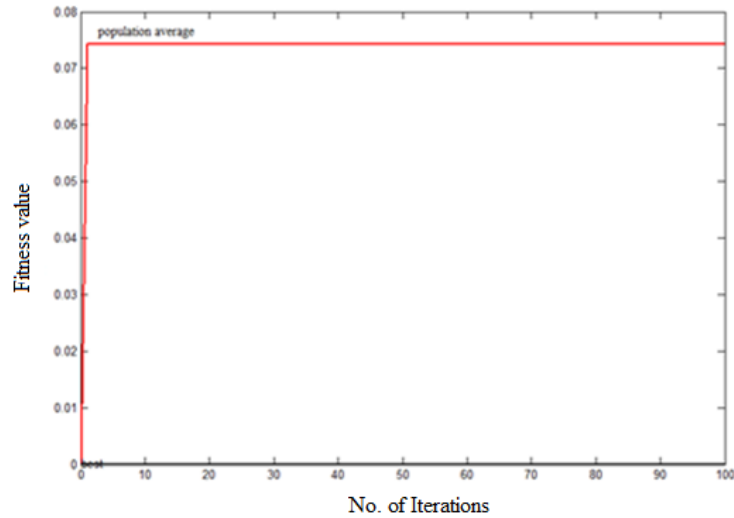
Figure 6.11 Convergence characteristics of PSO

Table 6.8 PSO optimal process parameters and their levels of Inconel 718

S.No	Cutting speed (m/min)	Feed rate (mm/rev)	Depth of cut (mm)	Workpiece temperature (^{o}C)	F_c (N)	R_a (µm)	V_{max} (mm)	MRR (g/min)
1	128.19	0.131	0.478	538	201.72	1.5112	0.32	37.97
2	127.14	0.051	0.419	548	252.10	0.818	0.21	32.33
3	127.14	0.103	0.453	470	180.06	1.228	0.28	33.45
4	128.19	0.051	0.396	570	261.56	0.81	0.21	33.184
5	121.72	0.085	0.298	493	202.29	0.961	0.24	28.03
6	108.29	0.089	0.286	568	189.95	0.823	0.22	25.34
7	113.53	0.053	0.205	583	223.114	0.63	0.168	21.8
8	101.67	0.092	0.446	524	165.11	0.779	0.22	20.897
9	128.44	0.097	0.272	495	212.78	1.152	0.26	35.22
10	115.85	0.066	0.438	569	210.16	0.705	0.21	27.19
11	104.45	0.096	0.492	534	167.56	0.826	0.23	23.0
12	112.04	0.086	0.308	490	183.59	0.862	0.22	23.21
13	101.67	0.142	0.461	577	199.6	1.44	0.3	30.75
14	121.56	0.051	0.268	429	237.14	0.906	0.20	25.95
15	128.24	0.074	0.402	417	194.64	1.109	0.24	31.45
16	127.45	0.051	0.324	473	247.17	0.910	0.213	30.23
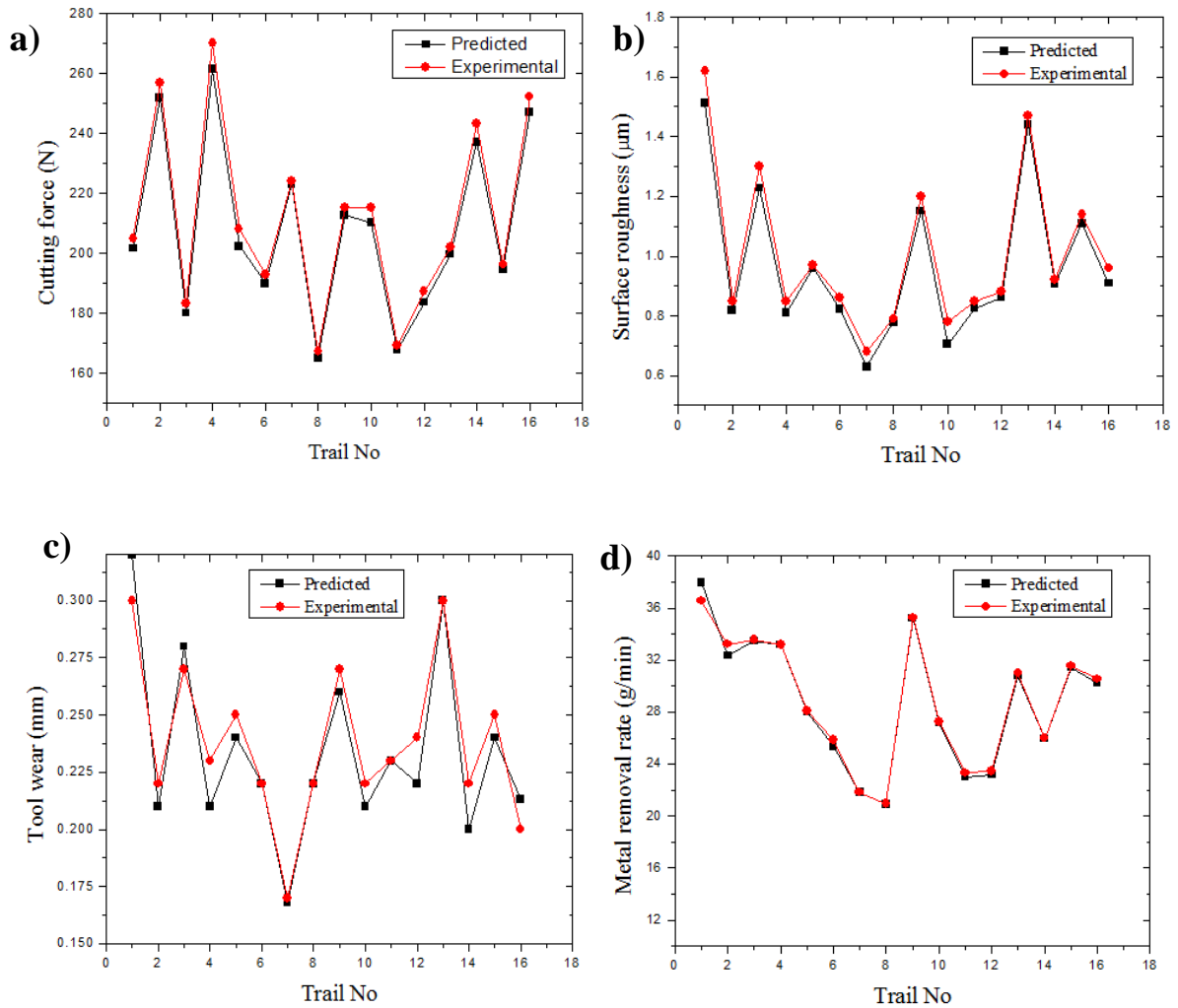
Figure 6.12 Experimental and PSO predicted values for Inconel 718 superalloy
(a) cutting force (b) surface roughness (c) tool wear (d) MRR

It is analyzed that the PSO optimized values were experimentally evaluated for process parameter combination as confirmation experimentation. The comparison of experimental and predicted values of Inconel 718 superalloy cutting force, surface roughness, tool wear and MRR, were displayed in Figure 6.12

147

6.10 VALIDATION OF PSO RESULTS

It is analyzed that the PSO optimized values were experimentally evaluated for process parameter combination as confirmation experimentation. The comparison of experimental and predicted values of Inconel 718 superalloy cutting force, surface roughness, tool wear and MRR were displayed in Figure 6.11 experimental values. As it is observed that the predicted values are closely follows the experimental values. The percentage error is calculated as follows.

$$\% \text{ Error} = \frac{(Y_i, \exp - Y_i, pred)}{Y_{i, \exp t}} \text{ X } 100 \qquad \text{................(6.13)}$$

Where Y_i, expt is the experimental value for i_{th} trial and Y_i, pred is the predicted by PSO for i^{th} trial. The error was found between the experimental and predicted value which is < 1.78 % for cutting force and error for surface roughness < 5 % and for tool wear is < 2 % and error for MRR < 1.7 % machining of Inconel 718 superalloy.

This clearly demonstrates predicted values are having good agreement with experimental value. Hence PSO can be used as tool to predict the thermally assisted machining parameters for Inconel 718 superalloy effectively.

6.11 SUMMARY

In this chapter, cutting force, surface roughness, tool wear and metal removal rate (MRR) were analyzed through experiments. Quadratic regression model has been developed to correlate the relation between input and output process parameters. The developed models are used in PSO objective functions to optimize the process parameters. Based on the experimental analysis, the following conclusions are drawn

- Mathematical model has been developed and it is adequate to use navigate the design space.
- Optimized process parameters were developed based on the particle swarm optimization technique. A sample technology table has been reported for machining of Inconel 718 superalloy can be usage in industrial applications.

- Percentage error of predicted and experimental values was very minimum for cutting force, surface roughness, tool wear and MRR. Hence PSO technique is quite effective in optimization.

CHAPTER 7

CONCLUSIONS AND SCOPE FOR FUTURE WORK

7.1 CONCLUSIONS

In the present work, the thermally assisted machining characteristics of Inconel 718 superalloy have been studied. Basically this study evaluates the machining performances of uncoated, TiAlN multilayer coating and TiCN/Al$_2$O$_3$/TiN triple layer coated cutting tools using a Kirloskar lathe machine. This study evaluates the major significant factors and their effect on cutting forces, surface and sub-surface properties, tool wear and MRR. The multiobjective optimization was performed using particle swarm optimization algorithm to achieve better cutting force, surface roughness, tool wear and MRR. The following conclusions are drawn from the current study:

1. Cutting forces in TAM were observed to be less compared to conventional machining; Surface roughness was improved remarkably in TAM. About 21.8 % reduction in surface roughness was observed in TAM compared to conventional machining, Tool wear was improved by 29 %, and MRR improved by 5.9 % in TAM compared to conventional machining.

2. From the results it was observed that cutting force is highly influenced by cutting speed followed by feed rate, depth of cut and workpiece temperature. Surface roughness is mostly influenced by feed rate and workpiece temperature. Whereas tool wear and MRR are mostly influenced by cutting speed followed by feed rate and depth of cut respectively.

3. Compared to uncoated, TiAlN and TiCN/Al$_2$O$_3$/TiN triple layer coated cutting tools, TiAlN nano multilayer coated tool is gave better performance in machining of Inconel 718 superalloy.

4. The microhardness increases as the workpiece temperature increases, hence TAM improves the performance of the product.

5. The XRD results of thermally assisted machining reveals that there are neither phase changes, nor broadening of the peaks that were observed at different machining conditions.

6. Tensile residual stresses are induced on the machined surface, as the workpiece temperature increases the residual stresses were decreased.

7. Mathematical models have been developed to correlate the process parameters and performance characteristics of thermally assisted machining using response surface methodology while machining Inconel 718 superalloy.

8. Optimized process parameters were determined based on the particle swarm optimization technique. A sample technology table has been reported for machining of Inconel 718 can be used in industrial applications.

7.2 SCOPE OF FUTURE WORK

Although the thermally assisted machining characteristics of Inconel 718 superalloy have been thoroughly studied, still there is scope for further investigation. The following suggestion may be useful for future work:

- Investigate on improvement in the machinability characteristics of hard materials like Titanium alloys, tool steel, high manganese steel using Oxy-LPG flame assisted machining.
- Examine the thermal model interface with a machining model for machinability analysis.
- Optimum incident angle and stand-off distance for flame can be obtained by varying incident angle and stand-off distance of the torch.
- Investigate machinability of hard metals using PCBN cutting tool.
- Investigate on chip morphology to understand the machinability characteristics.

- The technique of thermally assisted machining can be applied in cutting composites.
- Metallurgical aspects of the workpiece after hot machining can be studied.
- Use of Hybrid machining to improve the tool life and performances of hard metals.

REFERENCES

Anderson, M., Patwa, R. and A, Shin, Y.C. (2006). "Laser-assisted machining of Inconel 718 with an economic analysis". *International Journal of Machine Tools & Manufacture*, 46, 1879–1891.

Arunachalam, R.M., Mannan, M.A. and Spowage, A.C. (2004). "Residual stress and surface roughness when facing age hardened Inconel 718 with CBN and ceramic cutting tools". *International Journal of Machine Tools and Manufacture*, 44, 879–887.

Aslan, E. (2005). "Experimental investigation of cutting tool performance in high speed cutting of hardened X210 Cr12 cold-work tool steel (62 HRC)". *Materials and Design*, 26(1), 21–27.

Astakhov, V.P. (2004). "The assessment of cutting tool wear". *International Journal of Machine Tools and Manufacture*, 44(6), 637–647.

Attia, H., Tavakoli, S., Vargas, R. and Thomson, V. (2010). "Laser-assisted high-speed finish turning of superalloy Inconel 718 under dry conditions". *CIRP Annals-Manufacturing Technology*, 59(1), 83-88.

Bermingham, M.J., Palanisamy, S. and Dargusch, M.S. (2012). "Understanding the tool wear mechanism during thermally assisted machining Ti-6Al-4V". *International Journal of Machine Tools and Manufacture*, 62, 76–87.

Bhatt, A., Attia, H., Vargas, R. and Thomson, V. (2010). "Wear mechanisms of WC coated and uncoated tools in finish turning of Inconel 718". *Tribology International*, 43(5), 1113-1121.

Bushlya, V., Zhou, J. and Ståhl, J.E. (2012). "Effect of cutting conditions on machinability of superalloy Inconel 718 during high speed turning with coated and uncoated PCBN tools". *Procedia CIRP*, 3, 370-375.

Chen, W. (2000). "Cutting forces and surface finish when machining medium hardness steel using CBN tools". *International Journal of Machine Tools and Manufacture*, 40(3), 455–466.

Choudhury, I.A., and El-Baradie, M.A. (1998). "Machinability of nickel-base super alloys: a general review". *Journal of Materials Processing Technology*, 77(1), 278-284.

Choudhury, S.K. and Thandra, S.K. (2010). "Effect of cutting parameters on cutting force, surface finish and tool wear in hot machining". *International Journal of Machining and Machinability of Materials*, 7(3-4), 260-273.

Chryssolouris, G., Anifantis, N. and Karagiannis, S. (2014). "Laser Assisted Machining ∶ An Overview". *Journal of Manufacturing Science and Engineering*, 119, 766–769.

Chryssolouris G. and Anifantis N, K.S. (1994). "Laser assisted machining". *J. of Manf. Sc. & Engg,*, 119(1), 1–7.

Dabade, U.A., and Jadhav, M.R. (2016). "Experimental Study of Surface Integrity of Al/SiC Particulate Metal–matrix Composites in Hot Machining". *Procedia CIRP*, 41, 914–919.

Dandekar, C.R., Shin, Y.C. and Barnes, J. (2010). "Machinability improvement of titanium alloy (Ti-6Al-4V) via LAM and hybrid machining". *International Journal of Machine Tools and Manufacture*, 50(2),174–182.

Ding, H. and Shin, Y.C. (2010). "Laser-assisted machining of hardened steel parts with surface integrity analysis". *International Journal of Machine Tools and Manufacture*, 50(1), 106–114.

D Dudzinski, A Devillez, A Moufki, D Larrouquere, V Zerrouki, J Vigneal,l. (2004) A review of developments towards dry and high speed machining of Inconel 718 alloy, *International Journal of Machine Tools and Manufacture*, 44(4), 439-456.

Ezugwu, E.O., Wang, Z.M. and Machado, A.R. (1999). "The machinability of nickel-based alloys: a review". *Journal of Materials Processing Technology*, 86(1), 1-16.

Feyzi, T. and Safavi, S.M., (2013). "Improving machinability of Inconel 718 with a new hybrid machining technique". *International Journal of Advanced Manufacturing Technology*, 66(5-8), 1025-1030.

Gaitonde, V.N., Karnik, S.R., Figueira, L. and Davim, J.P., (2009). "Machinability investigations in hard turning of AISI D2 cold work tool steel with conventional and wiper ceramic inserts". *International Journal of Refractory Metals and Hard Materials*, 27(4), 754-763.

Garcí, V., Arriola, I., Gonzalo, O. and Leunda, J. (2013). "Mechanisms involved in the improvement of Inconel 718 machinability by laser assisted machining (LAM)". *International journal of machine tools and manufacture*, 74, 19-28.

Gaurav Bartarya, SK Choudhury. (2012)   State of the art in hard turning, *International Journal of Machine Tools and Manufacture*, 53(1), 1-14.

Germain, G., Dal Santo, P. and Lebrun, J.L. (2011). "Comprehension of chip formation in laser assisted machining". *International Journal of Machine Tools and Manufacture*, 51(3), 230–238.

154

Jiang, W., More, A.S., Brown, W.D. and Malshe, A.P. (2006). "A cBN-TiN composite coating for carbide inserts: Coating characterization and its applications for finish hard turning". *Surface and Coatings Technology*, 201(6), 2443-2449.

Jindal, P.C., Santhanam, A.T., Schleinkofer, U. and Shuster, A.F. (1999). "Performance of PVD TiN, TiCN, and TiAlN coated cemented carbide tools in turning". *International Journal of Refractory Metals and Hard Materials*, 17 (1),163-170.

Kaynak, Y. (2014). "Evaluation of machining performance in cryogenic machining of Inconel 718 and comparison with dry and MQL machining". *International Journal of Advanced Manufacturing Technology*, 72, 919–933.

Kitagawa, T., Maekawa, K. and Kubo, A. (1990). "Plasma hot machining for high hardness metals". *Bulletin of the Japan Society of Precision Engineering*, 22(2), 145–151.

Komanduri, R. and Brown, R.H. (1981). "On the mechanics of chip segmentation in machining". *Journal of Engineering for Industry*, 103(1), 33–51.

Konig, W. and Zaboklicki, A.K. (1994). "Laser-assisted hot machining processes: technological potentials". *Laser Assisted Net Shape Engineering Proceedings of the LANE'94*, 1, 389–404.

Lajis, M.A., Amin, A.K.M., Karim, A.N., Daud, C., Radzi, M. and Ginta, T.L. (2009). "Hot machining of hardened steels with coated carbide inserts". *American Journal of Engineering and Applied Sceices*, 2(2), 421-427.

Lee, T.H. and Mathew, P. (2007). "Experimental and theoretical investigation of AISI D2 hardened steel machining with varying nose radius CBN tools". *International Journal of Machining and Machinability of Materials*, 2(2), 254-269.

Lee, Y.Z. and Ponnambalam, S.G. (2012). "Optimisation of multipass turning operations using PSO and GA-AIS algorithms". *International Journal of Production Research*, 50(22), 6499–6518.

Leshock, C.E., Kim, J. and Shin, Y.C. (2001). "Plasma enhanced machining of Inconel 718: modeling of workpiece temperature with plasma heating and experimental results". *International Journal of Machine Tools and Manufacture*, 41, 877–897.

Li, L., He, N., Wang, M. and Wang, Z.G. (2002). "High speed cutting of Inconel 718 with coated carbide and ceramic inserts". *Journal of Materials Processing Technology*, 129(1), 127-130.

Lima, J.G., Avila, R.F., Abrao, A.M., Faustino, M. and Davim, J.P. (2005). "Hard

turning: AISI 4340 high strength low alloy steel and AISI D2 cold work tool steel". *Journal of Materials Processing Technology*, 169(3), 388-395..

Lin, Z.C. and Chen, D.Y. (1995). "A study of cutting with a CBN tool". *Journal of Materials Processing Tech.*, 49(1–2), 149–164.

Liu, F., Lin, X., Yang, G., Song, M., Chen, J. and Huang, W. (2011). "Microstructure and residual stress of laser rapid formed Inconel 718 nickel-base superalloy". *Optics & laser technology*, 43(1), 208-213.

Madhavulu, G. and Ahmed, B. (1994). "Hot machining process for improved metal removal rates in turning operations". *Journal of materials processing technology*, 44 (3-4), 199-206.

Maity, K.P. and Swain, P.K. (2008). "An experimental investigation of hot-machining to predict tool life". *Journal of materials processing technology*, 198(1), 344-349.

Masood, S.H., Armitage, K. and Brandt, M. (2011). "An experimental study of laser-assisted machining of hard-to-wear white cast iron". *International Journal of Machine Tools and Manufacture*, 51(6), 450–456.

Mukherjee, P.N. and Basu, S.K. (1973). "Statistical evaluation of metal-cutting parameters in hot-machining". *International Journal of Production Research*, 11(1), 21–36.

Outeiro, J.C., Pina, J.C., M'saoubi, R., Pusavec, F. and Jawahir, I.S., (2008). "Analysis of residual stresses induced by dry turning of difficult-to-machine materials". *CIRP Annals-Manufacturing Technology*, 57(1), 77-80.

Ozel, T., Hsu, T.K., and Zeren, E. (2005). "Effects of cutting edge geometry, workpiece hardness, feed rate and cutting speed on surface roughness and forces in finish turning of hardened AISI H13 steel". *International Journal of Advanced Manufacturing Technology*, 2(3–4), 262–269.

Ozler, L., Inan, A. and Özel, C. (2001). "Theoretical and experimental determination of tool life in hot machining of austenitic manganese steel". *International Journal of Machine Tools and Manufacture*, 41(2), 163–172.

Ozler, L. and Tosun, N. (2004). "Optimisation for hot turning operations with multiple performance characteristics". *The International Journal of Advanced Manufacturing Technology*, 23(11-12), 777-782.

Park, K.H., Olortegui-Yume, J., Yoon, M.C. and Kwon, P. (2010). "A study on droplets and their distribution for minimum quantity lubrication (MQL)". *International Journal of Machine Tools and Manufacture*, 50(9), 824-833.

Patrick A. Rebro, Yung C. Shin, Frank P. Incropera. (2002) Laser-Assisted Machining of Reaction Sintered Mullite Ceramics, *ASME Journal of Manufacturing Science and Engineering*, 124, 875-885.

Phadke, S.M., (1989). Quality Engineering Using Robust Design Prentice Hall

Poulachon, G. and Moisan, A.L. (2000). "Hard Turning: Chip Formation Mechanisms and Metallurgical Aspects". *Journal of Manufacturing Science and Engineering*, 122(3), 406.

Pramanik, A., Neo, K.S., Rahman, M., Li, X.P., Sawa, M., and Maeda, Y. (2003). "Cutting performance of diamond tools during ultra-precision turning of electroless-nickel plated die materials". *Journal of Materials Processing Technology*, 140 (1), 308-313..

Ranganathan, S. and Senthilvelan, T. (2011). "Multi-response optimization of machining parameters in hot turning using grey analysis". *International Journal of Advanced Manufacturing Technology*, 56, 455–462.

Ranganathan, S., Senthilvelan, T. and Sriram, G. (2010). "Evaluation of Machining Parameters of Hot Turning of Stainless Steel (Type 316) by Applying ANN and RSM". *Materials and Manufacturing Processes*, 25(10), 1131–1141.

Ravi, A.M., Murigendrappa, S.M. and Mukunda, P.G. (2014). "Experimental investigation on thermally enhanced machining of high-chrome white cast iron and to study its machinability characteristics using Taguchi method and artificial neural network". *International Journal of Advanced Manufacturing Technology*, 72, 1439–1454.

Rech, J. and Moisan, A. (2003). "Surface integrity in finish hard turning of case-hardened steels". *International Journal of Machine Tools and Manufacture*, 43(5), 543–550.

Ren, X. and Liu, Z. (2016). "Influence of cutting parameters on work hardening behavior of surface layer during turning superalloy Inconel 718". *The International Journal of Advanced Manufacturing Technology*, 86 (5-8), 2319-2327.

Ross, P.J., (1988). "Taguchi techniques for quality engineering: loss function, orthogonal experiments, parameter and tolerance design".

Rozzi, J.C., Pfefferkorn, F.E., Incropera, F.P. and Shin, Y.C. (2000). "Transient, three-dimensional heat transfer model for the laser assisted machining of silicon nitride: I. Comparison of predictions with measured surface temperature histories". *International Journal of Heat and Mass Transfer*, 43(8), 1409-1424..

Sahin, Y. (2009). "Comparison of tool life between ceramic and cubic boron nitride (CBN) cutting tools when machining hardened steels". *Journal of Materials*

Processing Technology, 209(7), 3478–3489.

Sanchez, L.E., Mello, H.J., Neto, R.R.I. and Davim, J.P. (2014). "Hot turning of a difficult-to-machine steel (sae xev-f) aided by infrared radiation". *The International Journal of Advanced Manufacturing Technology*, 73(5-8), 887-898.

Sarah, S.A., Daisy, I.J. and Varghese, R. (2010). "Optimization of process parameters using genetic algorithm and PSO". In *2010 International Conference on Communication and Computational Intelligence (INCOCCI)*.

Senthil Kumar, A., Durai, A.R. and Sornakumar, T. (2006). "The effect of tool wear on tool life of alumina-based ceramic cutting tools while machining hardened martensitic stainless steel". *Journal of Materials Processing Technology*, 173(2), 151-156.

Sharman, A.R.C., Hughes, J.I. and Ridgway, K. (2006). "An analysis of the residual stresses generated in Inconel 718 when turning". *Journal of Materials Processing Technology*, 173(3), 359-367.

Skvarenina, S. and Shin, Y.C. (2006). "Laser-assisted machining of compacted graphite iron". *International Journal of Machine Tools and Manufacture*, 46(1), 7–17.

Sobiyi, K., Sigalas, I., Akdogan, G. and Turan, Y. (2015). "Performance of mixed ceramics and CBN tools during hard turning of martensitic stainless steel". *The International Journal of Advanced Manufacturing Technology*, 77(5-8), 861-871.

Sun, S., Brandt, M. and Dargusch, M.S. (2010). "Thermally enhanced machining of hard-to-machine materials — A review". *International Journal of Machine Tools and Manufacture*, 50(8), 663–680.

Suresh, R., Basavarajappa, S., Gaitonde, V.N. (2012). "Machinability investigations on hardened AISI 4340 steel using coated carbide insert". *Int . Journal of Refractory Metals and Hard Materials RMHM*, 33, 75–86.

Suresh, R., Basavarajappa, S. and Samuel, G.L. (2012). "Some studies on hard turning of AISI 4340 steel using multilayer coated carbide tool". *Measurement*, 45 (7), 1872–1884.

Taylor, P., Lo, K.C. and Chen, N.N.S. (2007). "Prediction of tool life in hot machining of alloy steels". *International national journal of production research*. 15 (1), 47–63.

Thakur, A. and Gangopadhyay, S. (2016). "State-of-the-art in surface integrity in machining of nickel-based super alloys". *International Journal of Machine Tools and Manufacture*, 100, 25–54.

Thandra, S.K. and Choudhury, S.K. (2010). "Effect of cutting parameters on cutting force, surface finish and tool wear in hot machining". *International Journal of Machining and Machinability of Materials*, 7 (3-4), 278.

Trent, E.M., and Wright, P.K., (2000). *Metal cutting*, Butterworth-Heinemann.

Upadhyay, V., Jain, P.K. and Mehta, N.K. (2012). "Machinability Studies in Hot Machining of Ti-6Al-4V Alloy". *Advanced Materials Research*, 622–623, 361–365.

Wang, Y., Yang, L.J. and Wang, N.J. (2002). "An investigation of laser-assisted machining of Al_2O_3 particle reinforced aluminum matrix composite". 129, 268–272.

Xi, Y., Bermingham, M., Wang, G. and Dargusch, M., (2014). "SPH/FE modeling of cutting force and chip formation during thermally assisted machining of Ti6Al4V alloy". *Computational materials science*, 84, 188-197.

Xu, W., Liu, X., Sun, J. and Zhang, L. (2013). "Finite element simulation and experimental research on electric hot machining". *The International Journal of Advanced Manufacturing Technology*, 66(1-4), 407-415.

Yu, X.M., Xiong, X.Y. and Wu, Y.W. (2004). "A PSO-based approach to optimal capacitor placement with harmonic distortion consideration". *Electric Power Systems Research*, 71(1), 27–33.

Zhao, L.M., Hou, Z., Jia, D.P. and Wei, Q.K. (2012). "Online Temperature Detecting System in Hot Machining Process". *Applied Mechanics and Materials*,128, 657-660.

Zhou, J.M., Bushlya, V. and Stahl, J.E. (2012). "An investigation of surface damage in the high speed turning of Inconel 718 with use of whisker reinforced ceramic tools". *Journal of Materials Processing Tech.*, 212(2), 372–384.

Zhuang, K., Zhang, X., Zhu, D. and Ding, H. (2015). "Employing preheating-and cooling-assisted technologies in machining of Inconel 718 with ceramic cutting tools: towards reducing tool wear and improving surface integrity". *The International Journal of Advanced Manufacturing Technology*, 80(9-12), 1815-1822.

Table A1: Experimental observations for uncoated carbide tool based on L_{27} OA

Sl. No	Cutting forces (N)						Surface roughness (μm)		Tool wear (mm)		MRR (g/min)	
	F_c	S/N ratio	Ft	S/N ratio	Ff	S/N ratio	Ra	S/N ratio	Wear	S/N ratio	MRR	S/N ratio
1	272.00	-48.69	137.00	-42.73	169.00	-44.56	1.32	-2.41	0.11	19.17	2.14	6.19
2	245.75	-47.80	124.88	-41.93	152.88	-43.69	1.04	-0.34	0.09	20.91	2.86	9.37
3	224.00	-47.00	110.50	-40.87	140.50	-42.95	1.10	-0.83	0.12	18.41	4.45	13.94
4	241.50	-47.65	120.75	-41.64	152.75	-43.68	0.74	2.62	0.17	15.39	2.52	7.23
5	210.33	-46.45	105.17	-40.44	135.17	-42.62	1.20	-1.58	0.19	14.42	5.43	15.30
6	285.10	-49.09	142.55	-43.08	174.55	-44.84	1.65	-4.35	0.18	14.89	6.90	15.74
7	236.65	-47.48	118.33	-41.46	148.33	-43.42	1.72	-4.71	0.21	13.55	5.11	14.98
8	295.21	-49.40	147.61	-43.38	177.61	-44.99	1.91	-5.62	0.23	12.76	6.44	15.85
9	310.00	-49.82	149.09	-43.47	186.09	-45.39	1.85	-5.34	0.25	12.04	8.55	18.93
10	193.75	-45.74	104.88	-40.41	126.88	-42.07	0.79	2.05	0.25	12.04	2.35	6.36
11	204.21	-46.20	102.11	-40.18	132.11	-42.42	0.76	2.38	0.26	11.70	3.79	12.13
12	187.33	-45.45	93.67	-39.43	123.67	-41.84	0.65	3.74	0.29	10.75	6.63	16.73
13	234.00	-47.38	117.00	-41.36	147.00	-43.35	1.25	-1.94	0.29	10.75	4.62	13.55
14	194.00	-45.75	99.00	-39.91	130.00	-42.28	0.79	2.05	0.17	15.39	7.14	17.54
15	285.83	-49.12	142.92	-43.10	172.92	-44.76	1.54	-3.75	0.19	14.42	10.93	19.79
16	186.33	-45.40	94.17	-39.48	122.17	-41.74	1.57	-3.92	0.26	11.70	7.14	17.67
17	237.00	-47.49	118.50	-41.47	138.50	-42.83	2.68	-8.56	0.38	8.40	10.40	20.04
18	220.00	-46.84	110.00	-40.83	128.00	-42.14	1.87	-5.44	0.30	10.45	13.38	22.72
19	150.25	-43.53	75.13	-37.52	106.13	-40.52	1.13	-1.06	0.28	11.05	5.61	14.20
20	137.78	-42.78	66.39	-36.44	96.39	-39.68	0.69	3.22	0.36	8.87	11.13	21.16
21	110.00	-40.82	55.00	-34.81	85.00	-38.59	0.43	7.33	0.30	10.45	16.25	24.38
22	150.50	-43.55	75.25	-37.53	105.25	-40.44	1.17	-1.36	0.37	8.63	7.55	17.86
23	139.23	-42.87	69.62	-36.85	99.62	-39.97	1.19	-1.51	0.39	8.17	17.83	25.07
24	184.00	-45.29	92.00	-39.28	120.00	-41.58	1.62	-4.19	0.42	7.53	20.00	25.59
25	160.54	-44.11	80.27	-38.09	110.27	-40.85	1.50	-3.52	0.52	5.67	9.97	20.49
26	206.00	-46.27	101.50	-40.13	133.50	-42.51	2.35	-7.42	0.62	4.15	19.05	25.21
27	190.00	-45.57	94.50	-39.51	123.50	-41.83	1.78	-5.01	0.60	4.43	22.72	27.22

Table A2: Experimental observations for TiAlN multilayer coated insert based on L_{27} OA

Sl. No	Cutting forces (N)						Surface roughness (μm)		Tool wear (mm)		MRR (g/min)	
	F_c	S/N ratio	Ft	S/N ratio	Ff	S/N ratio	Ra	S/N ratio	Wear	S/N ratio	MRR	S/N ratio
1	202.54	-46.13	115.77	-41.27	138.24	-42.81	0.95	0.42	0.05	26.02	2.06	6.27
2	184.80	-45.33	107.52	-40.63	125.05	-41.94	0.71	2.93	0.07	23.09	2.96	9.43
3	166.45	-44.43	95.37	-39.59	116.93	-41.36	0.73	2.69	0.09	20.91	4.99	13.96
4	181.61	-45.18	102.03	-40.17	124.95	-41.93	0.59	4.53	0.15	16.47	2.52	8.03
5	158.17	-43.98	88.86	-38.97	111.56	-40.95	0.90	0.92	0.13	17.72	5.93	15.46
6	216.40	-46.70	122.45	-41.76	142.78	-43.09	1.30	-2.28	0.20	13.97	6.15	15.77
7	177.96	-45.01	99.98	-40.00	123.33	-41.82	1.23	-1.80	0.22	13.15	5.65	15.03
8	222.00	-46.93	124.67	-41.92	146.28	-43.30	1.74	-4.82	0.17	15.39	6.26	15.92
9	231.12	-47.28	125.98	-42.01	151.22	-43.59	1.52	-3.64	0.19	14.42	8.91	19.00
10	145.70	-43.27	88.62	-38.95	102.78	-40.24	0.71	3.02	0.20	13.97	2.29	7.18
11	156.57	-43.89	86.28	-38.72	106.06	-40.51	0.69	3.22	0.14	17.07	4.10	12.26
12	140.87	-42.98	79.15	-37.97	101.16	-40.10	0.59	4.58	0.16	15.91	6.88	16.75
13	175.97	-44.91	99.87	-39.99	120.25	-41.60	0.92	0.76	0.19	14.42	4.87	13.75
14	145.89	-43.28	83.66	-38.45	106.34	-40.53	0.60	4.39	0.15	16.47	7.63	17.64
15	218.94	-46.81	120.76	-41.64	145.44	-43.25	1.25	-1.94	0.23	12.76	10.01	20.01
16	140.12	-42.93	79.57	-38.01	100.93	-40.08	1.01	-0.12	0.21	13.55	7.79	17.83
17	178.22	-45.02	102.13	-40.18	113.29	-41.08	1.90	-5.58	0.26	11.70	10.40	20.34
18	165.44	-44.37	92.95	-39.36	105.70	-40.48	1.60	-4.08	0.24	12.39	13.69	22.73
19	114.99	-41.21	63.48	-36.05	84.81	-38.57	0.76	2.42	0.26	11.70	5.36	14.59
20	103.61	-40.31	54.10	-34.66	76.85	-37.71	0.58	4.68	0.29	10.75	11.47	21.19
21	82.72	-38.35	46.48	-33.34	69.53	-36.84	0.37	8.64	0.31	10.17	16.78	24.49
22	113.18	-41.08	63.59	-36.07	86.09	-38.70	0.77	2.31	0.26	11.70	7.86	17.90
23	104.70	-40.40	59.82	-35.54	81.49	-38.22	0.85	1.41	0.28	11.05	17.95	25.08
24	141.37	-43.01	77.74	-37.81	98.16	-39.84	1.20	-1.58	0.30	10.45	19.20	25.67
25	120.73	-41.64	66.83	-36.50	90.20	-39.10	0.99	0.12	0.31	10.17	10.67	20.56
26	152.91	-43.69	85.77	-38.67	108.20	-40.68	1.83	-5.25	0.29	10.75	18.30	25.25
27	142.88	-43.10	79.85	-38.05	101.02	-40.09	1.39	-2.86	0.36	8.87	23.07	27.26

Table A3: Experimental observations for TiCN/Al$_2$O$_3$/TiN triple layer insert based on L$_{27}$ OA

Sl. No	Cutting forces (N)						Surface roughness (μm)		Tool wear (mm)		MRR (g/min)	
	F$_c$	S/N ratio	Ft	S/N ratio	Ff	S/N ratio	Ra	S/N ratio	Wear	S/N ratio	MRR	S/N ratio
1	213.06	-46.57	118.72	-41.49	140.12	-42.93	1.00	0.00	0.09	20.91	2.06	6.28
2	191.41	-45.64	105.39	-40.46	127.65	-42.12	0.84	1.51	0.07	23.09	2.95	9.40
3	174.29	-44.83	98.15	-39.84	117.32	-41.39	0.85	1.41	0.10	20.00	4.98	13.95
4	194.06	-45.76	102.88	-40.25	129.55	-42.25	0.67	3.48	0.16	15.91	2.52	8.03
5	165.53	-44.38	90.60	-39.14	112.86	-41.05	0.96	0.35	0.17	15.39	5.93	15.45
6	220.37	-46.86	123.45	-41.83	145.75	-43.27	1.42	-3.05	0.23	12.76	6.14	15.76
7	186.24	-45.40	102.81	-40.24	123.85	-41.86	1.46	-3.29	0.19	14.42	5.63	15.01
8	232.33	-47.32	125.76	-41.99	148.30	-43.42	1.84	-5.30	0.18	14.89	6.33	16.02
9	243.97	-47.75	127.02	-42.08	157.38	-43.94	1.60	-4.08	0.23	12.76	8.95	19.03
10	153.48	-43.72	89.35	-39.02	105.94	-40.50	0.74	2.62	0.20	13.97	2.27	7.13
11	160.71	-44.12	87.99	-38.89	112.31	-41.01	0.73	2.73	0.16	15.91	4.08	12.21
12	147.43	-43.37	80.80	-38.15	103.26	-40.28	0.62	4.15	0.17	15.39	6.88	16.75
13	186.16	-45.40	99.68	-39.97	122.75	-41.78	0.98	0.18	0.21	13.55	4.87	13.75
14	152.68	-43.68	84.35	-38.52	108.55	-40.71	0.68	3.35	0.18	14.89	7.66	17.68
15	226.95	-47.12	124.76	-41.92	146.38	-43.31	1.35	-2.61	0.25	12.04	9.98	19.98
16	146.64	-43.33	80.23	-38.09	103.01	-40.26	1.13	-1.06	0.18	14.89	7.89	17.94
17	184.52	-45.32	100.96	-40.08	115.65	-41.26	2.07	-6.32	0.27	11.37	10.40	20.34
18	173.14	-44.77	93.72	-39.44	106.88	-40.58	1.70	-4.61	0.20	13.97	13.70	22.73
19	119.25	-41.53	66.01	-36.39	90.61	-39.14	0.86	1.31	0.22	13.15	5.36	14.59
20	108.43	-40.70	56.56	-35.05	80.49	-38.11	0.60	4.44	0.27	11.37	11.51	21.22
21	87.57	-38.85	46.86	-33.42	70.98	-37.02	0.40	7.96	0.32	9.89	16.67	24.44
22	118.44	-41.47	64.11	-36.14	87.88	-38.88	0.89	1.01	0.27	11.37	7.83	17.87
23	109.57	-40.79	59.31	-35.46	84.18	-38.50	0.90	0.92	0.29	10.75	17.96	25.08
24	146.81	-43.33	79.38	-37.99	100.20	-40.02	1.32	-2.41	0.31	10.17	19.12	25.63
25	126.34	-42.03	68.39	-36.70	94.08	-39.47	1.04	-0.34	0.29	10.75	10.72	20.60
26	160.12	-44.09	86.48	-38.74	111.47	-40.94	2.05	-6.24	0.32	9.89	18.30	25.25
27	149.53	-43.49	81.51	-38.22	103.12	-40.27	1.50	-3.52	0.38	8.40	23.00	27.23

Table A4. Upper percentage points of the F distribution with ν_1, ν_2 df

(a) 5% points

ν_1 =df for the numerator

ν_2	1	2	3	4	5	6	7	8	9	10	12	15	20	24	30	40	60	120	∞
1	161.448	199.500	215.707	224.583	230.162	233.986	236.768	238.883	240.543	241.882	243.906	245.950	248.013	249.052	250.095	251.143	252.196	253.253	254.314
2	18.513	19.000	19.164	19.247	19.296	19.330	19.353	19.371	19.385	19.396	19.413	19.429	19.446	19.454	19.462	19.471	19.479	19.487	19.496
3	10.1280	9.5521	9.2766	9.1172	9.0135	8.9406	8.8867	8.8452	8.8123	8.7855	8.7446	8.7029	8.6602	8.6385	8.6166	8.5944	8.5720	8.5493	8.5265
4	7.7086	6.9443	6.5914	6.3882	6.2561	6.1631	6.0942	6.0410	5.9988	5.9644	5.9117	5.8578	5.8025	5.7744	5.7459	5.7170	5.6877	5.6581	5.6281
5	6.6079	5.7861	5.4095	5.1922	5.0503	4.9503	4.8759	4.8183	4.7725	4.7351	4.6777	4.6188	4.5581	4.5272	4.4957	4.4638	4.4314	4.3985	4.3650
6	5.9874	5.1433	4.7571	4.5337	4.3874	4.2839	4.2067	4.1468	4.0990	4.0600	3.9999	3.9381	3.8742	3.8415	3.8082	3.7743	3.7398	3.7047	3.6689
7	5.5914	4.7374	4.3468	4.1203	3.9715	3.8660	3.7870	3.7257	3.6767	3.6365	3.5747	3.5107	3.4445	3.4105	3.3758	3.3404	3.3043	3.2674	3.2298
8	5.3177	4.4590	4.0662	3.8379	3.6875	3.5806	3.5005	3.4381	3.3881	3.3472	3.2839	3.2184	3.1503	3.1152	3.0794	3.0428	3.0053	2.9669	2.9276
9	5.1174	4.2565	3.8625	3.6331	3.4817	3.3738	3.2927	3.2296	3.1789	3.1373	3.0729	3.0061	2.9365	2.9005	2.8637	2.8259	2.7872	2.7475	2.7067
10	4.9646	4.1028	3.7083	3.4780	3.3258	3.2172	3.1355	3.0717	3.0204	2.9782	2.9130	2.8450	2.7740	2.7372	2.6996	2.6609	2.6211	2.5801	2.5379
11	4.8443	3.9823	3.5874	3.3567	3.2039	3.0946	3.0123	2.9480	2.8962	2.8536	2.7876	2.7186	2.6464	2.6090	2.5705	2.5309	2.4901	2.4480	2.4045
12	4.7472	3.8853	3.4903	3.2592	3.1059	2.9961	2.9134	2.8486	2.7964	2.7534	2.6866	2.6169	2.5436	2.5055	2.4663	2.4259	2.3842	2.3410	2.2962
13	4.6672	3.8056	3.4105	3.1791	3.0254	2.9153	2.8321	2.7669	2.7144	2.6710	2.6037	2.5331	2.4589	2.4202	2.3803	2.3392	2.2966	2.2524	2.2064
14	4.6001	3.7389	3.3439	3.1122	2.9582	2.8477	2.7642	2.6987	2.6458	2.6022	2.5342	2.4630	2.3879	2.3487	2.3082	2.2664	2.2229	2.1778	2.1307
15	4.5431	3.6823	3.2874	3.0556	2.9013	2.7905	2.7066	2.6408	2.5876	2.5437	2.4753	2.4034	2.3275	2.2878	2.2468	2.2043	2.1601	2.1141	2.0659
16	4.4940	3.6337	3.2389	3.0069	2.8524	2.7413	2.6572	2.5911	2.5377	2.4935	2.4247	2.3522	2.2756	2.2354	2.1938	2.1507	2.1058	2.0589	2.0096
17	4.4513	3.5915	3.1968	2.9647	2.8100	2.6987	2.6143	2.5480	2.4943	2.4499	2.3807	2.3077	2.2304	2.1898	2.1477	2.1040	2.0584	2.0107	1.9604
18	4.4139	3.5546	3.1599	2.9277	2.7729	2.6613	2.5767	2.5102	2.4563	2.4117	2.3421	2.2686	2.1906	2.1497	2.1071	2.0629	2.0166	1.9681	1.9168
19	4.3807	3.5219	3.1273	2.8951	2.7401	2.6283	2.5435	2.4768	2.4227	2.3779	2.3080	2.2341	2.1555	2.1141	2.0712	2.0264	1.9795	1.9302	1.8780
20	4.3512	3.4928	3.0984	2.8661	2.7109	2.5990	2.5140	2.4471	2.3928	2.3479	2.2776	2.2033	2.1242	2.0825	2.0391	1.9938	1.9464	1.8963	1.8432
21	4.3248	3.4668	3.0725	2.8401	2.6848	2.5727	2.4876	2.4205	2.3660	2.3210	2.2504	2.1757	2.0960	2.0540	2.0102	1.9645	1.9165	1.8657	1.8117
22	4.3009	3.4434	3.0491	2.8167	2.6613	2.5491	2.4638	2.3965	2.3419	2.2967	2.2258	2.1508	2.0707	2.0283	1.9842	1.9380	1.8894	1.8380	1.7831
23	4.2793	3.4221	3.0280	2.7955	2.6400	2.5277	2.4422	2.3748	2.3201	2.2747	2.2036	2.1282	2.0476	2.0050	1.9605	1.9139	1.8648	1.8128	1.7570
24	4.2597	3.4028	3.0088	2.7763	2.6207	2.5082	2.4226	2.3551	2.3002	2.2547	2.1834	2.1077	2.0267	1.9838	1.9390	1.8920	1.8424	1.7896	1.7331
25	4.2417	3.3852	2.9912	2.7587	2.6030	2.4904	2.4047	2.3371	2.2821	2.2365	2.1649	2.0889	2.0075	1.9643	1.9192	1.8718	1.8217	1.7684	1.7110
26	4.2252	3.3690	2.9752	2.7426	2.5868	2.4741	2.3883	2.3205	2.2655	2.2197	2.1479	2.0716	1.9898	1.9464	1.9010	1.8533	1.8027	1.7488	1.6906
27	4.2100	3.3541	2.9604	2.7278	2.5719	2.4591	2.3732	2.3053	2.2501	2.2043	2.1323	2.0558	1.9736	1.9299	1.8842	1.8361	1.7851	1.7306	1.6717
28	4.1960	3.3404	2.9467	2.7141	2.5581	2.4453	2.3593	2.2913	2.2360	2.1900	2.1179	2.0411	1.9586	1.9147	1.8687	1.8203	1.7689	1.7138	1.6541
29	4.1830	3.3277	2.9340	2.7014	2.5454	2.4324	2.3463	2.2783	2.2229	2.1768	2.1045	2.0275	1.9446	1.9005	1.8543	1.8055	1.7537	1.6981	1.6377
30	4.1709	3.3158	2.9223	2.6896	2.5336	2.4205	2.3343	2.2662	2.2107	2.1646	2.0921	2.0148	1.9317	1.8874	1.8409	1.7918	1.7396	1.6835	1.6223
40	4.0847	3.2317	2.8387	2.6060	2.4495	2.3359	2.2490	2.1802	2.1240	2.0772	2.0035	1.9245	1.8389	1.7929	1.7444	1.6928	1.6373	1.5766	1.5089
60	4.0012	3.1504	2.7581	2.5252	2.3683	2.2541	2.1665	2.0970	2.0401	1.9926	1.9174	1.8364	1.7480	1.7001	1.6491	1.5943	1.5343	1.4673	1.3893
120	3.9201	3.0718	2.6802	2.4472	2.2899	2.1750	2.0868	2.0164	1.9588	1.9105	1.8337	1.7505	1.6587	1.6084	1.5543	1.4952	1.4290	1.3519	1.2539
∞	3.8415	2.9957	2.6049	2.3719	2.2141	2.0986	2.0096	1.9384	1.8799	1.8307	1.7522	1.6664	1.5705	1.5173	1.4591	1.3940	1.3180	1.2214	1.0033

Table A5. Upper percentage points of the F distribution with ν_1, ν_2 df

(b) 2.5% points

ν_1 =df for the numerator

ν_2	1	2	3	4	5	6	7	8	9	10	12	15	20	24	30	40	60	120	∞
1	647.790	799.502	864.165	899.585	921.850	937.113	948.219	956.658	963.286	968.629	976.710	984.869	993.105	997.251	1001.416	1005.600	1009.802	1014.022	1018.260
2	38.506	39.000	39.166	39.248	39.298	39.331	39.355	39.373	39.387	39.398	39.415	39.431	39.448	39.456	39.465	39.473	39.481	39.490	39.498
3	17.4435	16.0441	15.4392	15.1010	14.8848	14.7347	14.6244	14.5399	14.4731	14.4190	14.3366	14.2527	14.1674	14.1242	14.0805	14.0365	13.9921	13.9473	13.9021
4	12.2179	10.6491	9.9792	9.6045	9.3645	9.1973	9.0741	8.9796	8.9047	8.8439	8.7512	8.6565	8.5599	8.5109	8.4613	8.4111	8.3604	8.3092	8.2573
5	10.0070	8.4336	7.7636	7.3879	7.1464	6.9777	6.8531	6.7572	6.6811	6.6192	6.5246	6.4277	6.3286	6.2780	6.2269	6.1751	6.1225	6.0693	6.0153
6	8.8131	7.2599	6.5988	6.2272	5.9876	5.8198	5.6955	5.5996	5.5234	5.4613	5.3662	5.2687	5.1684	5.1172	5.0652	5.0125	4.9589	4.9044	4.8491
7	8.0727	6.5415	5.8898	5.5226	5.2852	5.1186	4.9949	4.8993	4.8232	4.7611	4.6658	4.5678	4.4667	4.4150	4.3624	4.3089	4.2544	4.1989	4.1423
8	7.5709	6.0595	5.4160	5.0526	4.8173	4.6517	4.5286	4.4333	4.3572	4.2951	4.1997	4.1012	3.9995	3.9472	3.8940	3.8398	3.7844	3.7279	3.6702
9	7.2093	5.7147	5.0781	4.7181	4.4844	4.3197	4.1970	4.1020	4.0260	3.9639	3.8682	3.7694	3.6669	3.6142	3.5604	3.5055	3.4493	3.3918	3.3329
10	6.9367	5.4564	4.8256	4.4683	4.2361	4.0721	3.9498	3.8549	3.7790	3.7168	3.6209	3.5217	3.4185	3.3654	3.3110	3.2554	3.1984	3.1399	3.0798
11	6.7241	5.2559	4.6300	4.2751	4.0440	3.8807	3.7586	3.6638	3.5879	3.5257	3.4296	3.3299	3.2261	3.1725	3.1176	3.0613	3.0035	2.9441	2.8828
12	6.5538	5.0959	4.4742	4.1212	3.8911	3.7283	3.6065	3.5118	3.4358	3.3736	3.2773	3.1772	3.0728	3.0187	2.9633	2.9063	2.8478	2.7874	2.7249
13	6.4143	4.9653	4.3472	3.9959	3.7667	3.6043	3.4827	3.3880	3.3120	3.2497	3.1532	3.0527	2.9477	2.8932	2.8372	2.7797	2.7204	2.6590	2.5955
14	6.2979	4.8567	4.2417	3.8919	3.6634	3.5014	3.3799	3.2853	3.2093	3.1469	3.0502	2.9493	2.8437	2.7888	2.7324	2.6742	2.6142	2.5519	2.4872
15	6.1995	4.7650	4.1528	3.8043	3.5764	3.4147	3.2934	3.1987	3.1227	3.0602	2.9633	2.8621	2.7559	2.7006	2.6437	2.5850	2.5242	2.4611	2.3954
16	6.1151	4.6867	4.0768	3.7294	3.5021	3.3406	3.2194	3.1248	3.0488	2.9862	2.8890	2.7875	2.6808	2.6252	2.5678	2.5085	2.4471	2.3831	2.3163
17	6.0420	4.6189	4.0112	3.6648	3.4379	3.2767	3.1556	3.0610	2.9849	2.9222	2.8249	2.7230	2.6158	2.5598	2.5020	2.4422	2.3801	2.3153	2.2474
18	5.9781	4.5597	3.9539	3.6083	3.3820	3.2209	3.0999	3.0053	2.9291	2.8664	2.7689	2.6667	2.5590	2.5027	2.4445	2.3842	2.3214	2.2558	2.1869
19	5.9216	4.5075	3.9034	3.5587	3.3327	3.1718	3.0509	2.9563	2.8801	2.8172	2.7196	2.6171	2.5089	2.4523	2.3937	2.3329	2.2696	2.2032	2.1333
20	5.8715	4.4613	3.8587	3.5147	3.2891	3.1283	3.0074	2.9128	2.8365	2.7737	2.6758	2.5731	2.4645	2.4076	2.3486	2.2873	2.2234	2.1562	2.0853
21	5.8266	4.4199	3.8188	3.4754	3.2501	3.0895	2.9686	2.8740	2.7977	2.7348	2.6368	2.5338	2.4247	2.3675	2.3082	2.2465	2.1819	2.1141	2.0422
22	5.7863	4.3828	3.7829	3.4401	3.2151	3.0546	2.9338	2.8392	2.7628	2.6998	2.6017	2.4984	2.3890	2.3315	2.2718	2.2097	2.1446	2.0760	2.0032
23	5.7498	4.3492	3.7505	3.4083	3.1835	3.0232	2.9023	2.8077	2.7313	2.6682	2.5699	2.4665	2.3567	2.2989	2.2389	2.1763	2.1107	2.0415	1.9677
24	5.7166	4.3187	3.7211	3.3794	3.1548	2.9946	2.8738	2.7791	2.7027	2.6396	2.5411	2.4374	2.3273	2.2693	2.2090	2.1460	2.0799	2.0099	1.9353
25	5.6864	4.2909	3.6943	3.3530	3.1287	2.9685	2.8478	2.7531	2.6766	2.6135	2.5149	2.4110	2.3005	2.2422	2.1816	2.1183	2.0516	1.9811	1.9055
26	5.6586	4.2655	3.6697	3.3289	3.1048	2.9447	2.8240	2.7293	2.6528	2.5896	2.4908	2.3867	2.2759	2.2174	2.1565	2.0928	2.0257	1.9545	1.8781
27	5.6331	4.2421	3.6472	3.3067	3.0828	2.9228	2.8021	2.7074	2.6309	2.5676	2.4688	2.3644	2.2533	2.1946	2.1334	2.0693	2.0018	1.9299	1.8527
28	5.6096	4.2205	3.6264	3.2863	3.0626	2.9027	2.7820	2.6872	2.6106	2.5473	2.4484	2.3438	2.2324	2.1735	2.1121	2.0477	1.9797	1.9072	1.8291
29	5.5878	4.2006	3.6072	3.2674	3.0438	2.8840	2.7633	2.6686	2.5920	2.5286	2.4295	2.3248	2.2131	2.1540	2.0923	2.0276	1.9591	1.8861	1.8072
30	5.5675	4.1821	3.5894	3.2499	3.0265	2.8667	2.7460	2.6513	2.5746	2.5112	2.4120	2.3072	2.1952	2.1359	2.0739	2.0089	1.9400	1.8664	1.7867
40	5.4239	4.0510	3.4633	3.1261	2.9037	2.7444	2.6238	2.5289	2.4519	2.3882	2.2882	2.1819	2.0677	2.0069	1.9429	1.8752	1.8028	1.7242	1.6371
60	5.2856	3.9253	3.3425	3.0077	2.7863	2.6274	2.5068	2.4117	2.3344	2.2702	2.1692	2.0613	1.9445	1.8817	1.8152	1.7440	1.6668	1.5810	1.4822
120	5.1523	3.8046	3.2269	2.8943	2.6740	2.5154	2.3948	2.2994	2.2217	2.1570	2.0548	1.9450	1.8249	1.7597	1.6899	1.6141	1.5299	1.4327	1.3105
∞	5.0239	3.6889	3.1161	2.7858	2.5665	2.4082	2.2876	2.1918	2.1137	2.0483	1.9447	1.8326	1.7085	1.6402	1.5660	1.4836	1.3883	1.2685	1.0039

Table A6. Upper percentage points of the F distribution with v_1, v_2 df

(c) 1% points

$v_1 =$df for the numerator

v_2	1	2	3	4	5	6	7	8	9	10	12	15	20	24	30	40	60	120	∞
1	4052.19	4999.51	5403.36	5624.59	5763.66	5859.00	5928.37	5981.08	6022.48	6055.86	6106.33	6157.30	6208.74	6234.64	6260.66	6286.79	6313.04	6339.40	6365.87
2	98.50	99.00	99.17	99.25	99.30	99.33	99.36	99.37	99.39	99.40	99.42	99.43	99.45	99.46	99.47	99.47	99.48	99.49	99.50
3	34.1162	30.8165	29.4567	28.7099	28.2371	27.9107	27.6717	27.4892	27.3452	27.2288	27.0518	26.8722	26.6898	26.5975	26.5046	26.4108	26.3164	26.2212	26.1252
4	21.1977	18.0000	16.6944	15.9770	15.5219	15.2069	14.9758	14.7989	14.6591	14.5459	14.3736	14.1982	14.0196	13.9291	13.8377	13.7454	13.6522	13.5581	13.4631
5	16.2582	13.2739	12.0600	11.3919	10.9670	10.6723	10.4555	10.2893	10.1578	10.0510	9.8883	9.7222	9.5527	9.4665	9.3793	9.2912	9.2020	9.1118	9.0204
6	13.7450	10.9248	9.7795	9.1483	8.7459	8.4661	8.2600	8.1017	7.9761	7.8741	7.7183	7.5590	7.3958	7.3127	7.2285	7.1432	7.0567	6.9690	6.8800
7	12.2464	9.5466	8.4513	7.8466	7.4604	7.1914	6.9928	6.8401	6.7188	6.6201	6.4691	6.3143	6.1554	6.0743	5.9920	5.9085	5.8236	5.7373	5.6495
8	11.2586	8.6491	7.5910	7.0061	6.6318	6.3707	6.1776	6.0289	5.9106	5.8143	5.6667	5.5151	5.3591	5.2793	5.1981	5.1156	5.0316	4.9461	4.8588
9	10.5614	8.0215	6.9919	6.4221	6.0569	5.8018	5.6129	5.4671	5.3511	5.2565	5.1114	4.9621	4.8080	4.7290	4.6486	4.5666	4.4831	4.3978	4.3106
10	10.0443	7.5594	6.5523	5.9943	5.6363	5.3858	5.2001	5.0567	4.9424	4.8491	4.7059	4.5581	4.4054	4.3269	4.2469	4.1653	4.0819	3.9965	3.9090
11	9.6460	7.2057	6.2167	5.6683	5.3160	5.0692	4.8861	4.7445	4.6315	4.5393	4.3974	4.2509	4.0990	4.0209	3.9411	3.8596	3.7761	3.6904	3.6025
12	9.3302	6.9266	5.9525	5.4120	5.0643	4.8206	4.6395	4.4994	4.3875	4.2961	4.1553	4.0096	3.8584	3.7805	3.7008	3.6192	3.5355	3.4494	3.3608
13	9.0738	6.7010	5.7394	5.2053	4.8616	4.6204	4.4410	4.3021	4.1911	4.1003	3.9603	3.8154	3.6646	3.5868	3.5070	3.4253	3.3413	3.2548	3.1654
14	8.8616	6.5149	5.5639	5.0354	4.6950	4.4558	4.2779	4.1399	4.0297	3.9394	3.8001	3.6557	3.5052	3.4274	3.3476	3.2656	3.1813	3.0942	3.0040
15	8.6831	6.3589	5.4170	4.8932	4.5556	4.3183	4.1415	4.0045	3.8948	3.8049	3.6662	3.5222	3.3719	3.2940	3.2141	3.1319	3.0471	2.9595	2.8684
16	8.5310	6.2262	5.2922	4.7726	4.4374	4.2016	4.0259	3.8896	3.7804	3.6909	3.5527	3.4089	3.2587	3.1808	3.1007	3.0182	2.9330	2.8447	2.7528
17	8.3997	6.1121	5.1850	4.6690	4.3359	4.1015	3.9267	3.7910	3.6822	3.5931	3.4552	3.3117	3.1615	3.0835	3.0032	2.9205	2.8348	2.7459	2.6530
18	8.2854	6.0129	5.0919	4.5790	4.2479	4.0146	3.8406	3.7054	3.5971	3.5082	3.3706	3.2273	3.0771	2.9990	2.9185	2.8354	2.7493	2.6597	2.5660
19	8.1849	5.9259	5.0103	4.5003	4.1708	3.9386	3.7653	3.6305	3.5225	3.4338	3.2965	3.1533	3.0031	2.9249	2.8442	2.7608	2.6742	2.5839	2.4893
20	8.0960	5.8489	4.9382	4.4307	4.1027	3.8714	3.6987	3.5644	3.4567	3.3682	3.2311	3.0880	2.9377	2.8594	2.7785	2.6947	2.6077	2.5168	2.4212
21	8.0166	5.7804	4.8740	4.3688	4.0421	3.8117	3.6396	3.5056	3.3981	3.3098	3.1730	3.0300	2.8796	2.8011	2.7200	2.6359	2.5484	2.4568	2.3603
22	7.9454	5.7190	4.8166	4.3134	3.9880	3.7583	3.5867	3.4530	3.3458	3.2576	3.1209	2.9779	2.8274	2.7488	2.6675	2.5831	2.4951	2.4029	2.3055
23	7.8811	5.6637	4.7649	4.2636	3.9392	3.7102	3.5390	3.4057	3.2986	3.2106	3.0740	2.9311	2.7805	2.7017	2.6202	2.5355	2.4471	2.3542	2.2559
24	7.8229	5.6136	4.7181	4.2184	3.8951	3.6667	3.4959	3.3629	3.2560	3.1681	3.0316	2.8887	2.7380	2.6591	2.5773	2.4923	2.4035	2.3100	2.2107
25	7.7698	5.5680	4.6755	4.1774	3.8550	3.6272	3.4568	3.3239	3.2172	3.1294	2.9931	2.8502	2.6993	2.6203	2.5383	2.4530	2.3637	2.2696	2.1694
26	7.7213	5.5263	4.6366	4.1400	3.8183	3.5911	3.4210	3.2884	3.1818	3.0941	2.9578	2.8150	2.6640	2.5848	2.5026	2.4170	2.3273	2.2325	2.1315
27	7.6767	5.4881	4.6009	4.1056	3.7848	3.5580	3.3882	3.2558	3.1494	3.0618	2.9256	2.7827	2.6316	2.5522	2.4699	2.3840	2.2938	2.1985	2.0965
28	7.6356	5.4529	4.5681	4.0740	3.7539	3.5276	3.3581	3.2259	3.1195	3.0320	2.8959	2.7530	2.6017	2.5223	2.4397	2.3535	2.2629	2.1670	2.0642
29	7.5977	5.4204	4.5378	4.0449	3.7254	3.4995	3.3303	3.1982	3.0920	3.0045	2.8685	2.7256	2.5742	2.4946	2.4118	2.3253	2.2344	2.1379	2.0342
30	7.5625	5.3903	4.5097	4.0179	3.6990	3.4735	3.3045	3.1726	3.0665	2.9791	2.8431	2.7002	2.5487	2.4689	2.3860	2.2992	2.2079	2.1108	2.0062
40	7.3141	5.1785	4.3126	3.8283	3.5138	3.2910	3.1238	2.9930	2.8876	2.8005	2.6648	2.5216	2.3689	2.2880	2.2034	2.1142	2.0194	1.9172	1.8047
60	7.0771	4.9774	4.1259	3.6490	3.3389	3.1187	2.9530	2.8233	2.7185	2.6318	2.4961	2.3523	2.1978	2.1154	2.0285	1.9360	1.8363	1.7263	1.6007
120	6.8509	4.7865	3.9491	3.4795	3.1735	2.9559	2.7918	2.6629	2.5586	2.4721	2.3363	2.1915	2.0346	1.9500	1.8600	1.7628	1.6557	1.5330	1.3805
∞	6.6349	4.6052	3.7816	3.3192	3.0173	2.8020	2.6393	2.5113	2.4074	2.3209	2.1848	2.0385	1.8783	1.7908	1.6964	1.5923	1.4730	1.3246	1.0047

Table A7. Upper percentage points of the F distribution with v_1, v_2 df

(d) 0.5% points

$v_1 =$df for the numerator

v_2	1	2	3	4	5	6	7	8	9	10	12	15	20	24	30	40	60	120	∞
1	16210.8	19999.5	21614.8	22499.6	23055.8	23437.2	23714.6	23925.5	24091.1	24224.5	24426.4	24630.3	24836.0	24939.6	25043.7	25148.2	25253.2	25358.6	25464.5
2	198.5	199.0	199.2	199.2	199.3	199.3	199.4	199.4	199.4	199.4	199.4	199.4	199.4	199.5	199.5	199.5	199.5	199.5	199.5
3	55.5520	49.7993	47.4673	46.1947	45.3917	44.8385	44.4341	44.1256	43.8824	43.6858	43.3874	43.0847	42.7775	42.6223	42.4658	42.3082	42.1495	41.9895	41.8283
4	31.3328	26.2843	24.2591	23.1545	22.4564	21.9746	21.6217	21.3520	21.1391	20.9667	20.7047	20.4383	20.1673	20.0300	19.8915	19.7518	19.6107	19.4684	19.3247
5	22.7848	18.3138	16.5298	15.5561	14.9396	14.5133	14.2005	13.9610	13.7717	13.6182	13.3845	13.1463	12.9035	12.7802	12.6556	12.5297	12.4025	12.2737	12.1436
6	18.6350	14.5441	12.9166	12.0275	11.4637	11.0730	10.7859	10.5658	10.3915	10.2500	10.0343	9.8140	9.5888	9.4742	9.3582	9.2409	9.1219	9.0015	8.8793
7	16.2356	12.4040	10.8825	10.0505	9.5221	9.1553	8.8854	8.6781	8.5138	8.3803	8.1764	7.9678	7.7540	7.6450	7.5345	7.4224	7.3088	7.1933	7.0760
8	14.6882	11.0424	9.5965	8.8051	8.3018	7.9520	7.6941	7.4959	7.3386	7.2106	7.0149	6.8143	6.6082	6.5029	6.3961	6.2875	6.1772	6.0649	5.9506
9	13.6136	10.1067	8.7171	7.9559	7.4712	7.1339	6.8849	6.6933	6.5411	6.4172	6.2274	6.0325	5.8318	5.7292	5.6248	5.5186	5.4104	5.3001	5.1875
10	12.8265	9.4270	8.0807	7.3428	6.8724	6.5446	6.3025	6.1159	5.9676	5.8467	5.6613	5.4707	5.2740	5.1732	5.0706	4.9659	4.8592	4.7501	4.6385
11	12.2263	8.9123	7.6004	6.8809	6.4217	6.1016	5.8648	5.6821	5.5368	5.4183	5.2363	5.0489	4.8552	4.7557	4.6543	4.5508	4.4450	4.3367	4.2255
12	11.7542	8.5096	7.2258	6.5211	6.0711	5.7570	5.5245	5.3451	5.2021	5.0855	4.9063	4.7213	4.5299	4.4314	4.3309	4.2282	4.1229	4.0149	3.9039
13	11.3735	8.1865	6.9258	6.2335	5.7910	5.4819	5.2529	5.0761	4.9351	4.8199	4.6429	4.4600	4.2703	4.1726	4.0727	3.9704	3.8655	3.7577	3.6465
14	11.0603	7.9216	6.6804	5.9984	5.5623	5.2574	5.0313	4.8566	4.7173	4.6034	4.4281	4.2468	4.0585	3.9614	3.8619	3.7600	3.6553	3.5473	3.4359
15	10.7981	7.7008	6.4760	5.8029	5.3721	5.0708	4.8473	4.6744	4.5364	4.4235	4.2497	4.0698	3.8826	3.7859	3.6867	3.5850	3.4803	3.3722	3.2602
16	10.5755	7.5138	6.3034	5.6378	5.2117	4.9134	4.6920	4.5207	4.3838	4.2719	4.0994	3.9205	3.7342	3.6378	3.5389	3.4372	3.3324	3.2240	3.1115
17	10.3842	7.3536	6.1556	5.4967	5.0746	4.7789	4.5594	4.3894	4.2535	4.1424	3.9709	3.7929	3.6073	3.5112	3.4124	3.3108	3.2058	3.0971	2.9839
18	10.2181	7.2148	6.0278	5.3746	4.9560	4.6627	4.4448	4.2759	4.1410	4.0305	3.8599	3.6827	3.4977	3.4017	3.3030	3.2014	3.0962	2.9871	2.8732
19	10.0725	7.0935	5.9161	5.2681	4.8526	4.5614	4.3448	4.1770	4.0428	3.9329	3.7631	3.5866	3.4020	3.3062	3.2075	3.1058	3.0004	2.8908	2.7762
20	9.9439	6.9865	5.8177	5.1743	4.7616	4.4721	4.2569	4.0900	3.9564	3.8470	3.6779	3.5020	3.3178	3.2220	3.1234	3.0215	2.9159	2.8058	2.6904
21	9.8295	6.8914	5.7304	5.0911	4.6809	4.3931	4.1789	4.0128	3.8799	3.7709	3.6024	3.4270	3.2431	3.1474	3.0488	2.9467	2.8408	2.7302	2.6140
22	9.7271	6.8064	5.6524	5.0168	4.6088	4.3225	4.1094	3.9440	3.8116	3.7030	3.5350	3.3600	3.1764	3.0807	2.9821	2.8799	2.7736	2.6625	2.5455
23	9.6348	6.7300	5.5823	4.9500	4.5441	4.2591	4.0469	3.8822	3.7502	3.6420	3.4745	3.2999	3.1165	3.0208	2.9221	2.8197	2.7132	2.6015	2.4837
24	9.5513	6.6610	5.5190	4.8898	4.4857	4.2019	3.9905	3.8264	3.6949	3.5870	3.4199	3.2456	3.0624	2.9667	2.8679	2.7654	2.6585	2.5463	2.4276
25	9.4753	6.5982	5.4615	4.8351	4.4327	4.1500	3.9394	3.7758	3.6447	3.5371	3.3704	3.1963	3.0133	2.9176	2.8187	2.7160	2.6088	2.4961	2.3765
26	9.4059	6.5410	5.4091	4.7852	4.3844	4.1027	3.8928	3.7297	3.5989	3.4916	3.3252	3.1515	2.9685	2.8728	2.7738	2.6709	2.5633	2.4501	2.3297
27	9.3423	6.4885	5.3611	4.7396	4.3402	4.0594	3.8501	3.6875	3.5571	3.4499	3.2839	3.1104	2.9275	2.8318	2.7327	2.6296	2.5217	2.4079	2.2867
28	9.2838	6.4403	5.3170	4.6977	4.2996	4.0197	3.8110	3.6487	3.5186	3.4117	3.2460	3.0727	2.8899	2.7941	2.6949	2.5916	2.4834	2.3690	2.2470
29	9.2297	6.3958	5.2764	4.6591	4.2622	3.9831	3.7749	3.6131	3.4832	3.3765	3.2110	3.0379	2.8551	2.7594	2.6600	2.5565	2.4479	2.3331	2.2102
30	9.1797	6.3547	5.2388	4.6234	4.2276	3.9492	3.7416	3.5801	3.4505	3.3440	3.1787	3.0057	2.8230	2.7272	2.6278	2.5241	2.4151	2.2998	2.1760
40	8.8279	6.0664	4.9758	4.3738	3.9860	3.7129	3.5088	3.3498	3.2220	3.1167	2.9531	2.7811	2.5984	2.5020	2.4015	2.2958	2.1838	2.0636	1.9318
60	8.4946	5.7950	4.7290	4.1399	3.7599	3.4918	3.2911	3.1344	3.0083	2.9042	2.7419	2.5705	2.3872	2.2898	2.1874	2.0789	1.9622	1.8341	1.6885
120	8.1788	5.5393	4.4972	3.9207	3.5482	3.2849	3.0874	2.9330	2.8083	2.7052	2.5439	2.3727	2.1881	2.0890	1.9840	1.8709	1.7469	1.6055	1.4311
∞	7.8795	5.2983	4.2794	3.7151	3.3499	3.0913	2.8968	2.7444	2.6211	2.5188	2.3583	2.1868	1.9999	1.8983	1.7891	1.6692	1.5326	1.3638	1.0052

NATIONAL INSTITUTE OF TECHNOLOGY KARNATAKA,
SURATHKAL

List of Publications based on PhD Research Work

Sl. No.	Title of the Paper	Authors (In the same order as in the paper, underline the Research Scholar's name)	Name of the Journal / Conference / Symposium, Vol., No., Pages	Month & Year of Publication	Category *
1.	Multi response optimization of thermally enhanced machining parameters of Inconel 718 using Taguchi grey relation analysis.	Venkatesh G, K Srinivasa sagar, D. Chakradhar	International Journal Machining and Machinability of Materials, 19, 57-75. **DOI**: http://dx.doi.org/10.1504/IJMMM.2017.081189	January, 2017	1
2.	Influence of thermally assisted machining parameters on the machinability of Inconel 718 superalloy.	Venkatesh G, D. Chakradhar	Silicon	April, 2017 (SCI)	1
3.	Modeling and optimization of thermally assisted machining parameters in turning of Inconel 718 superalloy using response surface methodology and particle swarm optimization.	Venkatesh G, D. Chakradhar	Arabian Journal of Science and Engineering	Accepted for publication (SCI)	1
4.	Multi objective optimization of hot machining of 15-5PH stainless steel using grey relation analysis	Venkatesh G, D. Chakradhar	Procedia Materials Science, 5, 1810-1818.	March, 2014	1

5.	An Experimental Investigation of Hot Machining Performance Parameters using Oxy-Acetylene gas.	<u>Venkatesh G</u>, D. Chakradhar	5th International and 26th All India Manufacturing Technology, Design and Research Conference AIMTDR-2014, IIT- Guwahati, 371-376.	December, 2014	3
6.	Parametric Optimization in Hot Turning of Inconel 718 alloy using Taguchi Method.	<u>Venkatesh G</u>, D. Chakradhar	3rd International Engineering Symposium (IES 2015), Japan, 37(1-5).	March, 2015	3

* Category: 1 : Journal paper, full paper reviewed   2 : Journal paper, Abstract reviewed
                  3 : Conference/Symposium paper, full paper reviewed   4 : Conference/Symposium paper, abstract reviewed
                  5 : others (including papers in Workshops, NITK Research Bulletins,   Short notes etc.)

BIO DATA

1. **Name:** Venkatesh G

2. **Father's Name:** G. Nageswara Rao

3. **Date of Birth:** 18/06/1984

4. **Nationality:** Indian

5. **Marital Status:** Married

6. **Address:**

Permanent Address	**Present Address**
S/o. G. Nageswara Rao	Department of Mechanical Engineering
H.No: 87/1362-3f,	National Institute of Technology Karnataka
Chandrasekhar Nagar	Surathkal-575025, Srinivasanagar,
Kurnool- 518002	Dhakshina Kannada (Dist),
Andhra Pradesh, India	Karnataka, India.

7. **Mobile Number:** +91-9491825550

8. **E-mail id.:** venkatesh.8056@gmail.com

9. **Educational Qualification:**

Qualification	College/school	University/Board	Year of Passing	Performance
Ph.D. (Mechanical Engineering)	National Institute of Technology Karnataka, Surathkal, India	National Institute of Technology Karnataka, Surathkal, India	Pursuing	------
M. Tech (Manufacturing Engineering)	National Institute of Technology Warangal, India.	National Institute of Technology Warangal, India.	2010	8.19 (CGPA)
B. E (Industrial & Production Engineering)	G. Pulla Reddy Engineering College.	Sri Krishnadevaraya, University, Ananthapur, India.	2007	70.05 %

10. **Work Experience**

Name of the Organization	Duration	Position
Kottam Karunakara Reddy Institute of Technology, Kurnool, Andhra Pradesh, India.	June 2010 to Dec 2012	Assistant Professor
National Institute of Technology Karnataka, Surathkal, India.	Dec 2016 to till date	Assistant Lecturer

I declare that above information is true and correct to best of my knowledge.

(Venkatesh Ganta.)